geodiversitas

2026 • 48 • 11

A new Carboniferous coelacanth illuminates the evolution of the actinistian hyobranchial skeleton

Jorge MONDÉJAR FERNÁNDEZ, Rohan MANSUIT, Richard FLAMENT, Richard CLOUTIER, Royal MAPES, Gaël CLÉMENT & Alan PRADEL

art. 48 (11) — Published on 16 June 2026
www.geodiversitas.com

PUBLICATIONS SCIENTIFIQUES

MUSÉUM NAL HIST NATURELLE

Directeur de la publication / *Publication director* : Gilles Bloch,
Président du Muséum national d'Histoire naturelle

Rédacteur en chef / *Editor-in-chief*: Sylvain Charbonnier

Rédacteur associé / *Associate editor*: Didier Merle

Éditeur technique (suivi éditorial) / *Desk editor (editorial process)*: Emmanuel Côtez (geodiv@mnhn.fr)

Éditeur technique (production) / *Desk editor (production)*: Audrina Neveu (audrina.neveu@mnhn.fr)

Comité scientifique / *Scientific board*:
Christine Argot (Muséum national d'Histoire naturelle, Paris)
Beatrix Azanza (Museo Nacional de Ciencias Naturales, Madrid)
Raymond L. Bernor (Howard University, Washington DC)
Henning Blom (Uppsala University)
Gaël Clément (Muséum national d'Histoire naturelle, Paris)
Ted Daeschler (Academy of Natural Sciences, Philadelphie)
Cédric Del Rio (Muséum national d'Histoire naturelle)
Gregory D. Edgecombe (The Natural History Museum, Londres)
Ursula Göhlich (Natural History Museum Vienna)
Jin Meng (American Museum of Natural History, New York)
Brigitte Meyer-Berthaud (CIRAD, Montpellier)
Zhu Min (Chinese Academy of Sciences, Pékin)
Isabelle Rouget (Muséum national d'Histoire naturelle, Paris)
Sevket Sen (Muséum national d'Histoire naturelle, Paris, retraité)
Stanislav Štamberg (Museum of Eastern Bohemia, Hradec Králové)
Paul Taylor (The Natural History Museum, Londres, retraité)

Couverture / *Cover*:
Réalisée à partir des Figures de l'article/*Made from the Figures of the article*.

Geodiversitas est indexé dans / Geodiversitas *is indexed in:*
– Science Citation Index Expanded (SciSearch®)
– ISI Alerting Services®
– Current Contents® / Physical, Chemical, and Earth Sciences®
– Scopus®

Geodiversitas est distribué en version électronique par / Geodiversitas *is distributed electronically by:*
– BioOne® (http://www.bioone.org)

Les articles ainsi que les nouveautés nomenclaturales publiés dans *Geodiversitas* sont référencés par /
Articles and nomenclatural novelties published in Geodiversitas *are referenced by:*
– ZooBank® (http://zoobank.org)

Geodiversitas est une revue en flux continu publiée par les Publications scientifiques du Muséum, Paris
Geodiversitas *is a fast track journal published by the Museum Science Press, Paris*

Les Publications scientifiques du Muséum publient aussi / *The Museum Science Press also publish:* ***Adansonia***, ***Zoosystema***, ***Anthropozoologica***, ***European Journal of Taxonomy***, ***Naturae***, ***Cryptogamie*** **sous-sections** ***Algologie***, ***Bryologie***, ***Mycologie, Comptes Rendus Palevol***

Diffusion – Publications scientifiques Muséum national d'Histoire naturelle
CP 41 – 57 rue Cuvier F-75231 Paris cedex 05 (France)
Tél. : 33 (0)1 40 79 48 05 / Fax : 33 (0)1 40 79 38 40
diff.pub@mnhn.fr / http://sciencepress.mnhn.fr

Les articles publiés dans *Geodiversitas* sont distribués sous licence CC-BY 4.0/*Articles published in* Geodiversitas *are distributed under a CC-BY 4.0 license*.
ISSN (imprimé / *print*) : 1280-9659/ ISSN (électronique / *electronic*) : 1638-9395

A new Carboniferous coelacanth illuminates the evolution of the actinistian hyobranchial skeleton

Jorge MONDÉJAR FERNÁNDEZ
Division Palaeontology and Historical Geology, Senckenberg Research Institute and Natural History Museum, Senckenberganlage 25, 60325 Frankfurt am Main (Germany)
and CR2P (CNRS, MNHN, Sorbonne Université), Département Origines et Évolution, Muséum national d'Histoire naturelle, case postale 38, 57 rue Cuvier, F-75231 Paris cedex 05 (France)
jorge.mondejar.fernandez@gmail.com (corresponding author)

Rohan MANSUIT
CR2P (CNRS, MNHN, Sorbonne Université), Département Origines et Évolution, Muséum national d'Histoire naturelle, case postale 38, 57 rue Cuvier, F-75231 Paris cedex 05 (France)
and UniLaSalle, Université d'Artois, Interactions de l'Environnement et de l'Alimentation sur la Santé animale et la Santé humaine (IDEALISS), ULR 7519, 3 rue du Tronquet, 76130 Mont-Saint-Aignan (France)
rohan.mansuit@unilasalle.fr

Richard FLAMENT
Département de Biologie, Chimie et Géographie, Université du Québec à Rimouski, 300, allée des Ursulines, C.P. 3300, succ. A, Rimouski, QC G5L 3A1 (Canada)
richard.flament@uqar.ca

Richard CLOUTIER
Département de Biologie, Chimie et Géographie, Université du Québec à Rimouski, 300, allée des Ursulines, C.P. 3300, succ. A, Rimouski, QC G5L 3A1 (Canada)
and Centre of Excellence in Basin Studies and Applied Palaeontology, Palaeontological Research and Education Centre, Mahasarakham University, 67X3+3HM, Kham Riang, Kantharawichai District, Maha Sarakham 44150 (Thailand)
richard_cloutier@uqar.ca

Royal MAPES
Division of Paleontology (Invertebrates), American Museum of Natural History, 200 Central Park W, New York, NY 10024 (United States)
mapes@ohio.edu

Gaël CLÉMENT
Alan PRADEL
CR2P (CNRS, MNHN, Sorbonne Université), Département Origines et Évolution, Muséum national d'Histoire naturelle, case postale 38, 57 rue Cuvier, F-75231 Paris cedex 05 (France)
gael.clement@mnhn.fr
alan.pradel@mnhn.fr

Submitted on 16 June 2025 | Accepted on 22 September 2025 | Published on 16 June 2026

urn:lsid:zoobank.org:pub:32D7A51A-BD46-4DA4-AA8C-FAC9B10C143D

Mondéjar Fernández J., Mansuit R., Flament R., Cloutier R., Mapes R., Clément G. & Pradel A. 2026. — A new Carboniferous coelacanth illuminates the evolution of the actinistian hyobranchial skeleton. *Geodiversitas* 48 (11): 185-226. https://doi.org/10.5252/geodiversitas2026v48a11. http://geodiversitas.com/48/11

ABSTRACT
The hyobranchial skeleton plays a fundamental role in breathing and feeding in gnathostomes (jawed vertebrates). Nevertheless, despite a relatively rich fossil record spanning more than 400 million years, our knowledge of the anatomy and evolution of the hyoid and branchial arches of coelacanths is limited due to the extremely delicate and poorly ossified small elements forming the arches, which are rarely preserved. Comparative data are mainly available from the extant *Latimeria chalumnae* Smith, 1939, which represents a crucial landmark for all morphological descriptions of extinct coelacanth taxa. Here we introduce a new genus and species, *Aemilia stellata* n. gen., n. sp., from the Late Carboniferous (Pennsylvanian) of Texas, United States. The use of micro-computed tomography (µCT) has revealed in exquisite detail the complete series of the hyoid and branchial arches as well as part of the braincase, dermal skull roof and cheek, and pectoral girdle. Our new data shed light on the organisation of the skull in coelacanths and allow us to identify new trends in the evolution of the neurocranium and hyobranchial skeleton. A phylogenetic analysis of actinistian interrelationships reconstructs *Aemilia stellata* n. gen., n. sp. as the oldest representative of a large Mesozoic radiation of coelacanths, which extends its roots into the Carboniferous. Based on the new topology, coelacanth systematics are reviewed, and we propose a new phylogenetic definition of the order Coelacanthiformes. By its unexpected combination of features, *Aemilia stellata* n. gen., n. sp. bridges the gap between Devonian and post-Carboniferous coelacanths and reveals that the hyobranchial skeleton displays a certain degree of evolutionary plasticity in the traditionally considered "static" coelacanth anatomy.

KEY WORDS
Branchial arches,
Palaeozoic,
coelacanth,
microtomography,
evolution,
Latimeria,
new genus,
new species.

RÉSUMÉ
Un nouveau cœlacanthe du Carbonifère éclaire l'évolution du squelette hyobranchial des actinistiens.
Le squelette hyobranchial joue un rôle fondamental dans la respiration et la prise alimentaire chez les gnathostomes (vertébrés à mâchoires). Néanmoins, malgré un registre fossile relativement riche s'étendant sur plus de 400 millions d'années, nos connaissances sur l'anatomie et l'évolution des arcs hyoïdien et branchiaux des cœlacanthes sont limitées en raison des petits éléments extrêmement délicats et peu ossifiés qui les forment, et qui sont rarement préservés. Les données comparatives proviennent principalement du cœlacanthe actuel *Latimeria chalumnae* Smith, 1939, qui constitue la référence pour toutes les descriptions morphologiques de cœlacanthes éteints. Nous présentons ici un nouveau genre et une nouvelle espèce de cœlacanthe paléozoïque, *Aemilia stellata* n. gen., n. sp., du Carbonifère supérieur (Pennsylvanien) du Texas, aux États-Unis. L'utilisation de la microtomographie assistée par ordinateur (µCT) a révélé avec les plus grands détails la série complète des arcs hyoïdien et branchiaux, ainsi qu'une partie de la boîte crânienne, le toit crânien, la joue, et la ceinture pectorale. Nos nouvelles données éclairent la mise en place du crâne des cœlacanthes et nous permettent d'identifier de nouvelles tendances dans l'évolution du neurocrâne et du squelette hyobranchial. L'analyse phylogénétique pour les actinistiens positionne *Aemilia stellata* n. gen., n. sp. comme le plus ancien représentant d'une vaste radiation mésozoïque, dont les racines s'étendent jusqu'au Carbonifère. Sur la base de cette nouvelle topologie, la systématique des cœlacanthes est revue et nous proposons une nouvelle définition phylogénétique de l'ordre des Cœlacanthiformes Huxley, 1861 sensu Forey (1998). Par sa combinaison de caractères inattendue, *Aemilia stellata* n. gen., n. sp. comble le fossé entre les cœlacanthes du Dévonien et ceux du post-Carbonifère et révèle que le squelette hyobranchial présente un certain degré de plasticité évolutive dans une anatomie traditionnellement considérée comme « statique » chez les cœlacanthes.

MOTS CLÉS
Arcs branchiaux,
Paléozoïque,
cœlacanthe,
microtomographie,
évolution,
Latimeria,
genre nouveau,
espèce nouvelle.

INTRODUCTION

Since their first appearance in the fossil record at the beginning of the Devonian period (late Lockhovian, *c.* 410 Ma), coelacanths stand out among other sarcopterygians (lobe-finned fishes) by a unique set of features, many of them retained by the iconic extant *Latimeria* Smith, 1939 (*L. chalumnae* Smith, 1939 from the Eastern African coast, *L. menadoensis* Pouyaud, Wirjoatmodjo, Rachmatika, Tjakrawidjaja, Hadiaty & Hadie, 1999, and a possible third species (Kadarusman *et al.* 2020) from Indonesia). Anatomically modern coelacanths (i.e., forms with an elongated preorbital portion of the skull roof, two pairs of parietals, and a trilobed caudal fin; Zhu *et al.* 2012; Clement *et al.* 2024), broadly similar to *Latimeria*, can be traced back

to the Early Devonian (Johanson *et al.* 2006) and include Palaeozoic taxa such as *Euporosteus* Jaeckel, 1927, *Diplocercides* Stensiö, 1922, *Rhabdoderma* Newberry 1856, and *Coelacanthus* Agassiz, 1839 (Stensiö 1922, 1937; Moy-Thomas & Westoll 1935; Moy-Thomas 1937; Schaumberg 1978; Forey 1981, 1998; Zhu *et al.* 2012). This apparent evolutionary conservatism of their anatomy, as displayed in *Latimeria* is one of the most remarkable traits of coelacanths among osteichthyans (bony fishes). Other Devonian species like *Miguashaia bureaui* Schultze, 1973 (Schultze 1973; Cloutier 1996), *Gavinia syntrips* Long, 1999 (Long 1999), and *Ngamugawi wirngarri* Clement, Cloutier, Lee, King, Vanhaesebroucke, Bradshaw, Dutel, Trinajstic & Long, 2024 (Clement *et al.* 2024) are considered morphologically primitive coelacanths due to the retention of a generalized sarcopterygian arrangement of the skull roof and a heterocercal caudal fin (when found).

The fossil record reveals that the peak of coelacanth diversity occurred during the Early Triassic, with minor peaks in the Late Devonian, Early Carboniferous and Late Jurassic (Cloutier 1991a, b; Forey 1991, 1998; Schultze 2004; Toriño *et al.* 2021a; Ferrante *et al.* 2022; Clement *et al.* 2024; Ferrante & Cavin 2025). However, it is during the Devonian and Carboniferous that the highest morphological disparity is recorded in the Palaeozoic (e.g., Clement *et al.* 2024), evidenced by forms such as *Allenypterus montanus* Melton, 1969 (Lund & Lund 1984, 1985; Forey 1998) and *Holopterygius nudus* Jessen, 1973 (Friedman & Coates 2006). In contrast, post-Carboniferous taxa retained a more stereotypical coelacanth shape despite a higher taxonomical diversity, with the exceptions of the unusual Triassic *Rebellatrix divaricerca* Wendruff & Wilson, 2012 (Wendruff & Wilson 2012), *Foreyia maxkuhni* Cavin, Mennecart, Obrist, Costeur & Furrer, 2017 (Cavin *et al.* 2017), and *Rieppelia heinzfurreri* Ferrante & Cavin, 2023 (Ferrante & Cavin 2023). These departures from the "typical" coelacanth body-plan challenge the traditional portrayal of coelacanths as morphologically invariant.

The anatomy of the extant *Latimeria chalumnae* is among the best-known in vertebrates (e.g., Millot & Anthony 1958, 1965; Millot *et al.* 1978; Forey 1998; Amemiya *et al.* 2013; Cupello *et al.* 2017a, b; Dutel *et al.* 2019; Manuelli *et al.* 2023; Datovo & Johnson 2025). However, some important aspects of the anatomical and physiological evolution of coelacanths are still incompletely understood, especially those dealing with key internal structures of the skull such as the braincase (neurocranium) or the visceral skeleton (splanchnocranium). The visceral skeleton of gnathostomes (jawed vertebrates) is constituted of the mandibular arch (i.e., the jaws), followed by the hyoid arch and the subsequent branchial (or gill) arches, ventrally linked to the median basibranchial series, and as such it plays a major role in breathing and feeding (e.g., Nelson 1969; Janvier 1996; Dutel *et al.* 2013, 2015a). Nevertheless, despite a relatively rich fossil diversity, our knowledge on the morphology and evolution of the hyoid and branchial arches of coelacanths is extremely limited. This is caused by the poor preservation of many small elements forming the arches due to their weakly-ossified and presumed to be mainly cartilaginous nature. As such, the bones easily disarticulate after death and, when preserved, are found scattered and displaced from their original position. Unfortunately, three-dimensionally preserved Palaeozoic coelacanths are rare since many Devonian and Carboniferous coelacanths are usually preserved as fragmentary, flattened or highly compressed specimens, complicating the access to these important, but delicate internal features of the skull.

Here we describe a new three-dimensionally preserved coelacanth from the Late Carboniferous (Pennsylvanian) of Texas, United States, using micro-computed tomography (µCT). It exquisitely preserves the complete series of the hyoid and branchial arches as well as part of the skull roof, cheek, palate, braincase, and pectoral girdle. Through comparisons with other extinct and extant taxa, we reveal and discuss new evolutionary trends, shedding light on the anatomical organization and evolution of the skull of coelacanths.

MATERIAL AND METHODS

Locality and stratigraphic information

The specimen (AMNH FF 20686) is preserved in a phosphatic nodule from dark grey shale near the base of the Finis Shale Member, Graham Formation (Pennsylvanian age, early Virgilian corresponding to the early Gzhelian; Fig. 1). The hillside exposure, which contains a diverse fauna and plant remains, is the Lost Creek Lake emergency spillway (approximately 4.0 km northeast of Jacksboro, Texas and 1.5 km south of Texas Highway 59: American Museum of Natural History loc. 5562; Mapes loc. TXV-200: Jacksboro NE 71/2' quadrangle). The fossil specimen was recovered in a bed of phosphatic nodules and broken shell debris, which is interpreted as a storm deposit in a marine environment. The dark grey shale surrounding the specimen has yielded numerous other nodules containing a diverse calcified fauna, including vertebrates and cephalopods.

Specimen

The specimen (AMNH FF 20686; Fig. 2A-D) consists of a partial skull of a coelacanth including elements of the skull roof, cheek, hyoid and branchial arches, shoulder girdle, and a partially preserved braincase. Due to its preservation in a nodule, many osseous elements have not been subject to substantial crushing and are still in close articulation. The specimen measures approximately 5 cm in length and 4 cm at its widest width. It exposes certain dermal bones of the cheek and skull roof, evidenced by their tubercular ornamentation, as well as the basisphenoid and both palatoquadrates. Several elements from the hyobranchial skeleton, like the urohyal and both ceratohyals, are exposed as imprints on the lateral and ventral surfaces.

Micro-computed tomography scanning

The specimen (AMNH FF 20686; Fig. 2A-D) was scanned at the American Museum of Natural History (AMNH) in 2013 on a 2010 GE phoenix v|tome|x s240 high-resolution microfocus computed tomography system (General Electric, Fairfield, CT,

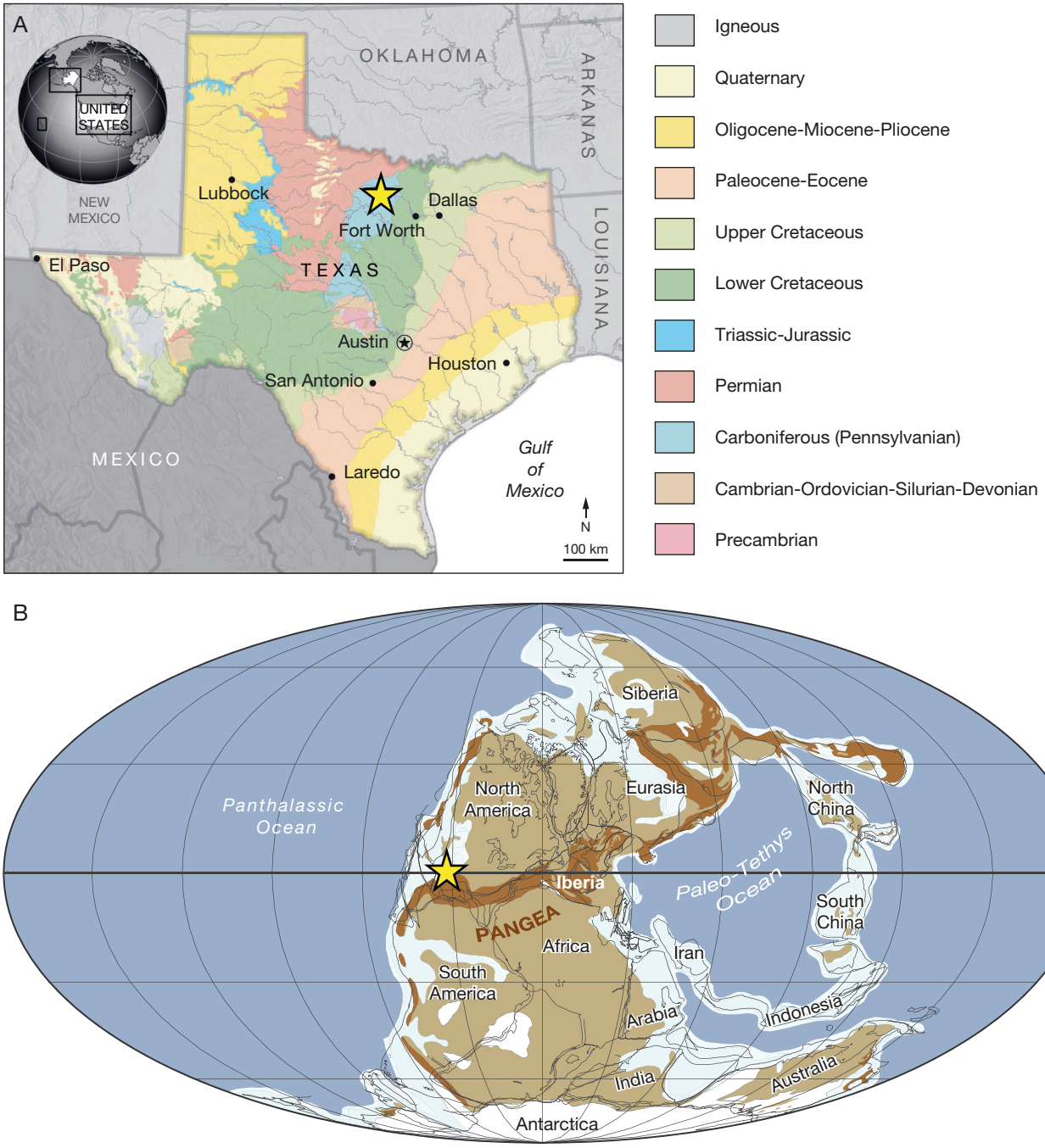

FIG. 1. — Geological and palaeogeographical context of *Aemilia stellata* n. gen., n. sp.; **yellow star** indicates locality: **A**, geological map of Texas (United States); **B**, palaeogeographical reconstruction of the latest Carboniferous-earliest Permian (Gzhelian-Asselian, 296-285 Ma). Credits: maps modified after Ferring (2007) (A) and Golonka (2000) (B).

United States), using a diamond target and 0.5 mm copper filter, at 100 kV, 120 µA, producing 1002 images with a voxel size of 0.01299285 mm. Image stacks were reconstructed using GE phoenix datos|x and FIJI software (Schindelin *et al.* 2012). Data were segmented manually in Mimics Innovation Suite V.18.0 (http://biomedical.materialise.com/mimics; Materialise, Leuven, Belgium). Meshes were exported as .ply files and rendered in Blender V.2.80 (http://www.blender.org; Blender Institute, Amsterdam, the Netherlands). Image stacks and .stl files are available in the Appendices 1 and 2.

ABBREVIATIONS

Institutional abbreviations

AMNH American Museum of Natural History, New York;
MHNG Muséum d'Histoire naturelle de Genève;
MNHN Muséum national d'Histoire naturelle, Paris.

Anatomical abbreviations

a.Cz anterior catazygal;
a.occ canal for the anterior branches of the occipital commissure;

a.w.Boc	anterior wings of the basioccipital;
art.Bb	articular surface for the basibranchial;
art.Cb1-4	articular surface for the first to fourth ceratobranchials;
art.Cb1	articular surface for the first ceratobranchial;
art.Cb2	articular surface for the second ceratobranchial;
art.Cb3	articular surface for the third ceratobranchial;
art.Cb4	articular surface for the fourth ceratobranchial;
art.Ch	articular surface for the ceratohyal;
art.Ch+Sy	articular surface for the ceratohyal and symplectic;
art.Eb1	articular surface for the first epibranchial;
art.Eb2	articular surface for the second epibranchial;
art.Ih	articular surface for the interhyal;
art.Ih+Sy	articular surface for the interhyal and symplectic;
art.pa.pr	articular facet for the putative parampullary process of the braincase;
art.Pro	articular facet for the prootic;
art.Rart	articular surface for the retroarticular;
art.Uh	articular surface for the urohyal;
Az	anazygal;
Bb	basibranchial;
bh.c	buccohypophysial canal;
Boc	basioccipital;
Bsph	basisphenoid;
c.a.br	canal for the branchial artery;
c.ju	jugular canal;
c.n.VII	canal for the otic ramus of the facial nerve;
c.v.ju	canal for the jugular vein;
Cb1.l	first left ceratobranchial;
Cb1.r	first right ceratobranchial;
Cb2.l	second left ceratobranchial;
Cb2.r	second right ceratobranchial;
Cb3.l	third left ceratobranchial;
Cb3.r	third right ceratobranchial;
Cb4.l	fourth left ceratobranchial;
Cb4.r	fourth right ceratobranchial;
Cb5.l	fifth left ceratobranchial;
Cb5.r	fifth right ceratobranchial;
Ch	ceratohyal;
Ch.l	left ceratohyal;
Ch.r	right ceratohyal;
Cl	cleithrum;
Cl.l	left cleithrum;
Cl.r	right cleithrum;
Cla	cavicle;
Cla.l	left clavicle;
Cla.r	right clavicle;
d.p.Pp	descending process of the postparietal;
ds	dorsum sellae;
Eb1	first epibranchial;
Eb2	second epibranchial;
Eb3	third epibranchial;
Eb4	fourth epibranchial;
Eb1.l	first left epibranchial;
Eb1.r	first right epibranchial;
Eb2.l	second left epibranchial;
Eb2.r	second right epibranchial;
Eb3.l	third left epibranchial;
Eb3.r	third right epibranchial;
Eb4.l	fourth left epibranchial;
Eb4.r	fourth right epibranchial;
Ecl	extracleithrum;
Ecl.l	left extracleithrum;
Ecl.r	right extracleithrum;
Ectp	ectopterygoid;
Entp	entopterygoid;
f	fang;
f.a.br	foramen for the branchial artery;
gr.a.br	groove for the branchial artery;
gr.car	groove for the carotid artery;
gr.Cb	ceratobranchial groove for the branchial artery;
gr.Entp	dorsal groove for the articulation with the entopterygoid;
gr.hyp	groove for the hypophysial canal;
gr.lig.pmh	groove for the posterior mandibulohyoid ligament;
gr.m.bc	groove for the basicranial muscle;
hyo.fac	hyomandibular facet;
Ib2.l	second left infrapharyngobranchial;
Ib2.r	second right infrapharyngobranchial;
Ih	interhyal;
Ih.l	left interhyal;
Ih.r	right interhyal;
iPb1	infrapharyngobranchial portion of the first pharyngobranchial;
lat.co	lateral commissure;
m.r.Uh	median ridge of the urohyal;
m.s	median suture;
m.w	medial wall;
n.c	notochordal canal;
ncp	notochordal pit;
oc	otic sensory canal;
op.lig	process for the attachment of the opercular ligament;
ot.ca	otic capsule;
ot.sh	otic shelf;
ov.Pp	overlapping facet for the postparietal;
ov.Ta	overlapping facet for the tabular;
p.Cz	posterior catazygal;
p.w.Pro	posterior wing of the prootic;
?Pb2	undetermined second infra- or suprapharyngobranchial;
?Pb.2.l	second left infra- or supraphrayngobranchial;
?Pb.2.r	second right infra- or supraphrayngobranchial;
po.a.occ	pores associated with the anterior branches of the occipital commissure;
po.oc	pores associated with the otic sensory canal;

Po.r	right postorbital;
po.sf	posterior shelf;
Pp	postparietals;
Pp.l	left postparietal;
Pp.r	right postparietal;
Pq.l	left palatoquadrate;
Pq.r	right palatoquadrate;
pr.con	processus connectens;
pre.e	prefacial eminence;
Pro.l	left prootic;
Pro.r	right prootic;
Psph	parasphenoid;
r.s	replacement socket;
re.sh	spiraculo-hyomandibalur recess;
Sb2.l	second left suprapharyngobranchial;
Sb2.r	second right suprapharyngobranchial;
Scc	scapulocoracoid;
Scc.l	left scapulocoracoid;
Scc.r	right scapulocoracoid;
So.l	left supraorbital;
So.r	right supraorbital;
sPb1	suprapharyngobranchial portion of the first pharyngobranchial;
sph.co	sphenoid condyles;
Sq.r	right squamosal;
Sy	symplectic;
Sy.l	left symplectic;
Sy.r	right symplectic;
t	teeth;
Ta	tabular;
Ta.l	left tabular;
Ta.r	right tabular;
Uh	urohyal;
v.fl.Ch	ventro-lateral flange of the ceratohyal.

PHYLOGENETIC ANALYSIS

The phylogenetic analysis was based on a modified version of the discrete matrix from Clement *et al.* (2024) composed of 268 characters and 90 species. Three coelacanth taxa were added to the original matrix and coded based on the published descriptions: *Rieppellia heinzfurreri* Ferrante & Cavin, 2023 (Ferrante & Cavin 2023), *Graulia branchiodonta* Manuelli, Mondéjar Fernández, Dollman, Jakata & Cavin, 2024 (Manuelli *et al.* 2024), and *Aemilia stellata* n. gen., n. sp. (this study). The matrix was modified in MorphoBank. Only 59 out of 268 characters could be coded for *Aemilia stellata* n. gen., n. sp., 45 of which are hyoid and branchial arches characters that are poorly known in most coelacanths. Of these codings, 30 are plesiomorphic conditions, while 29 are apomorphic conditions.

A few codings were modified from the original matrix of Clement *et al.* (2024). The coding of character 82 for *Graulia branchiodonta* was based on the CT-scan rendering that shows the presence of the postorbital limb of the lacrimojugal (Manuelli *et al.* 2024: figs 5, 10A, B); however, the reconstruction of *G. branchiodonta* (Manuelli *et al.* 2024: figs 5, 10A, B) does not show a clear postorbital limb. The coding of characters 207(0), 245(1), and 247(0) for *Macropomoides orientalis* Woodward, 1942 was completed from new observations on specimens from the Oishi Fossils Gallery of the Mizuta Memorial Museum of Tokyo, Japan (RC, pers. observ.). The coding of character 29 for *Ngamugawi wirngarri* was corrected to correspond to the apomorphic condition in which the postparietal is fused to the tabular (as described in Clement *et al.* 2024). We added a new apomorphic character-state for character 60 to take into account the condition of the lateral rostral of *Rieppelia heinzfurreri*: elongated vertically (length/height ratio < 1). Ferrante & Cavin (2023) described a one-to-two ratio between the radials and the lepidotrichia based on the numerous lepidotrichia identified in the caudal fin of *R. heinzfurreri*. However, after careful examination (JMF) and discussions with C. Ferrante, we consider that the hemilepidotrichia were incorrectly identified as lepidotrichia, and thus the total amount of lepidotrichia (formed of two symmetrical hemilepidotrichia) is half of what was originally identified. Thus, the caudal fin of *R. heinzfurreri* shows a one-to-one ratio between its radials and the lepidotriochia (character 54; character 106 of Ferrante & Cavin [2023, 2025]). Finally, the definition of character 56 of Clement *et al.* (2024) (size of sensory pores [Forey 1991: char. 38]) was modified to: pores on ethmosphenoid shield similar to postparietal shield pores (0), pores on ethmosphenoid shield larger than postparietal shield pores (1).

The stratigraphic information (first and last appearance dates, FAD and LAD, respectively) used for the tip-dating analysis of *Aemilia stellata* n. gen., n. sp. and *Graulia branchiodonta* (Manuelli *et al.* 2024) corresponds to the standards used by Clement *et al.* (2024: SI). The FAD and LAD of *Rieppelia heinzfurreri* correspond to the error on the dating (242.1 +/- 0.6) provided in figure 1 of Ferrante & Cavin (2023). The outgroup for the analyses is represented by five species of Onychodontida Andrews, 1973 from the Devonian.

Parsimony analysis

We performed a parsimony analysis using TNT 1.6 (Goloboff & Morales 2023) using the New Traditionnal Search with Ratchet and Drift. We added ten initial sequences and set the parameters to find minimum length at least ten times. The analysis produced 34 equally parsimonious trees with a score of 1335. We also performed 1000 bootstrap replications. All the results are available in the Appendix 3.

Bayesian tip-dating

We performed Bayesian tip-dated phylogenetic analyses using BEAST 2.7.7 (Bouckaert *et al.* 2019). This approach was particularly suitable given the extensive missing data in *Aemilia stellata* n. gen., n. sp., which precluded a reliable parsimony analysis but could be appropriately handled within a Bayesian framework. The most appropriate tree prior was the fossilized birth-death (FBD) model, implemented in the FBD package for BEAST 2 (Heath *et al.* 2014).

We also conducted a complementary analysis using the Birth Death Skyline (BDSKY) model (Stadler *et al.* 2013), which produced similar topologies (see Appendix 3). Both analyses employed an optimized relaxed clock model, and Markov Chain Monte Carlo (MCMC) sampling as implemented in BEAST 2. We used coupled MCMC with four chains, which yielded consistent and converging results. Output log files were inspected using Tracer 1.7.2 (Rambaut *et al.* 2018), confirming robust parameter estimates with high effective sample sizes (ESS) (see .log files in the Appendix 3). The final tree was summarized using the Maximum Clade Credibility (MCC) approach with median node heights, via TreeAnnotator (from the BEAST 2 package), and visualized using FigTree 1.4.4 (Rambaut 2018).

SYSTEMATIC PALEONTOLOGY

Class OSTEICHTHYES Huxley, 1880
Subclass SARCOPTERYGII Romer, 1955
Infraclass ACTINISTIA Cope, 1871
Order COELACANTHIFORMES Huxley, 1861, *sensu* Forey (1998)
Family incertae sedis

Genus *Aemilia* n. gen.

urn:lsid:zoobank.org:act:7407645D-1643-4B4E-ADCE-FF29C837CC56

ETYMOLOGY. — *Aemilia* from the Latin *aemulus* meaning emulate, referencing the completeness of its hyobranchial skeleton, rivalling with that of the extant *Latimeria.*

TYPE SPECIES. — *Aemilia stellata* n. sp.

DIAGNOSIS. — Same as for the type species, by monotypy.

Aemilia stellata n. gen., n. sp.
(Figs 2-13)

urn:lsid:zoobank.org:act:15405ABA-87C4-4D88-9209-2A6C8DB118C4

TYPE MATERIAL. — **Holotype. United States** • Texas, Jack County, northeast of Jacksboro, TXV 200 Mapes locality; AMNH FF 20686, nodule comprising a partially preserved braincase and associated elements of the skull roof, cheek, hyoid and branchial arches, and shoulder girdle in close articulation (Fig. 2A-D).

ETYMOLOGY. — *stellata* from the Latin *stella* meaning star, referencing the Lone Star State of Texas (United States) where the specimen was found.

DIAGNOSIS. — Coelacanth characterized by the following unique association of characters: descending process in the form of a longitudinal ridge on the ventral surface of the postparietal; presence of pores on the posterior margin of the postparietal corresponding to anterior branches of the occipital commissure from the median extrascapular; squamosal and postorbital ornamented with pointed tubercles; dentition of the ectopterygoid composed of a single row of small teeth and a large fang; braincase composed of separate ossifications (parasphenoid, basisphenoid, prootics, and basioccipital); buccohypophysial canal open on the parasphenoid; prominent prefacial eminence on the prootic; presence of a postero-dorsal process on the prootic for the contact with the tabular; complex suture between the prootic and the basioccipital; cleithrum and extracleithrum ornamented with tubercles; fully ossified boomerang-shaped first pharyngobranchial; fully ossified fourth epibranchial.

TYPE LOCALITY. — United States, Texas, Jack County, northeast of Jacksboro, TXV 200 Mapes locality.

TYPE HORIZON AND AGE. — Finis Shale member, Graham Formation, Cisco Group, Lower Gzhelian (Virgilian), Upper Carboniferous (Pennsylvanian).

DESCRIPTION

Dermal skull

The dermocranium is only poorly represented and comprises parts of the skull roof (postparietals, tabulars, and possible supraorbitals) and the cheek (postorbital, squamosal).

Skull roof

Postparietal. The two postparietals (Pp; Figs 2E; 3E, H; 5A-D) are broad and overall flattened bones but are poorly preserved, lacking most of their anterior and lateral margins; only the medial margin displaying a straight median suture (m.s; Fig. 5B, D) and the posterior margin of the right element can be identified confidently. The inner surface is smooth and otherwise featureless, but a reduced descending process (d.p.Pp; Fig. 5D) in the form of a longitudinal ridge is present on the left postparietal, running diagonally across the anterior portion of the bone. The course of the otic canal on the antero-lateral margin cannot be reconstructed. The presence of pores in the posterior portion of both postparietals (po.a.occ; Fig. 5B) are associated with anterior branches of the occipital commissure (corresponding to the supratemporal commissure).

Tabular. The two disarticulated tabulars (Ta; Figs 2E; 3E, H; 5A-D; corresponding to the supratemporal of Forey 1998) are preserved; the right one (Ta.r; Figs 2E; 3E, H; 5F, H) is fairly complete, whereas the left one (Ta.l; Figs 3E, H) is only represented by a small portion of a canal-bearing process. The exposed surface of the right tabular is densely pitted and pierced by large pores associated with the trajectory of the otic sensory canal (po.oc; Fig. 5F). The medial and lateral margins display articulation surfaces for the adjoining bones in the form of depressed smooth flanges separated from the elevated exposed and ornamented surface of the bone. The lateral margin shows ventrally a moderate process, probably for the attachment of the opercular ligament (op.lig; Fig. 5F, H) as in *Latimeria chalumnae* and other fossil coelacanths (Forey 1998). The posterior margin carries a small shelf (po. sf; Fig. 5F) projecting postero-ventrally with a distinctive concave, oval depression, certainly for the articulation of a convex process of the unpreserved lateral extrascapular. The ventral surface is smooth, and no distinctive ventral process has been identified. The otic canal (oc; Fig. 5F, H) penetrates

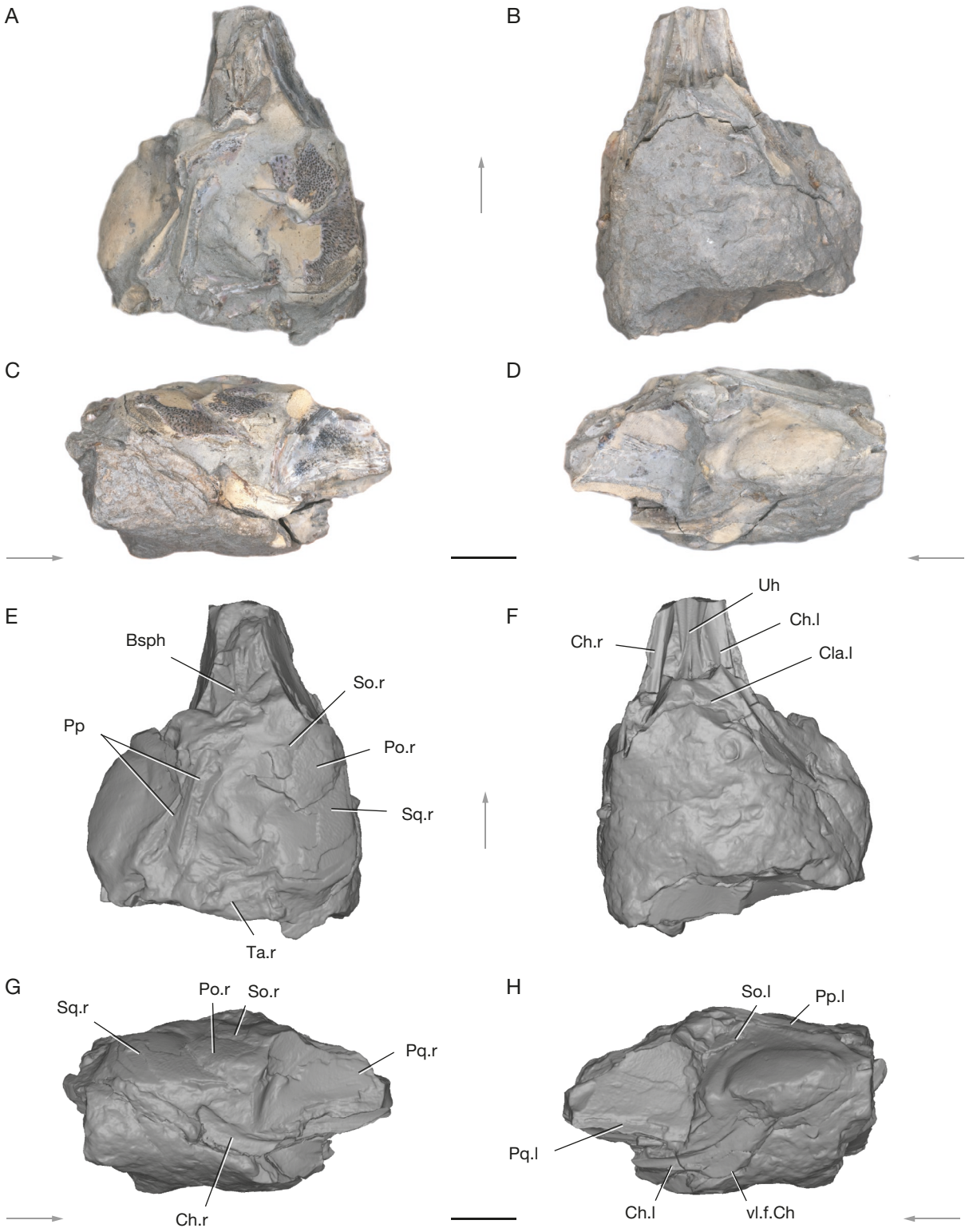

Fig. 2. — Fossil nodule specimen of *Aemilia stellata* n. gen., n. sp. (AMNH FF 20686) (**A**-**D**) and virtual render of the surface (**E**-**H**) in dorsal (**A**, **E**), ventral (**B**, **F**), lateral right (**C**, **G**) and lateral left (**D**, **H**) views. Abbreviations: **Bsph**, basisphenoid; **Ch.l**, left ceratohyal; **Ch.r**, right ceratohyal; **Cla.l**, left clavicle; **Po.r**, right postorbital; **Pp**, postparietals; **Pp.l**, left postparietal; **Pq.l**, left palatoquadrate; **Pq.r**, right palatoquadrate; **So.r**, right supraorbital; **Sq.r**, right squamosal; **Ta.r**, right tabular; **Uh**, urohyal; **vl.f.Ch**, ventrolateral flange of the ceratohyal. **Arrows** point anteriorly. Scale bars: 10 mm. Credits: photos by Alan Pradel.

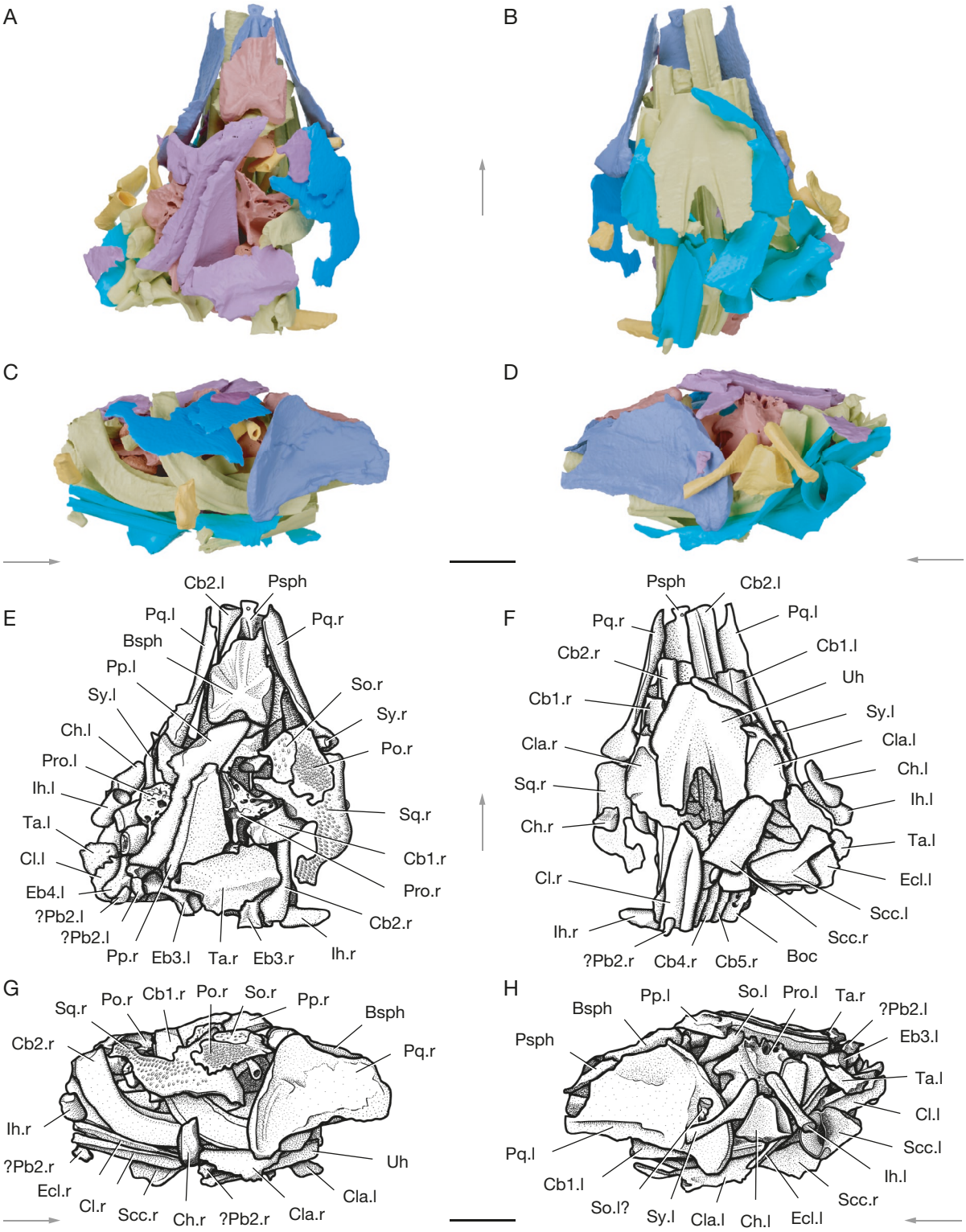

FIG. 3. — Preserved bones inside of the nodule of *Aemilia stellata* n. gen., n. sp. (AMNH FF 20686). Virtual renders (**A**-**D**) and interpretative drawings (**E**-**H**) in dorsal (**A**, **E**), ventral (**B**, **F**), lateral right (**C**, **G**) and lateral left (**D**, **H**) views. Color legend: **blue**, cheek; **golden**, hyoid arch; **light blue**, lower jaw; **light green**, opercular series; **maroon**, skull roof; **pink**, neurocranium; **purple**, palate; **turquoise**, pectoral girdle; **yellow**, branchial arches. Abbreviations: **Bsph**, basisphenoid; **Cb1.l**, first left ceratobranchial; **Cb1.r**, first right ceratobranchial; **Cb2.l**, second left ceratobranchial; **Cb2.r**, second right ceratobranchial; **Cb4.r**, fourth right ceratobranchial; **Cb5.r**, fifth right ceratobranchial; **Ch.l**, left ceratohyal; **Ch.r**, right ceratohyal; **Cl.l**, left cleithrum; **Cl.r**, right cleithrum; **Cla.l**, left clavicle; **Cla.r**, right clavicle; **Eb3.l**, third left epibranchial; **Eb3.r**, third right epibranchial; **Eb4.l**, fourth left epibranchial; **Ecl.l**, left extracleithrum; **Ecl.r**, right extracleithrum; **Ih.l**, left interhyal; **Ih.r**, right interhyal; **?Pb.2**, **l**, second left infra- or supraphrayngobranchial; **Po.r**, right postorbital; **Pp.l**, left postparietal; **Pp.r**, right postparietal; **Pq.l**, left palatoquadrate; **Pq.r**, right palatoquadrate; **Pro.l**, left prootic; **Pro.r**, right prootic; **Psph**, parasphenoid; **Scc.l**, left scapulocoracoid; **Scc.r**, right scapulocoracoid; **So.l**, left supraorbital; **So.r**, right supraorbital; **Sq.r**, right squamosal; **Sy.l**, left symplectic; **Sy.r**, right symplectic; **Ta.l**, left tabular; **Ta.r**, right tabular; **Uh**, urohyal. **Arrows** point anteriorly. Scale bars: 10 mm. Credits: 3D models and drawings made by Jorge Mondéjar Fernández.

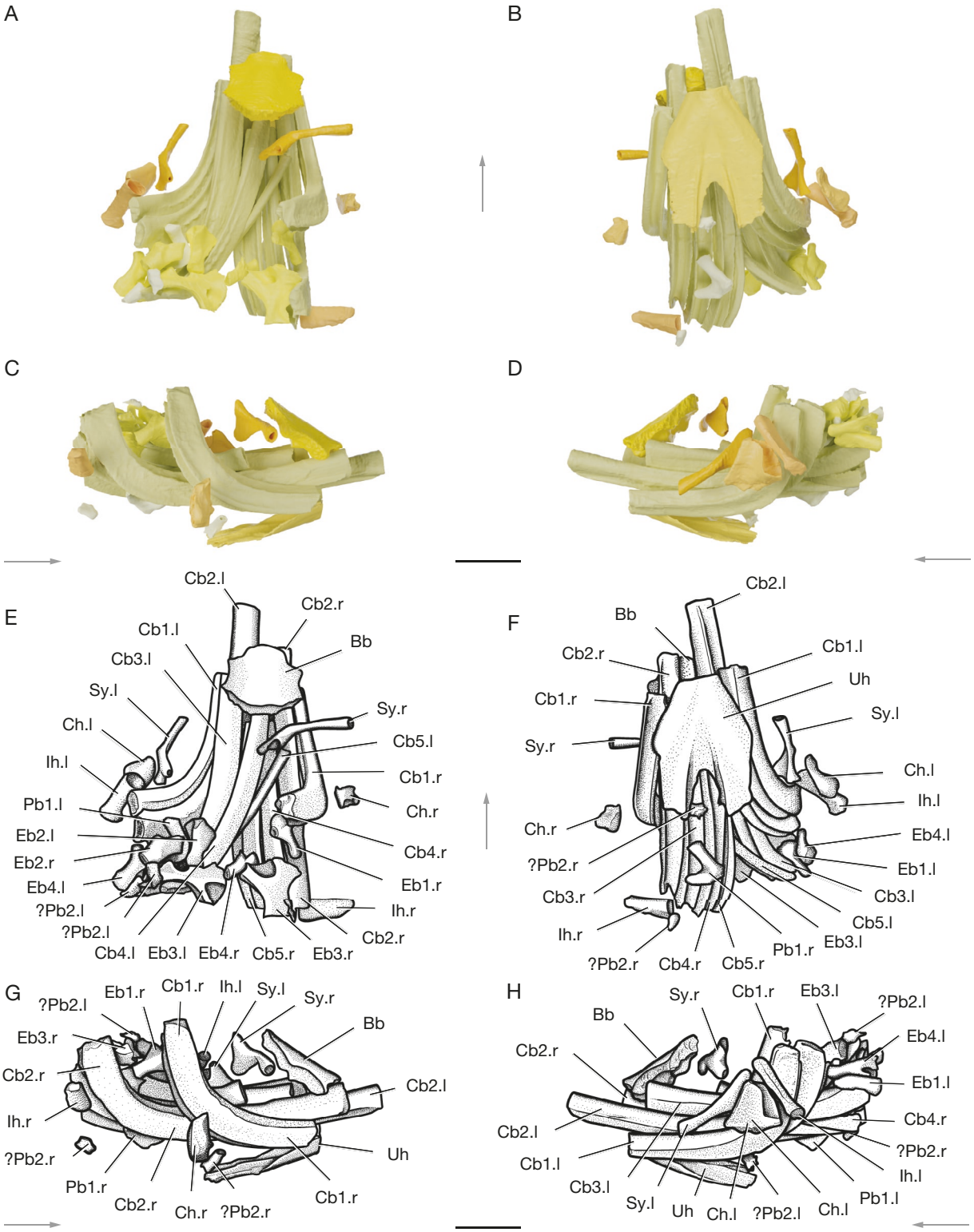

Fig. 4. — Hyobranchial skeleleton of *Aemilia stellata stellata* n. gen., n. sp. (AMNH FF 20686). Virtual renders (**A**-**D**) and interpretative drawings (**E**-**H**) in dorsal (**A**, **E**), ventral (**B**, **F**), lateral right (**C**, **G**) and lateral left (**D**, **H**) views. Abbreviations: **Bb**, basibranchial; **Cb1.l**, first left ceratobranchial; **Cb1.r**, first right ceratobranchial; **Cb2.l**, second left ceratobranchial; **Cb2.r**, second right ceratobranchial; **Cb3.l**, third left ceratobranchial; **Cb3.r**, third right ceratobranchial; **Cb4.l**, fourth left ceratobranchial; **Cb4.r**, fourth right ceratobranchial; **Cb5.l**, fifth left ceratobranchial; **Cb5.r**, fifth right ceratobranchial; **Ch.l**, left ceratohyal; **Ch.r**, right ceratohyal; **Eb1.l**, first left epibranchial; **Eb1.r**, first right epibranchial; **Eb2.l**, second left epibranchial; **Eb2.r**, second right epibranchial; **Eb3.l**, third left epibranchial; **Eb3.r**, third right epibranchial; **Eb4.l**, fourth left epibranchial; **Eb4.r**, fourth right epibranchial; **Ih.l**, left interhyal; **Ih.r**, right interhyal; **?Pb.2.l**, second left infra- or suprapharyngobranchial; **?Pb.2.r**, second right infra- or supraphrayngobranchial; **Sy.l**, left symplectic; **Sy.r**, right symplectic. **Arrows** point anteriorly. Scale bars: 10 mm. Credits: 3D models and drawings made by Jorge Mondéjar Fernández.

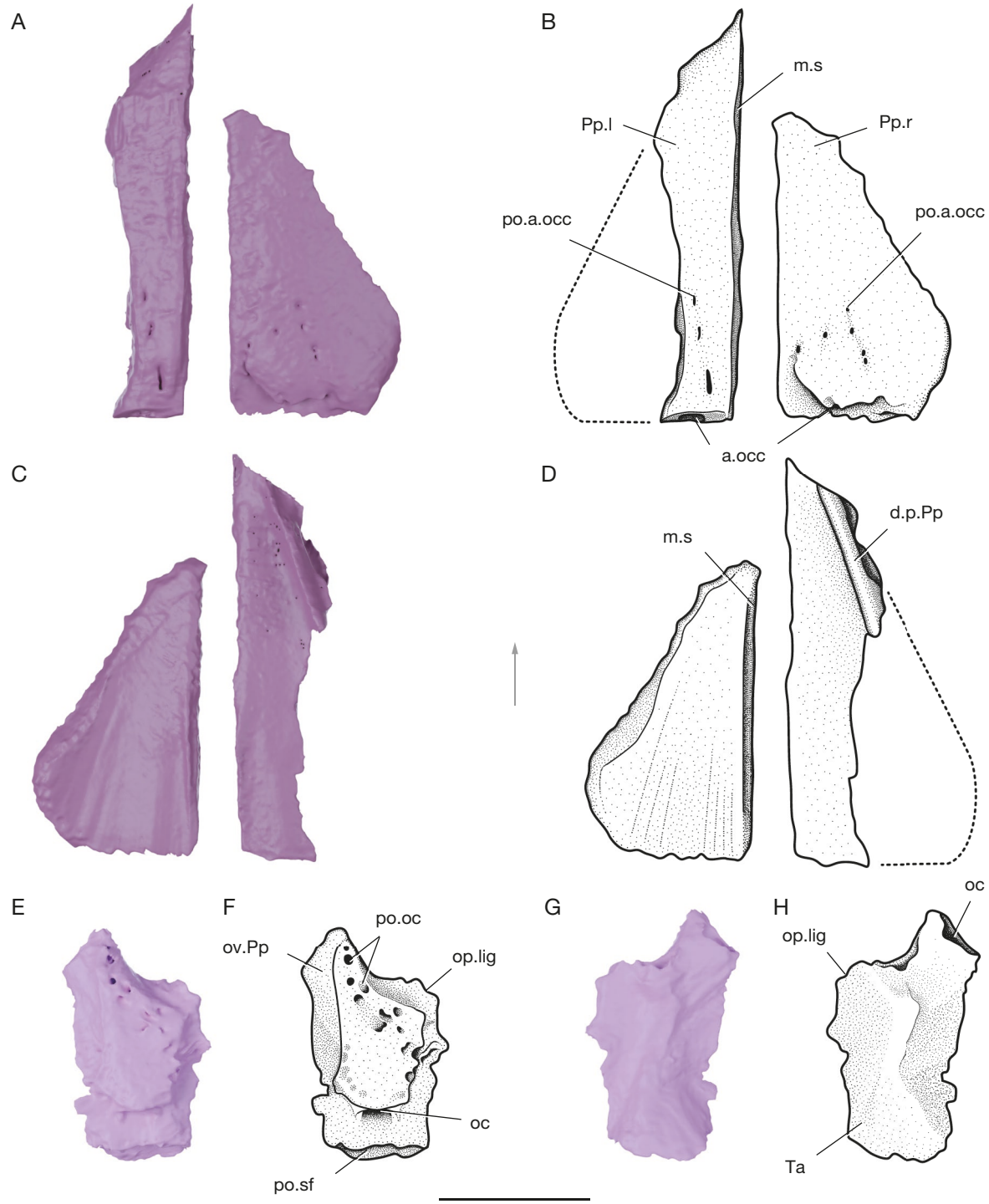

FIG. 5. — Skull roof of *Aemilia stellata* n. gen., n. sp. (AMNH FF 20686). Virtual renders (**A**, **C**, **E**, **G**) and interpretative drawings (**B**, **D**, **F**, **H**) in dorsal (**A**, **E**) and ventral (**C**, **G**) views. Abbreviations: **a.occ**, canal for the anterior branches of the occipital commissure; **d.p.Pp**, descending process of the postparietal; **m.s**, median suture; **oc**, otic sensory canal; **op.lig**, process for the attachment of the opercular ligament; **ov.Pp**, overlapping facet for the postparietal; **ov.Ta**, overlapping facet for the tabular; **po.a.occ**, pores associated with the anterior branches of the occipital commissure; **po.oc**, pores associated with the otic sensory canal; **po.sf**, posterior shelf; **Pp.l**, left postparietal; **Pp.r**, right postparietal; **Ta**, tabular. **Arrows** point anteriorly. Scale bar: 10 mm. Credits: 3D models and drawings made by Jorge Mondéjar Fernández.

the tabular through an antero-medial process and exits posteriorly through a large single opening. There is no evidence of a triple junction of the otic, occipital commissure and main lateral line canals in the tabular, which most probably occurred in the lateral extrascapular.

Supraorbitals. A small bony element, ornamented with sparse rounded tubercles, lies dorsal to the postorbital on the right side of the specimen. Given its small size and ornamentation, it is similar to a spiracular (corresponding to the postspiracular of other sarcopterygians). However, it

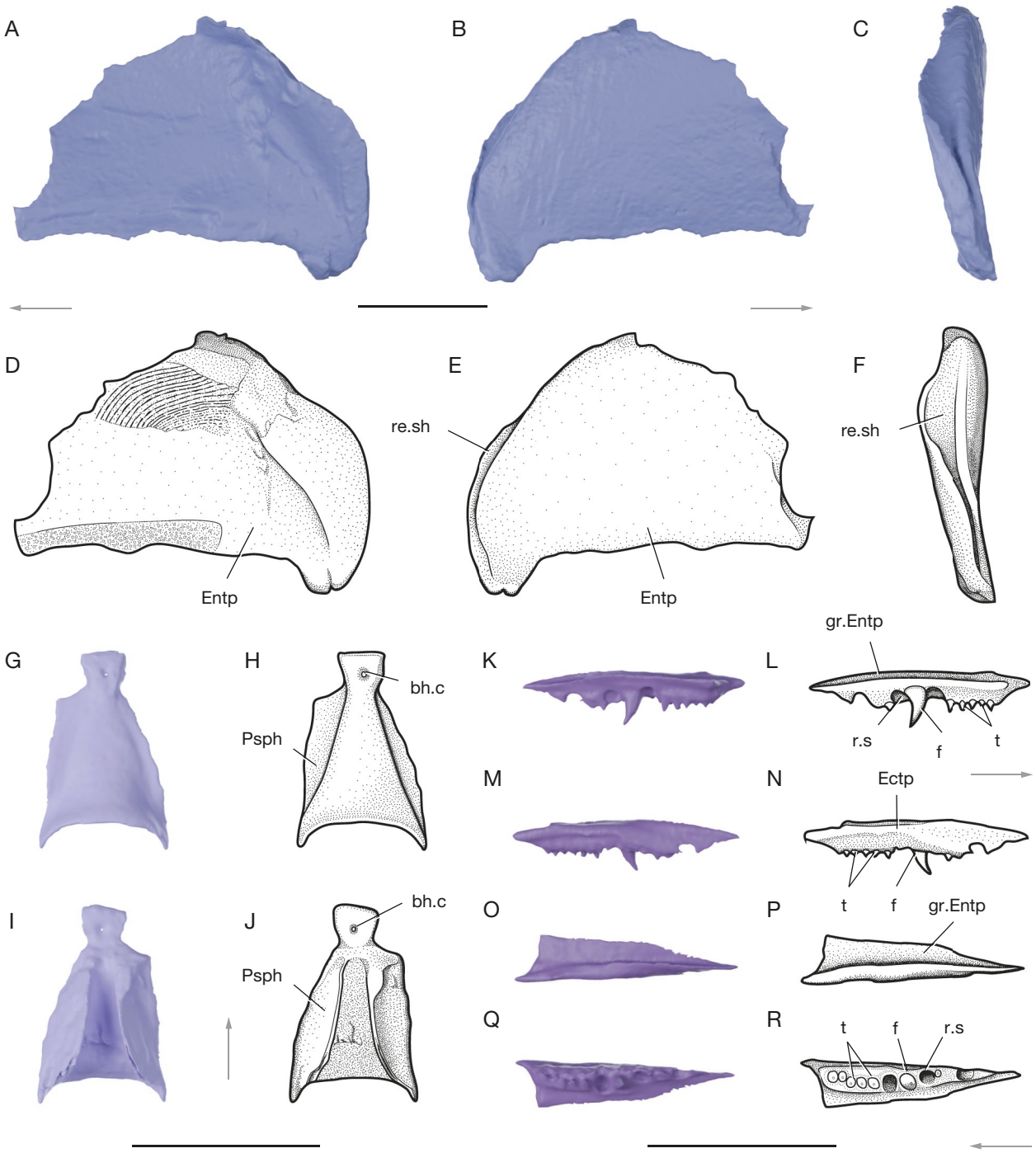

FIG. 6. — Palate of *Aemilia stellata* n. gen., n. sp. (AMNH FF 20686): **A**-**F**, left palatoquadrate complex: virtual renders (**A**-**C**) and interpretative drawings (**D**-**F**) in lateral (**A**, **D**), medial (**B**, **E**) and posterior (**C**, **F**) views**;** **G**-**J**: parasphenoid: virtual renders (**GI**,) and interpretative drawings (**H**, **J**) in ventral (**G**, **H**) and dorsal (**I**, **J**) views; **K**-**R**, left ectopterygoid: virtual renders (**K**, **M**, **O**, **Q**,) and interpretative drawings (**L**, **N**, **P**, **R**) in lateral (**A**, **D**), medial (**B**, **E**) and posterior (**C**, **F**) views. Abbreviations: **bh.c**, buccohypophysial canal; **Ectp**, ectopterygoid; **Entp**, entopterygoid; **f**, fang; **gr.Entp**, dorsal groove for the articulation with the entopterygoid; **Psph**, parasphenoid; **r.s**, replacement socket; **re.sh**, spiraculo-hyomandibalur recess; **t**, teeth. **Arrows** point anteriorly (**A**-**D**, **G**-**J**, **K**-**L**, **M**-**R**). Scale bars: 10 mm. Credits: 3D models and drawings made by Jorge Mondéjar Fernández.

carries a well-developed canal visible in internal view and thus it may correspond to the posteriormost supraorbital bone (So.r; Figs 2E, G; 3E, H). A similar element lies on the left side of the specimen (So.l; Figs 2H; 3E, H), it is a small ossification with an enlarged middle section, probably for the course of the supraorbital sensory canal. However, as opposed to the one on the right side, the left element is not ornamented, possibly due to a greater erosion of the left side of the fossil nodule. Several small, ossified elements displaced from their original position are located between the branchial arches, but are not visible in the figures (see Appendix 2). They are roughly square

elements, usually pierced by pores related to a possible internal canal and display dorsal and ventral gutters. We tentatively assign them to the supraorbital series due to their similarity with the supraorbitals of *Graulia branchiodonta* (Manuelli *et al.* 2024).

Cheek

Postorbital. The right postorbital (Po.r; Figs 2E, G; 3E, G) is incompletely preserved, slightly displaced from its original position and overlapping the antero-ventral portion of the squamosal. The preserved fragment is roughly triangular and does not show any trace of a lateral sensory canal, usually found in the anterior most region, suggesting that the bone lacks the anterior portion and was quite large posteriorly. The external surface is profusely ornamented by rounded to pointed tubercles.

Squamosal. The right squamosal (Sq.r; Figs 2E, G, 3E-G) is the largest bone retrieved from the cheek; however, it is incompletely preserved. The external surface is richly ornamented with tubercles, more elongate and antero-posteriorly oriented dorsally, and more rounded ventrally. The internal surface displays a prominent canal for the horizontal course of the jugal canal. The ventral margin shows an overlapping facet for a putative preopercular.

Palate

Several elements of the palate have been identified: both palatoquadrates, a left ectopterygoid, and the parasphenoid.

Palatoquadrate. The palatoquadrate complex (Pq; Figs 2G, H; 3E-H) is a single ossification, roughly triangular in shape, comprising both dermal (entopterygoid) and endoskeletal (quadrate and metapterygoid) elements. Only the entopterygoids appear to be preserved and no distinctive autopalatines have been found.

Entopterygoid. Both entopterygoids (Entp; Fig. 6D, E) are almost entirely preserved, only the anterior most portion is missing. The lingual side is slightly concave, covered in a shagreen of small denticles arranged in concentric lines following the postero-dorsal margins of the bone (Fig. 2C, D). In posterior view, a groove on the postero-dorsal margin corresponds to the spiraculo-hyomandibular recess (re.sh; Fig. 6E, F). The ventral margin of the anterior projection is straight and carries a narrow antero-posterior depression, likely for the contact with the lingual lamina of the ectopterygoid. The postero-ventral corner displays a ventral projection probably fitting inside a groove for the articulation with the unpreserved quadrate.

Ectopterygoid. The right ectopterygoid (Ectp; Fig. 6L, N, P, Q) is elongate, triangular in dorsal view, carrying teeth on a horizontal lamina close to the labial side. Its small size may result from a lack of preservation of its most anterior portion. The dentition is organised into a single row of small teeth (t; Fig. 6L, N, R) associated with a large, pointed, posteriorly recurved fang (f; Fig. 6L, N, R), flanked by two replacement sockets (r.s; Fig. 6L, N, R). The dorsal surface carries a deep groove for the articulation with the ventral margin of the anterior projection of the entopterygoid (gr. Entp; Fig. 6L, P).

Parasphenoid. The parasphenoid (Psph; Figs 3E, F, H; 6H, J; 9A-E) is only partially preserved posteriorly; the anterior denticulated section is missing. The ventral surface is convex and displays an hour-glass-shaped median section that broadens posteriorly. The dorsal surface is open, composed of two laterally depressed flanges delimiting a median furrow between their parallel ridges. The posterior margin is broad and comprises a deep pit to accommodate the anterior expansion of the basisphenoid, dorsally articulating with the latter. A foramen in the anterior extremity of the preserved section of the parasphenoid indicates that the buccohypophysial canal (bh.c; Figs 3E, F, H; 6H, J) was open.

Braincase

Numerous endoskeletal elements of the neurocranium have been preserved and include: the basisphenoid, basioccipital, and the paired prootics. The zygal series comprises the anazygal, and the anterior and posterior catazygals. The separate ossifications of the parasphenoid, basisphenoid, prootics, and basioccipital confirm that the braincase was not ossified as a single unit. No supraoccipital or exoccipitals have been found.

Basisphenoid. The basisphenoid (Bsph; Figs 2E, H; 3E, H, 7B, D; 9A-E) is incompletely preserved, with its dorsal surface exposed in the nodule. The paired *processus connectens* (pr.con; Fig. 7B) are mildly developed as blunt, elongate, and anteriorly tapering lateral margins; they did not contact the parasphenoid and were certainly capped by large cartilage pads to articulate with the otic shelves of the prootics. The antero-lateral margins of the basisphenoid are broken with only the broad proximal portion of the antotic processes being preserved. A pair of sphenoid condyles (sph.co; Fig. 7B,D) are well developed posteriorly and separated by a gap to articulate with the anazygal. The *dorsum sellae* (ds; Fig. 7B) forms the elevated merging surface between two triangular slight depressions dorsal to the *processus connectens* laterally and the sphenoid condyles posteriorly. Anterior to the *dorsum sellae*, two thin parallel ridges frame a narrow groove likely for the course of the hypophysial canal (gr.hyp; Fig. 7B). In ventral view, a large notochordal pit (ncp; Fig. 7D) is anteriorly bordered by a small ridge and laterally by the ventral edge of the *processus connectens*. Anterior to it, two lateral deep notches, seemingly converging anteriorly, mark the trajectory of the internal carotid arteries (gr.car; Fig. 7D). No distinct foramina can be reconstructed suggesting that the oculomotor (III) and profundus (V1) nerves left the cranial cavity anterior to the basisphenoid. There is no evidence of a basipterygoid nor of a suprapterygoid process.

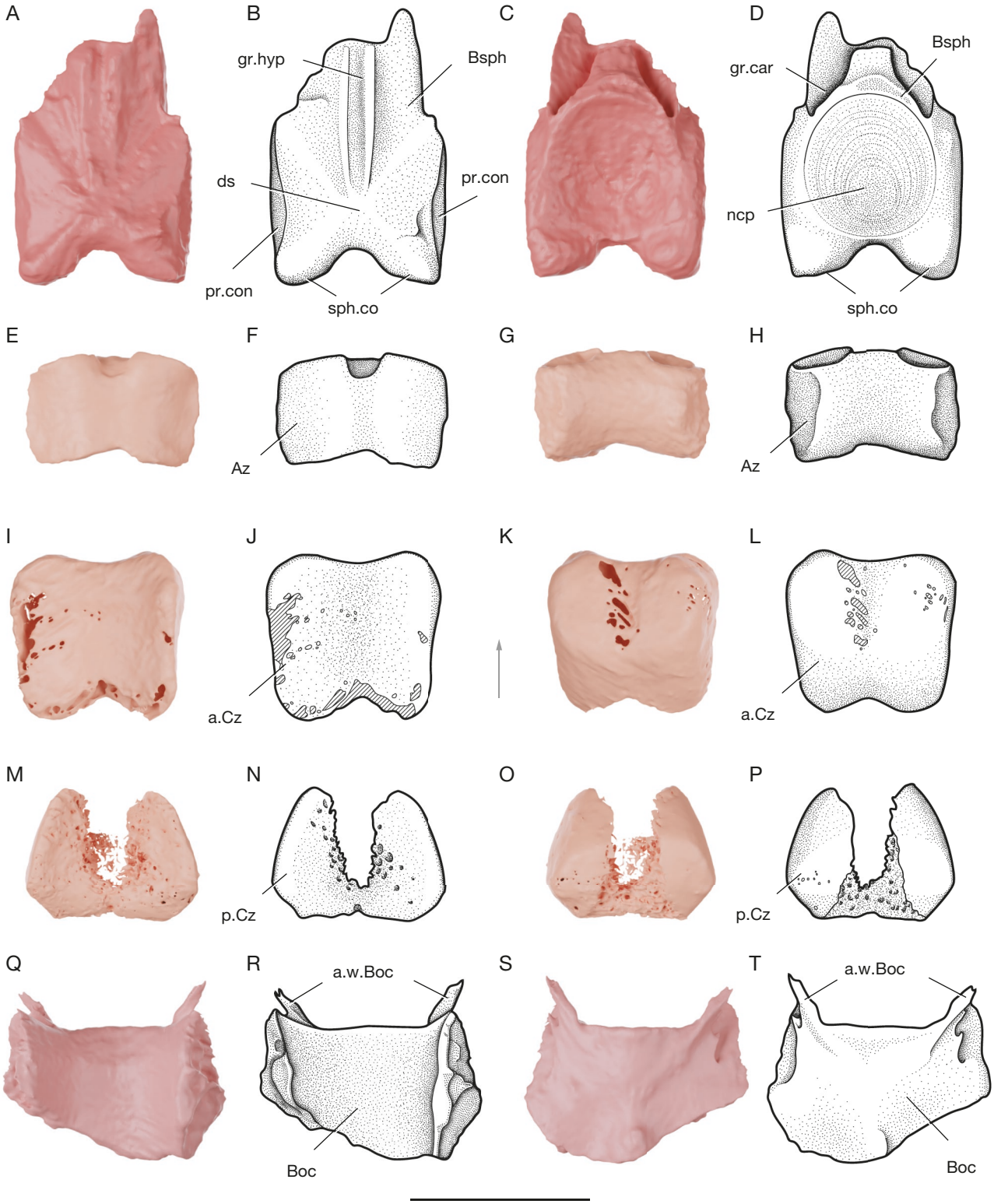

FIG. 7. — Braincase of *Aemilia stellata* n. gen., n. sp. (AMNH FF 20686): **A**-**D**, basisphenoid:virtual renders (**A**, **C**) and interpretative drawings (**B**, **D**) in dorsal (**A**, **B**) and ventral (**C**, **D**) views; **E**-**H**, anazygal: virtual renders (**E**, **G**) and interpretative drawings (**F**, **H**) in dorsal (**E**-**F**) and ventral (**G**-**H**) views. **I**-**P.** Catazygal series: virtual renders of the anterior catazygal (**I**, **K**) and posterior catazygal (**M**, **O**) and interpretative drawings (**J**, **L**; **N**, **P**) in dorsal (**I**-**J; M**-**N**) and ventral (**K**-**L; O**-**P**) views. **Q**-**T.** Basioccipital: virtual renders (**Q**, **S**) and interpretative drawings (**R**, **T**) in dorsal (**Q**-**R**) and ventral (**S**-**T**) views**.** Abbreviations: **a.Cz**, anterior catazygal; **a.w.Boc**, anterior wings of the basioccipital; **Az**, anazygal; **Boc**, basioccipital; **Bsph**, basisphenoid; **ds**, dorsum sellae; **gr.car**, groove for the carotid artery; **gr.hyp**, groove for the hypophysial canal; **ncp**, notochordal pit; **p.Cz**, posterior catazygal; **pr.con**, processus connectens; **sph.co**, sphenoid condyles. **Arrow** points anteriorly. Scale bar: 10 mm. Credits: 3D models and drawings made by Jorge Mondéjar Fernández.

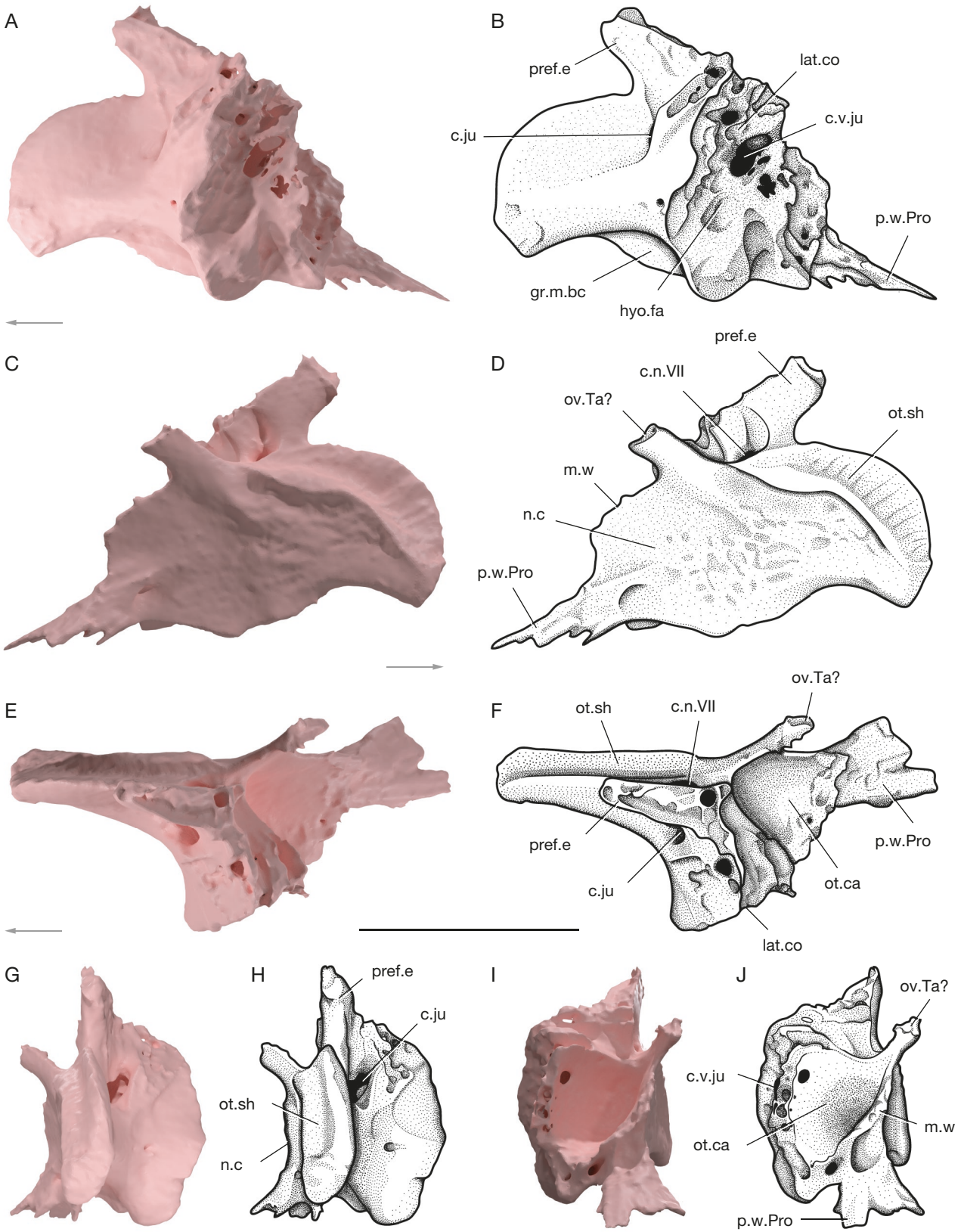

FIG. 8. — Braincase of *Aemilia stellata* n. gen., n. sp. (AMNH FF 20686): **A**-**J**, left prootic: virtual renders (**A**, **C**, **E**, **G**, **I**) and interpretative drawings (**B**, **D**, **F**, **H**, **J**) in lateral (**A**, **B**), medial (**C**, **D**), dorsal (**E**, **F**), anterior (**G**, **H**), and posterior (**I**, **J**) views. Abbreviations: **c.ju**, jugular canal; **c.n.VII**, canal for the otic ramus of the facial nerve; **c.v.ju**, canal for the jugular vein; **gr.m.bc**, groove for the basicranial muscle; **hyo.fac**, hyomandibular facet; **lat.co**, lateral commissure; **m.w**, medial wall; **n.c**, notochordal canal; **ot.ca**, otic capsule; **ot.sh**, otic shelf; **ov.Ta?**, overlapping facet for the tabular; **p.w.Pro**, posterior wing of the prootic; **pre.e**, prefacial eminence. **Arrows** point anteriorly (**A**-**F**). Scale bar: 10 mm. Credits: 3D models and drawings made by Jorge Mondéjar Fernández.

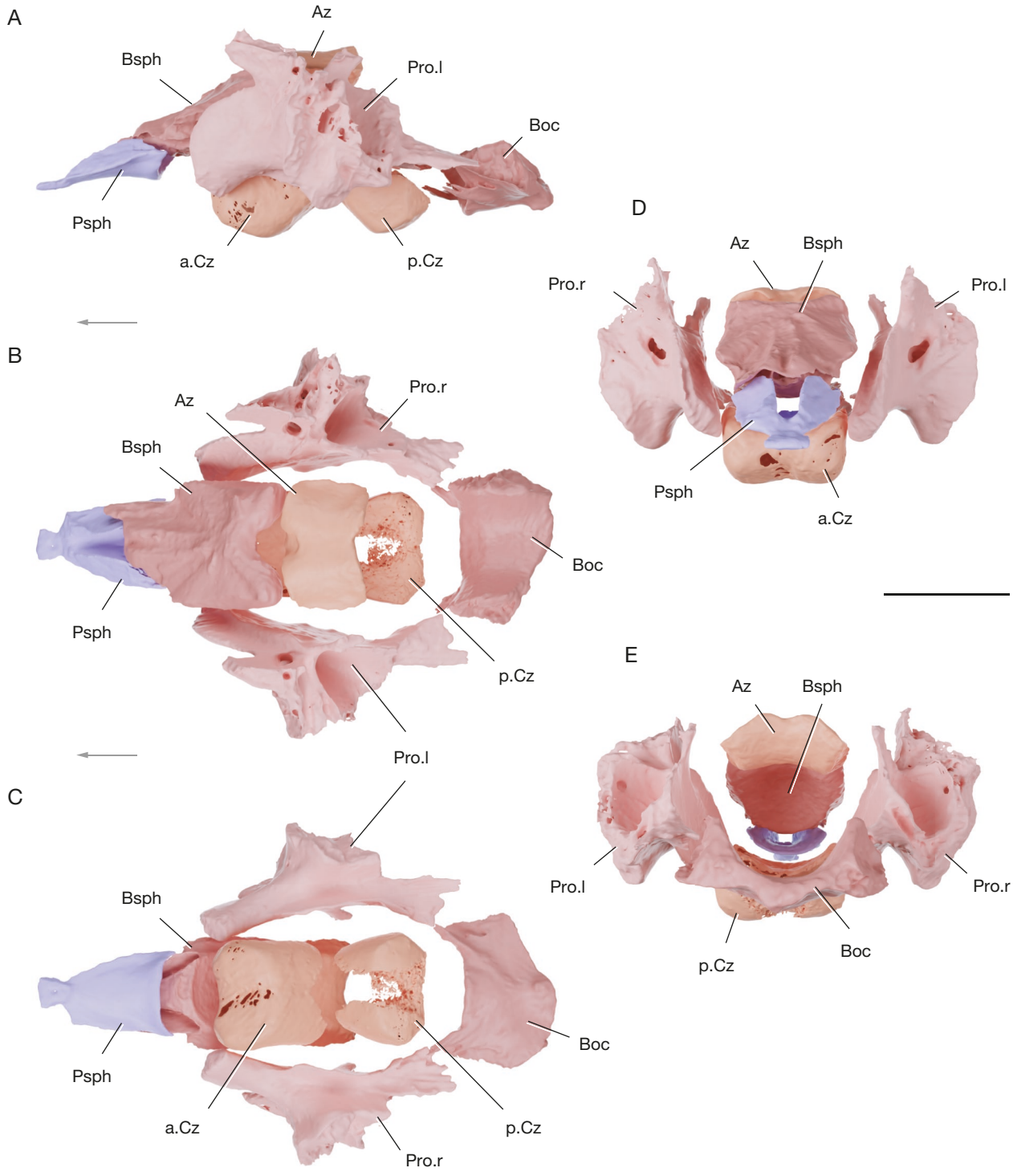

Fig. 9. — Braincase and parasphenoid of *Aemilia stellata* n. gen., n. sp. (AMNH FF 20686): **A**-**E**, reconstrution of the braincase with slightly expanded articular positions of the parasphenoid, basisphenoid, anazygal, catazygals, prootics, and basioccipital in lateral (**A**), dorsal (**B**), ventral (**C**), anterior (**D**), and posterior (**E**) views. Abbreviations: **a.Cz**, anterior catazygal; **Az**, anazygal; **Boc**, basioccipital; **Bsph**, basisphenoid; **p.Cz**, posterior catazygal; **Pro.l**, left prootic; **Pro.r**, right prootic. **Arrows** point anteriorly (**A**-**C**). Scale bar: 10 mm. Credits: 3D models made by Jorge Mondéjar Fernández.

Prootic. The two prootics (Pro; Figs 3E, H; 8; 9A-E) are fully preserved as separate elements of the otico-occipital portion of the neurocranium. The otic shelf (ot.sh; Fig. 8D, F, H) is short, with a concave dorsal margin, and carries a groove to accommodate the *processus connectens* of the basisphenoid. The dorsal and postero-lateral margins appear jagged owing to the lack of preservation of an important cartilaginous connection with the rest of the braincase. The hyomandibular facet (hyo.fa; Fig. 8B) is postero-laterally directed but cannot be confidently reconstructed as the

entire lateral commissure (lat.co; Fig. 8B, F) was entirely made of cartilage. Similarly, any putative articulatory surfaces for the pharyngo- and epibranchial elements of the branchial series have not been preserved. Dorsal to the otic shelf, a prominent antero-dorsal projection (the prefacial eminence [pref.e]; Fig. 8B, D, F, H) carries an overlapping surface, probably for the contact with the ventral ridge of the postparietal. Medial to it, a postero-dorsally oriented process displays a small overlapping surface on its dorsal edge, probably for a contact with the tabular (ov.Ta?; Fig. 8D, F, J), but this is difficult to ascertain. The medial surface is smooth and slightly concave, framing the notochord. The ventral surface carries a groove for the course of the basicranial muscle (gr.m.bc; Fig. 8B), which probably inserted on the posterior wing of the prootic, medially framed by a sharp ridge forming the medial wall of the notochordal canal (n.c; Fig. 8D, H) and laterally by the lateral commissure. The canal for the otic ramus of the facial nerve (c.n.VII; Fig. 8D, F) opens dorsally through a foramen at the medial base of the prefacial eminence, dorsal to the posterior edge of the otic shelf, and exits laterally through a large common foramen for the jugular canal (c.ju; Fig. 8B, F, H). The canal for the jugular vein (c.v.ju; Fig. 8B, J) crosses the prootic antero-posteriorly through a mildly-developed groove, entering the bone between the lateral commissure and the prefacial eminence, and exiting lateral to the saccular chamber through a large foramen associated with the passage of the hyomandibular ramus of the facial nerve. The large saccular chamber (or otic capsule [ot.ca]; Fig. 8F, J) is ovoid, postero-dorsally open, and laterally framed by the irregularly delimited lateral commissure. The medial wall (m.w; Fig. 8D, J) separates the saccular chamber from the notochordal canal and displays a serrated outline, with a convex postero-dorsal expansion. The floor of the otic capsule projects posteriorly into the posterior wing of the prootic (p.w.Pro; Fig. 8B, D, F, J), which is medially inclined and terminated by a complex interdigitated margin for the suture with the basioccipital.

Basioccipital. The basioccipital (Boc; Figs 7R, T; 9A-E) is entirely preserved, detached from the rest of the braincase. It has a semilunar shape, dorsally concave and ventrally convex. The dorsal surface is smooth and perfectly semicircular, accommodating the notochord. The ventral surface displays a median ridge that bifurcates anteriorly towards two antero-lateral projections. These antero-lateral projections have an interdigitating anterior margin to match the posterior wings of the prootics. The lateral margins are incompletely ossified, suggesting the occurrence of a cartilaginous connection with the prootics.

Zygals. The complete zygal series is preserved, represented by the anazygal and the anterior and posterior catazygals. The anazygal lies dorsal to the notochord, articulating with the basisphenoid. The catazygals ventrally frame the notochord, occupying the basicranial fenestra, and they are posteriorly followed by the basioccipital.

Anazygal. The anazygal (Az; Figs 7F, H; 9A-E) has a quadrangular saddle-shape, ventrally concave and dorsally convex with a faint midline groove. It articulates with the basisphenoid condyles via two well-developed anterior depressions separated by a narrow gap. The bone is well ossified, but the lateral margins are unfinished suggesting the occurrence of cartilaginous lateral extensions.

Catazygals. The catazygals are crescent-shaped bones, dorsally concave and ventrally convex, without articulation facets as they do not contact any bone of the neurocranium. The anterior catazygal (a.Cz; Figs 7J, L; 9A-E) is slightly larger than the posterior catazygal (p.Cz; Figs 7N, P; 9A-E), which is less ossified along its median portion than the anterior catazygal.

Hyoid and branchial arches

The hyoid and branchial arches are overall complete on each side of the skull. The hyoid arch comprises the interhyal, symplectic, and fragments of the ceratohyal. There are five branchial arches composed of five ceratobranchials, four epibranchials and three pharyngobranchials. No distinctive hypohyals or hypobranchials have been identified. A single basibranchial is entirely preserved while the anterior portion of the urohyal is missing.

Hyoid arch

Interhyal. The interhyals (Ih; Figs 3E-H; 4E-H; 10D, H; 12A-E) consist of small, elongate, weakly-ossified tubular bones made of thin periosteal walls. They lie near to the dorsal fragment of the ceratohyals and the symplectics and would have articulated ventrally with the latter.

Symplectic. The symplectics (Sy; Figs 3E-H; 4E-H; 10F, J; 12A-E) are also elongate with thin periosteal walls, and they display a characteristic inverted tripodal shape, slightly curved inwards in dorsal view. The ventral portion is cylindrical and hollow with a circular ventral extremity. The enlarged triangular dorsal portion shows a concave inner surface, probably for the course of the posterior mandibulohyoid ligament (gr.lig.pmh; Fig. 10J), running on the medial side of the symplectic, connecting the retroarticular to the interhyal (Forey 1998).

Ceratohyal. The two ceratohyals (Ch; Figs 2F-H; 3E-H; 4E-H; 10B; 12A-E) are incompletely preserved. Most of the bones' contour has been preserved as imprints in the outer surface of the specimen and only fragments of the posterior (dorsal) portion were modelled. The ceratohyals are curved and elongate, with a well-developed and characteristic ventro-lateral flange (v.fl.Ch; Figs 2H; 10A), visible as an imprint on the left side of the nodule. The preserved dorsal portion of the left ceratohyal is triangular in shape with a concave lateral surface and a large extremity to accommodate a probably well-developed cartilage pad for the articulation with the symplectic and interhyal, as in *Latimeria chalumnae* (Millot & Anthony 1958).

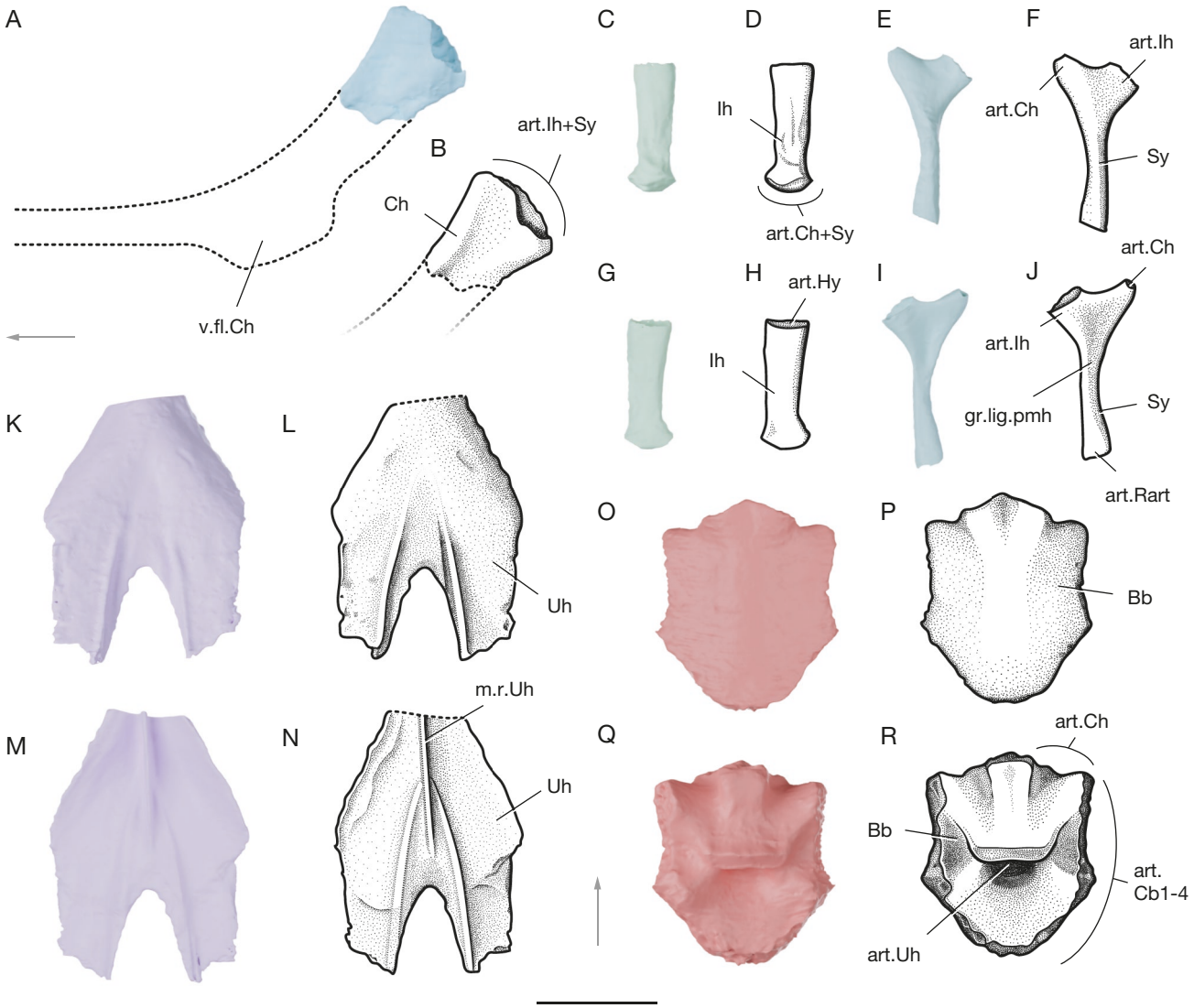

FIG. 10. — Hyoid arch and basibrancial series of *Aemilia stellata* n. gen., n. sp. (AMNH FF 20686): **A**, **B**, left ceratohyal: virtual render (**A**) and interpretative drawing (**B**) of the small preserved dorsal portion in lateral view; **C**, **D**, **G**, **H**, left interhyal: virtual render (**C**, **G**) and interpretative drawing (**D**, **H**) in lateral (**C**, **D**) and medial (**G**-**H**) view; **E**, **F**, **I**, **J**, left symplectic: virtual render (**E**, **I**) and interpretative drawing (**F**, **J**) in lateral (**E**, **F**) and medial (**I**, **J**) view; **K**-**N**, urohyal: virtual render (**K**, **M**) and interpretative drawings (**L**, **N**) in ventral (**K**, **L**) and dorsal (**M**, **N**) views; **O**-**R**, basibranchial: virtual renders (**O**, **Q**) and interpretative drawings (**P**, **R**) in ventral (**O**-**P**) and dorsal (**Q**, **R**) views. Abbreviations: **art.Cb1-4**, articular surface for the first to fourth ceratobranchials; **art.Ch**, articular surface for the ceratohyal; **art.Ch+Sy**, articular surface for the ceratohyal and symplectic; **art.Ih**, articular surface for the interhyal; **art.Ih+Sy**, articular surface for the interhyal and symplectic; **art.Rart**, articular surface for the retroarticular; **art.Uh**, articular surface for the urohyal; **Bb**, basibranchial; **Ch**, ceratohyal; **gr.lig.pmh**, groove for the posterior mandibulohyoid ligament; **Ih**, interhyal; **m.r.Uh**, median ridge of the urohyal; **Sy**, symplectic; **Uh**, urohyal; **v.fl.Ch**, ventro-lateral flange of the ceratohyal. **Arrows** point anteriorly (**A**-**F**, **K**-**R**). Scale bar: 10 mm. Credits: 3D models and drawings made by Jorge Mondéjar Fernández.

Branchial arches

Pharyngobranchials. Three pairs of pharyngobranchials (Pb; Figs 3E-H; 4E-H; 11G, I; 12A-E) are preserved on each side of the skull. The first pharyngobranchial (Pb1; Figs 3E-H; 4E-H; 11G; 12A-E) has a distinctive boomerang shape and displays three surfaces of articulation: a large ventral one in the shape of a bean for the first epibranchial (art.Eb1; Fig. 11G) and two reduced dorsal surfaces at the extremities of long processes, which can be recognised as the infra- and suprapharyngobranchial portions. The infra- and suprapharyngobranchial processes differ in width, with the suprapharyngobranchial portion (s.Pb1; Fig. 11G) being larger and cylindrical in outline, whereas the infrapharyngobranchial portion (i.Pb1; Fig. 11G) is slender and gently tapers anteriorly. The articulation surface of the suprapharyngobranchial portion might have contacted the so-called parampullary process of the prootic (art.pa.pr; Fig. 11G) as known in other coelacanths like *Diplocercides*, *Rhabdoderma* or *Latimeria* (Jarvik 1954; Forey 1998). The infrapharyngobranchial portion carries a small articulation surface anteriorly, probably contacting an unpreserved articulatory facet on the postero-lateral margin of the prootic (art.Pro; Fig. 11G). The rest of the pharyngobranchial series is difficult to identify and may correspond to separate supra- and infrapharyngobranchials from the second arch (?Pb2; Figs 3E-H; 4E-H; 11I; 12A-E;

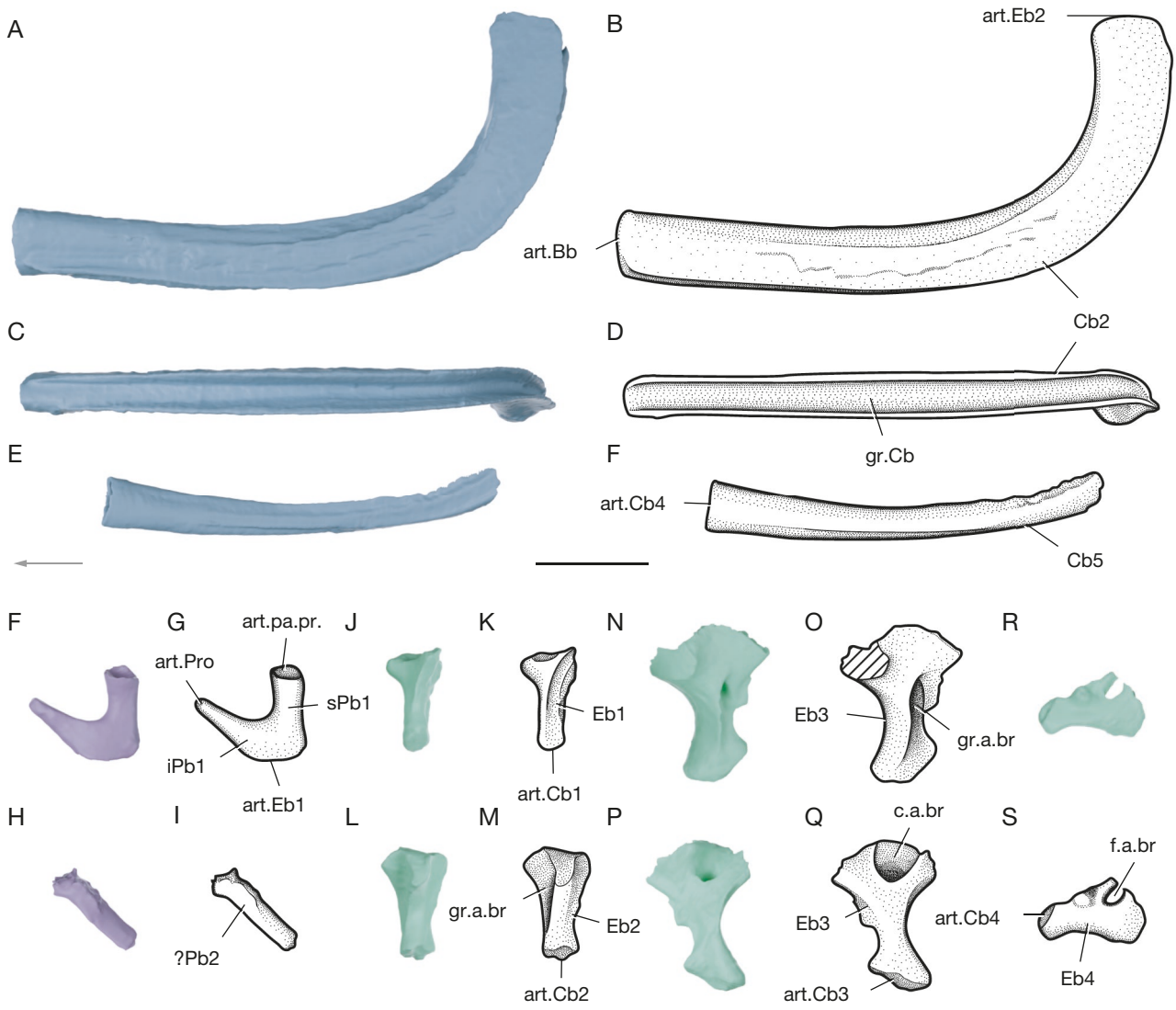

FIG. 11. — Branchial arches of *Aemilia stellata* n. gen., n. sp. (AMNH FF 20686): **A**-**F**, ceratobranchial series: virtual renders (**A**, **C**, **E**) and interpretative drawings (**B**, **D**, **F**) of the second left ceratobranchial (**A**-**D**) and fifth left ceratobranchial (**E**, **F**) in lateral (**A**, **B**, **E**, **F**) and ventral (**C**, **D**) views; **F**-**I**, pharyngobranchial series: virtual renders (**F**, **H**) and interpretative drawings (**G**, **I**) of the left first pharyngobranchial (**F**, **G**) and putative second pharyngobranchial (**H**, **I**) in lateral views; **J**-**S**, epibranchial series: virtual renders (**J**, **L**, **N**, **P**, **R**) and interpretative drawings (**K**, **M**, **O**, **Q**, **S**) of the first left epibranchial (**J**, **K**), second left epibranchial (**L**, **M**), third left epibranchial (**N**-**Q**),v and fourth left epibranchial (**R**, **S**) in lateral (**J**-**O**) and medial (**P**-**S**) views. Abbreviations: **art.Bb**, articular surface for the basibranchial; **art.Cb1**, articular surface for the first ceratobranchial; **art.Cb2**, articular surface for the second ceratobranchial; **art.Cb3**, articular surface for the third ceratobranchial; **art.Cb4**, articular surface for the fourth ceratobranchial; **art.Eb1**, articular surface for the first epibranchial; **art.Eb2**, articular surface for the second epibranchial; **art.pa.pr**, articular facet for the putative parampullary process of the braincase; **art.Pro**, articular facet for the prootic; **c.a.br**, canal for the branchial artery; **Cb2**, second ceratobranchial; **Cb5**, fifth ceratobranchial; **Eb1**, first epibranchial; **Eb2**, second epibranchial; **Eb3**, third epibranchial; **Eb4**, fourth epibranchial; **f.a.br**, foramen for the branchial artery; **gr.a.br**, groove for the branchial artery; **gr.Cb**, ceratobranchial groove for the branchial artery; **iPb1**, infrapharyngobranchial portion of the first pharyngobranchial; **sPb1**, suprapharyngobranchial portion of the first pharyngobranchial; **?Pb2**, undetermined second infra- or suprapharyngobranchial. **Arrow** points anteriorly (**A**-**F**). Scale bar: 10 mm. Credits: 3D models and drawings made by Jorge Mondéjar Fernández.

?Pb2l, r. 14A,C-D), represented by small rod-like elements decreasing in size medially of which only a small portion of the middle section was lightly ossified.

Epibranchials. The epibranchials (Eb; Figs 3E-H; 4E-H; 11K, M, O, Q, S; 12A-E) are robust bones, four in number on each side of the specimen and variable in size and shape. The first two epibranchials (Eb1,Eb2; Figs 3E-H; 4E-H; 11K, M; 12A-E) are somewhat pear-shaped with a well-developed longitudinal ridge and associated dorsal groove (gr.a.br; Fig. 11M). Their anterior (dorsal) articulation head is expanded, roughly triangular in outline, and larger than the more circular proximal (ventral) extremity, articulating with the ceratobranchial (art.Cb; Fig. 11K, M). The third epibranchial (Eb3; Figs 3E-H; 4E-H; 11O, Q; 12A-E) is the largest of the series and carries a large canal for the passage of the efferent branchial artery (ca.a.br; Fig. 11Q) that pierces the bone antero-posteriorly, with the posterior opening prolonging itself into a postero-dorsal groove (gr.a.br; Fig. 11O). The most medial epibranchial (Eb4; Figs 3E-H; 4E-H; 11S;

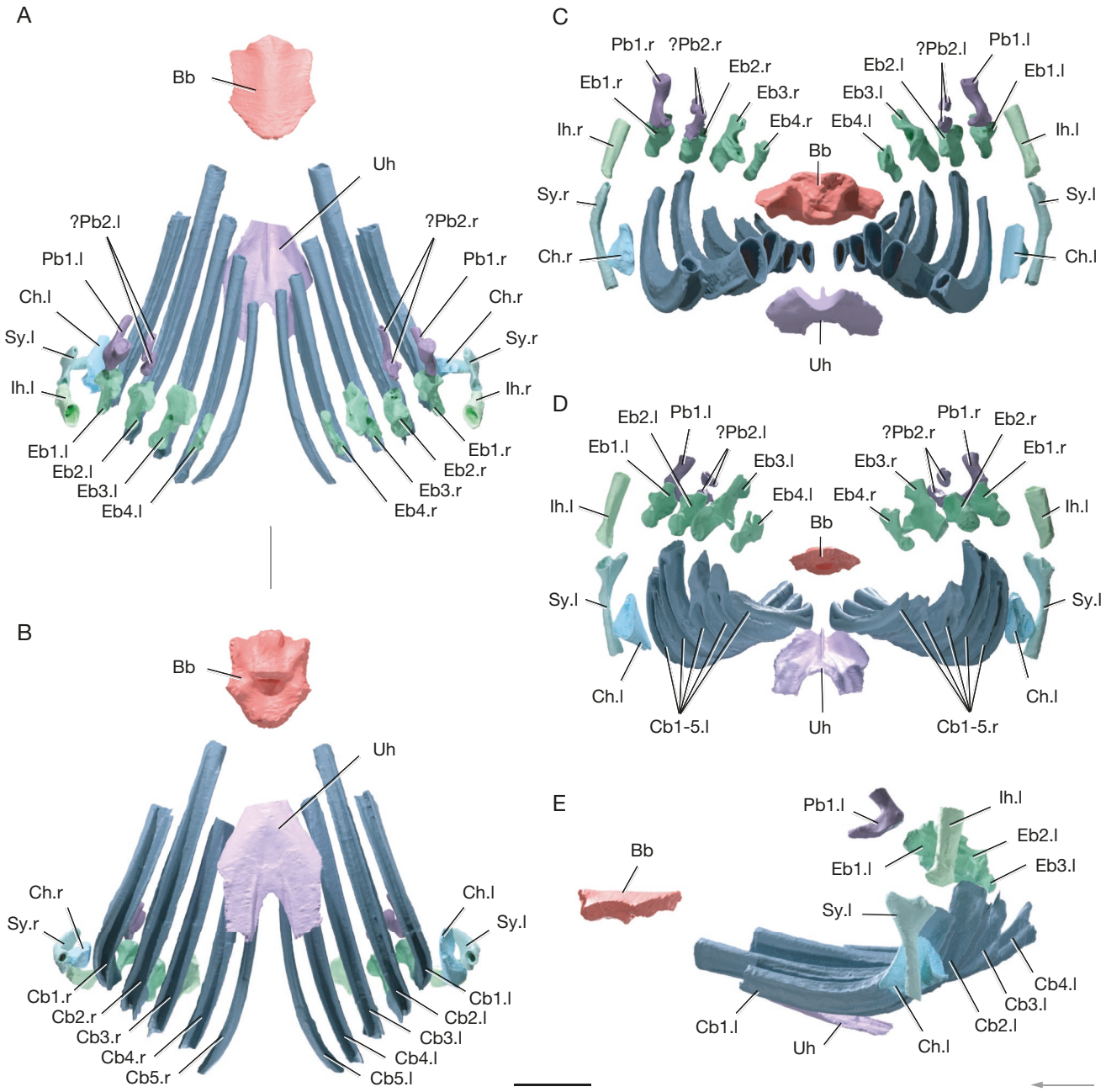

Fig. 12. — Hyobranchial skeleleton of *Aemilia stellata* n. gen., n. sp. (AMNH FF 20686): **A**-**E**, reconstrution of the hyobranchial skeleton with slightly expanded articular positions of its elements in dorsal (**A**), ventral (**B**), anterior (**C**), posterior (**D**), and left lateral (**E**) views. Abbreviations: **Bb**, basibranchial; **Cb1.l**, first left ceratobranchial; **Cb1.r**, first right ceratobranchial; **Cb2.l**, second left ceratobranchial; **Cb2.r**, second right ceratobranchial; **Cb3.l**, third left ceratobranchial; **Cb3.r**, third right ceratobranchial; **Cb4.l**, fourth left ceratobranchial; **Cb4.r**, fourth right ceratobranchial; **Cb5.l**, fifth left ceratobranchial; **Cb5.r**, fifth right ceratobranchial; **Ch.l**, left ceratohyal; **Ch.r**, right ceratohyal; **Eb1.l**, first left epibranchial; **Eb1.r**, first right epibranchial; **Eb2.l**, second left epibranchial; **Eb2.r**, second right epibranchial; **Eb3.l**, third left epibranchial; **Eb3.r**, third right epibranchial; **Eb4.l**, fourth left epibranchial; **Eb4.r**, fourth right epibranchial; **Ih.l**, left interhyal; **Ih.r**, right interhyal; **?Pb.2.l**, second left infra- or supraphrayngobranchial; **?Pb.2.r**, second right infra- or supraphrayngobranchial; **Sy.l**, left symplectic; **Sy.r**, right symplectic. Arrows point anteriorly (**A**-**B**, **E**). Scale bar: 10 mm. Credits: 3D models and drawings made by Jorge Mondéjar Fernández.

12A-E) is again more elongate with a slightly-developed dorsal process displaying an antero-dorsal foramen for the efferent branchial artery (f.a.br; Fig. 11S), as in *Latimeria chalumnae* (Millot & Anthony 1958). There is no fifth epibranchial.

Ceratobranchials. The ceratobranchials (Cb; Figs 3E-H; 4E-H, 11B, D, F; 12A-E) are the largest elements of the branchial arches. They are five in number on each side, decreasing in size postero-medially, and all display a similar curved shape with an elongate, cylindrical anterior (ventral) section and a shorter, cylindrical, oval or trapezoidal (depending of the element) posterior (dorsal) section. The cross sections reveal a weakly developed ossification, decreasing medially along the series, with a hollow internal cavity and thin periosteal walls. The anterior (ventral) tips are circular in outline and appear open since they were

probably capped with large cartilaginous heads. The first pair of ceratobranchials (Cb1; Figs 3E-H; 4E-H; 11B, D; 12A-E) are the longest ones but both are anteriorly broken with the missing section preserved as an imprint in the fossil nodule. The posterior (dorsal) tips of the ceratobranchials 3-5 are also missing due a posterior breakage of the nodule. Ceratobranchials 1 and 2 are completely preserved posteriorly (dorsally) but the lack of cartilage heads hampers a confident reconstruction of their relationship with the epibranchials (art.Eb2; Fig. 11B). The ventral surface of the ceratobranchials 1-4 (Cb1-4; Figs 3E-H; 4E-H; 11B, D; 12A-E) carries a large groove (gr.Cb; Fig. 11D) for the passage of the afferent and efferent branchial arteries. The first four ceratobranchials (Cb1-4) were connected to the basibranchial (art.Bb; Fig. 11B). The fifth ceratobranchial (Cb5; Figs 3E-H; 4E-H; 11F; 12A-E) is the smallest of the series, lacks a groove and is inwardly curved, articulating anteriorly and posteriorly with the ceratobranchial 4 (art.Cb4; Fig. 11F) as in *Latimeria chalumnae* (Millot & Anthony 1958; Datovo & Johnson 2025) and other sarcopterygians (Janvier 1996).

Basibranchial series

Basibranchial. A single basibranchial (Bb; Figs 3E-H; 4E, F; 10P, R; 12A-E) is entirely preserved. It is mainly perichondrally ossified and roughly hexagonal in outline, without traces of partial division. In lateral view, the anterior portion is thickened, becoming more flattened towards the rear. The anterior margin presents a large, inverted trapezoidal surface towards the symphysis of the lower jaw that carries two dorsal depressions for the articulation with the ceratohyals (art.Ch; Fig. 10R). The dorsal surface is slightly convex with two lateral depressions bordering a more elevated median section. The ventral surface displays a ventral process in the shape of a shelf, anteriorly bordering the circular facet for the articulation with the urohyal (art.Uh; Fig. 10R). The lateral margins display two slightly concave articulatory surfaces for the ceratobranchials 1-4 (art.Cb1-4; Fig. 10R) that were probably covered by large cartilage pads, as in *Latimeria chalumnae* (Millot & Anthony 1958).

Urohyal. The well-ossified urohyal (Uh; Figs 2F; 3F-H; 4E-H; 10L, N; 12A-E) is only partially preserved on its posterior third while the middle section is visible as an imprint in the fossil specimen. It is dorso-ventrally flattened and is composed of a wide bifid posterior portion narrowing towards an elongate middle and anterior portion (unpreserved). The posterior expansion displays two lateral flanges with small ridges on the ventral surface framing the median gap and a prominent median ridge on the dorsal surface (m.r.Uh; Fig. 10N). The imprint in the nodule reveals that the ridge does not reach the anterior end, which is partially missing.

Branchial dentition. Numerous scattered branchial platelets have been modelled (but are not shown in the figures, see Appendix 2). These dental plates were certainly associated with the ceratobranchials and the large basibranchial. They display a similar square to rectangular shape. Unfortunately, their precise number, arrangement, and distribution on the branchial elements cannot be reconstructed.

Pectoral girdle

The ventral part of both pectoral girdles is well-preserved comprising the clavicle, the extracleithrum, the ventral blade of the cleithrum, and the scapulocoracoid. There is no evidence of an interclavicle. The dorsal series of post-temporal, supracleithrum and anocleithrum has not been retrieved.

Clavicle. The clavicles (Cla; Figs 2F; 3F-H; 13C, D, G, H) are overall well-preserved, but parts of the antero-ventral blade are missing from both sides of the skull. The clavicle can be divided into two distinct portions: a large dorso-lateral section overlapping the ventral edge of the cleithrum and the extracleithrum, and a dorso-ventrally flattened antero-ventral flange. The internal surface of the dorso-lateral section is strongly concave and is funnel-shaped. The anteriormost portion of the dorso-lateral section displays a wing-like pointed process embracing a groove present in the antero-lateral portion of the cleithrum and overlapping it.

Cleithrum. Both cleithra (Cl; Figs 3E-H; 13C, D, G, H) are incompletely preserved, lacking the dorsal blade. The cleithrum is narrow throughout its length and its external surface displays a smooth anterior margin and a more rugose and ornamented postero-dorsal corner. The external surface is slightly convex, except for the anterior narrow groove accommodating the clavicle. The internal surface is concave and displays a prominent ridge towards the medial margin certainly housing a large cartilaginous blade supporting the scapulocoracoid, as in *Latimeria chalumnae* (Millot & Anthony 1958).

Extracleithrum. The extracleithra (Ecl; Figs 3F-H; 13C, D, G-H) are narrow and elongate bones. The external surface is ornamented with tubercles as on the cleithrum, and similar to those present on the postorbital and squamosal. The dorsal end is levelled with the articulatory head of the scapulocoracoid. The ventral margin is serrated and is overlapped by the clavicle abutting a ventro-lateral buttress, while the major part of the bone fits in a postero-lateral depression of the cleithrum. The postero-dorsal edge displays a small depression concomitant with a similar depression in the posterior margin of the cleithrum.

Scapulocoracoid. The ossified articulatory portion of both scapulocoracoids (Scc; Figs 3F-H; 13C, D, G-H) is completely preserved. It is a remarkably large, shoe-shaped element, internally hollow with extremely thin periosteal walls. The base is quadrangular, slightly narrowing ventrally. The medial columnar section is dorso-posteriorly inclined and the proximal edge would have likely housed a convex cartilaginous articulatory head for the humerus. There are no traces of perforations in the outer surface of the bone.

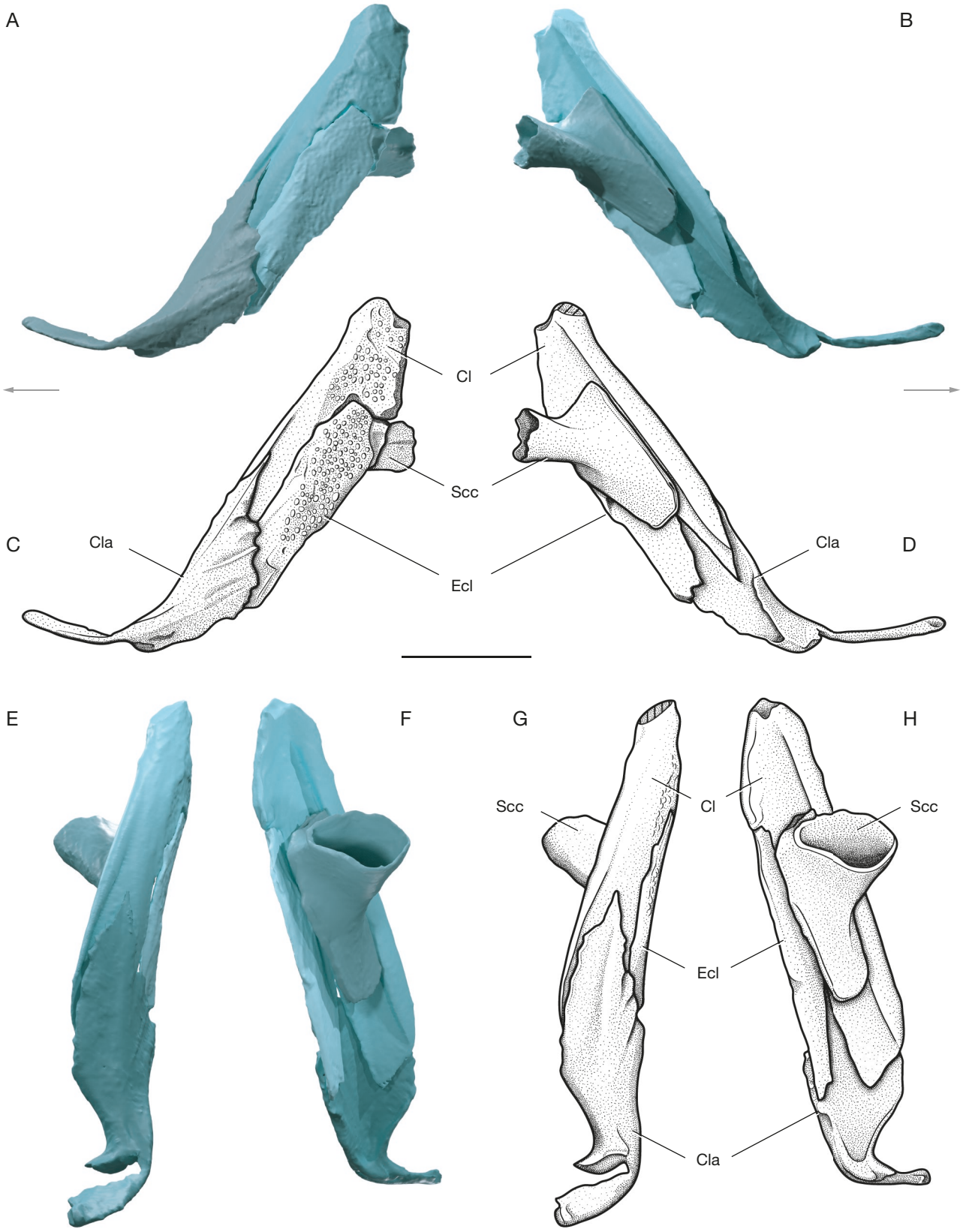

Fig. 13. — Pectoral girdle of *Aemilia stellata* n. gen., n. sp. (AMNH FF 20686): **A**-**H**, left pectoral girdle: virtual renders (**A**, **B**, **E**, **F**) and interpretative drawings (**C**, **D**, **G**, **H**) in lateral (**A**, **C**), medial (**B**, **D**), anterior (**E**, **G**) and posterior (**F**, **H**) views. Abbreviations: **Cl**, cleithrum; **Cla**, cavicle; **Ecl**, extracleithrum; **Scc**, scapulocoracoid. **Arrows** point anteriorly (**A**-**D**). Scale bar: 10 mm. Credits: 3D models and drawings made by Jorge Mondéjar Fernández.

Phylogenetic results

The phylogenetic position of *Aemilia stellata* n. gen., n. sp. was evaluated through maximum parsimony and Bayesian inference using the revised and enhanced matrix of Clement *et al.* (2024). The differences between the parsimony (Appendix 3) and Bayesian (Fig. 15) analyses will only be briefly described here.

The parsimony analyses yielded unreliable results (Appendix 3). The strict consensus produced a poorly resolved tree from 34 equally parsimonious trees (length = 2033; consistency index = 0.18; retention index = 0.23) as well as the 50% majority rule consensus tree (tree length = 1475; consistency index = 0.25; retention index = 0.49). The resulting large polytomy is certainly due to the fact that *Aemilia stellata* n. gen., n. sp. lacks numerous important phylogenetic characters owing to the limited available material. The bootstrap replications yield an average support value of 7.9 for the resulting tree, which falls below the threshold required to consider the tree as robust. For a fully resolved parsimony analysis and the characters supporting each node, see Ferrante & Cavin (2025).

The Bayesian analyses provided a clearer outcome (Fig. 15). *Aemilia stellata* n. gen., n. sp. is reconstructed as the sister group and earliest representative of a Permian-Triassic-Jurassic clade of coelacanths (clade 3; Fig. 15), comprising well-known taxa like *Diplurus newarki* Newberry, 1878 (Jurassic), *Piveteauia madagascarensis* Lehman, 1952, *Rieppelia heinzfurreri* Ferrante & Cavin, 2023, and *Foreyia maxkuhni* Cavin, Mennecart, Obrist, Costeur & Furrer, 2017 (Triassic), among others. This clade is in turn reconstructed as the sister group of an exclusively Triassic clade (clade 4; Fig. 15) mainly comprising the different species of *Whiteia* Moy-Thomas, 1935, as well as *Rebellatrix divaricerca* Wendruff & Wilson, 2012, *Sassenia tuberculata* Stensiö, 1921, and *Heptanema paradoxum* Belloti, 1857.

Several clades can be associated with previously identified families of coelacanths, although their composition may vary with respect to earlier studies (e.g., Schultze 1993, 2004; Forey 1998; Manuelli *et al.* 2024; Ferrante & Cavin 2025). Among the most clearly recognizable families, we note the Laugiidae Berg, 1940 (clade 1; Fig. 15), Axeliidae Ferrante & Cavin, 2025 (clade 2; Fig. 15), Mawsoniidae Schultze, 1993 (clade 5; Fig. 15), and Latimeriidae Berg, 1940 (clade 6; Fig. 15). Other traditional coelacanth families like Miguashaiidae Schultze, 1993, Diplocerciidae Stensiö, 1921, Hadronectoridae Lund & Lund, 1984, Rhabdodermatidae Berg, 1958, Whiteiidae Schultze, 1993, and Sasseniidae Forey, 1998 were not retrieved as monophyletic and will not be further discussed here.

The family Laugiidae Berg, 1940 (clade 1; Fig. 15) maintains its traditional composition (e.g., Forey 1998; Schultze 2004) and corresponds to the clade including *Laugia groenlandica* Stensiö, 1932 and *Coccoderma suevicum* Quenstedt, 1858, with the exlusion here of *Piveteauia madagascarensis* Lehman, 1952, usually retrieved among the laugiids (e.g., Toriño *et al.* 2021a; Ferrante & Cavin 2023, 2025; Manuelli *et al.* 2024). The family Axeliidae Ferrante & Cavin, 2025 (clade 2; Fig. 15; reconstructed as a subset of Whiteiidae (node E1) by Arratia & Schultze (2015) and defined by Ferrante & Cavin (2025)) is composed of *Axelia robusta* Stensiö, 1921, *Wimania sinuosa* Stensiö, 1921, and *Atacamaia solitaria* Arratia & Schultze, 2015; its sister group is here represented by *Coelacanthus granulatus* Agassiz, 1839. Ferrante & Cavin (2025) reconstructed the family Whiteiidae Schultze, 1993 including *Whiteia* Moy-Thomas, 1935, *Guizhoucoelacanthus* Liu, Yin, Luo, Wang & Wang, 2006, and *Garnbergia* Martin & Wenz, 1984. In our analysis, all surveyed species of the genus *Whiteia* (*W. durabilis* Wendruff, 2011, *W. lepta* Wendruff, 2011, *W. woodwardi* Moy-Thomas, 1935, *W. uyenoteruya* Yabumoto, Brito, Iwata & Abe, 2019, *W. nielseni* Forey, 1998, and *W. oishoii* Yabumoto & Brito, 2016) cluster close together in a larger clade (clade 4; Fig. 15) that also includes *Rebellatrix divaricerca* Wendruff & Wilson, 2012, *Sassenia tuberculata* Stensiö, 1921, and *Heptanema paradoxum* Belloti, 1857. However, *Guizhoucoelacanthus* is found within clade 3, whereas *Garnbergia* is reconstructed among the Mawsoniidae.

The families Mawsoniidae Schultze, 1993 (clade 5; Fig. 15) and Latimeriidae Berg, 1940 (clade 6; Fig. 15) are also clearly recognizable as sister clades whithin the suborder Latimerioidei Schultze, 1993 (for a different composition see Dutel *et al.* 2012; Cavin & Grădinaru 2014; Arratia & Schultze 2015; Toriño *et al.* 2021a; Ferrante & Cavin 2023, 2025; Manuelli *et al.* 2024). One puzzling result is that *Graulia branchiodonta* Manuelli, Mondéjar Fernández, Dollman, Jakata & Cavin, 2024 is no longer found as a basal Mawsoniidae (as opposed to Manuelli *et al.* 2024) but appears well-nested within the Latimeriidae, whereas *Dobrogeria aegyssensis* Cavin & Grădinaru, 2014 also switches position from the Latimeriidae (Ferrante & Cavin 2023, 2025; Manuelli *et al.* 2024) to the Mawsoniidae. Within the Latimeriidae, the subfamily Ticinepomiinae Ferrante & Cavin, 2023, previously containing the species *Ticinepomis peyeri* Rieppel, 1980, *Foreyia maxkuhni* Cavin, Mennecart, Obrist, Costeur & Furrer, 2017, and *Rieppelia heinzfurreri* Ferrante & Cavin, 2023 known exclusively from the Triassic of Switzerland (Ferrante & Cavin 2023, 2025) has surprinsingly exploded, with *Ticinepomis peyeri* retrieved as an early latimeriid in a clade containing *Holophagus gulo* Egerton, 1861, *Undina* (*U. penicillata* Münster, 1834 and *U. cirinensis* Saint-Seine, 1949), and *Macropoma willemoesii* Vetter, 1881. On the other hand, *Rieppelia heinzfurreri* and *Foreyia maxkuhni* were reconstructed as crownward members of the clade including *Aemilia stellata* n. gen., n. sp. (clade 3; Fig. 15).

The analysis also revealed probable polyphyletic taxa, notably *Rhabdoderma* Newberry, 1856, *Sassenia* Stensiö, 1921, *Changxingia* Wang & Liu, 1981, *Whiteia* Moy-Thomas, 1935, and *Macropoma* Agassiz, 1835, as well as paraphyletic genera like *Diplocercides* Stensiö, 1922, *Euporosteus* Jaeckel, 1927, *Undina* Münster, 1834, and *Axelrodichthys* Maisey, 1986. Among the multispecific genera of coelacanths surveyed, only *Miguashaia* (*M. bureaui* Schultze, 1973 and *M. grossi* Forey, Ahlberg, Lukševičs & Zupiņš, 2000) and *Mawsonia* (*M. gigas* Woodward, 1907, *M. soba* Brito, Cupello, Yabumoto, Hell, Brunet & Otero, 2018, *M. brasiliensis* Yabumoto, 2002, and *M. tegamensis* Wenz, 1973) were retrieved as monophyletic. It is not in the scope of this study to discuss the probable causes

for this odd distribution of taxa, but we encourage future surveys to thoroughly review these polyspecific genera and shed light on these problematic phylogenetic reconstructions.

DISCUSSION

Anatomical comparisons

The new features revealed by *Aemilia stellata* n. gen., n. sp. broaden our understanding of the organization and evolution of the neurocranium and hyobranchial skeleton of coelacanths, two of their most conspicuous and incompletely known anatomical systems. However, comparisons with other taxa are challenging, due to the scarcity of data concerning the internal structures of the skull, especially in Palaeozoic coelacanths. We will first discuss the new anatomical features of the skull roof, cheek, braincase and pectoral girdle, and their evolutionary implications highlighted by the new material of *Aemilia stellata* n. gen., n. sp., and then focus exclusively on the hyobranchial skeleton to decipher the assembly and evolution of the hyoid and branchial arches in coelacanths.

Skull roof

The dermal skull roof of coelacanths is divided by the intracranial joint into an anterior parietonasal and a posterior postparietal shields. *Latimeria* Smith, 1939 is the only living vertebrate to retain this plesiomorphic feature of sarcopterygians (Janvier 1996). The joint between the parietal (or posterior parietal *sensu* Teng *et al.* 2019) and postparietal bones can be straight and simple as in *Latimeria* (Millot & Anthony 1958; Forey 1998) or digitated as in *Ngamugawi* Clement, Cloutier, Lee, King, Vanhaesebroucke, Bradshaw, Dutel, Trinajstic & Long, 2024 (Clement *et al.* 2024). The straight condition can be considered plesiomorphic, when compared with early coelacanths (e.g., *Miguashaia* Schultze, 1973; Cloutier 1996) and other sarcopterygians (e.g., Jarvik 1980; Janvier 1996). Unfortunately, in *Aemilia stellata* n. gen., n. sp. the parietals are unknown and the postparietal shield is too badly preserved to ascertain whether the joint was either simple or digitated (Fig. 5).

The ventral surface of the postparietals of *Aemilia stellata* n. gen., n. sp. is more phylogenetically informative as it displays a reduced descending process represented by a ridge (d.p.Pp; Fig. 5D) as in other Palaeozoic coelacanths (e.g., *Coelacanthus* Agassiz, 1839, *Spermatodus* Cope, 1894, and *Rhabdoderma* Newberry, 1856; Forey 1998; Ferrante & Cavin 2025) compared with the stronger and more developed processes of the Mesozoic and Recent Latimerioidei (e.g., *Graulia* Manuelli, Mondéjar Fernández, Dollman, Jakata & Cavin, 2024, *Macropoma* Agassiz, 1835, *Latimeria*; Forey 1998; Manuelli *et al.* 2024;). The tabular of *Aemilia stellata* n. gen., n. sp. (Fig. 5) does not carry a significantly developed descending process, a plesiomorphic condition also known in *Diplocercides* Stensiö, 1922 (Stensiö 1922, 1937; Forey 1998), but variably found among younger fossil coelacanths (e.g., *Mawsonia* Woodward, 1907, *Axelrodichthys* Maisey, 1986, *Trachymetopon* Hennig, 1951; Forey 1998; Dutel *et al.* 2015b; Toriño *et al.* 2021b; Ferrante & Cavin 2025), in which it likely represents a derived loss from well-developed processes in Palaeozoic and early Mesozoic taxa like *Rhabdoderma*, *Laugia*, *Dobrogeria* Cavin & Grădinaru, 2014, and *Graulia* (Forey 1998; Cavin & Grădinaru 2014; Manuelli *et al.* 2024).

The pores associated with the otic sensory canal open within the bones lateral to the postparietals, in case of *Aemilia stellata* n. gen., n. sp. it is the tabular (po.oc; Fig. 5F), a plesiomorphic feature for many sarcopterygians and early coelacanths like *Miguashaia* (Cloutier 1996) and *Diplocercides* (Forey 1998). Finally, the presence of pores on the preserved posterior portion of the postparietals in *Aemilia stellata* n. gen., n. sp. suggests the earliest occurrence of anterior branches of the occipital commissure piercing the postparietal (po.a.occ; Fig. 5B), a character previously known only in Mesozoic and Recent coelacanths (e.g., the Latimerioidei *Graulia*, *Macropoma*, *Swenzia* Clément, 2005, and *Latimeria*; Forey 1998; Clément 2005; Manuelli *et al.* 2024).

The posterior margin of the tabular of *Aemilia stellata* n. gen., n. sp. carries a small shelf projecting posteriorly and receiving the unpreserved lateral extrascapular (po.sf; Fig. 5F), a condition similar to *Laugia*, *Coccoderma* Quenstedt, 1858, and *Spermatodus* (Forey 1998; Westoll 1939). The occurrence of separated tabulars and postparietals is the most common arrangement in coelacanths, with only a few exceptions of tabulars fused to the postparietals (e.g., *Ngamugawi*, *Foreyia* Cavin, Mennecart, Obrist, Costeur & Furrer, 2017, *Ticinepomis* Rieppel, 1980, *Hainbergia* Schweizer, 1966; Schweizer 1966; Cavin *et al.* 2017; Ferrante *et al.* 2023; Clement *et al.* 2024). The posterior extension of the tabular among the postparietal shield is difficult to reconstruct in *Aemilia stellata* n. gen., n. sp. as the tabular was not found articulated with the postparietal. The plesiomorphic condition (e.g., *Miguashaia* and onychodontids; Cloutier 1996; Mondéjar-Fernández 2020) is the posterior margin of the tabular ending anteriorly to the posterior margin of the postparietals (Clement *et al.* 2024). Tabulars levelled with the posterior margin of the postparietals are seen in many Palaeozoic taxa (e.g., *Diplocercides*, *Hadronector* Lund & Lund, 1984, *Rhabdoderma*; Forey 1998). A tabular extending beyond the posterior margin of the postparietals and the extrascapulars is considered the consequence of the fusion of the lateralmost extrascapular with the tabular (Stensiö 1921; Forey 1998; Ferrante & Cavin 2025). As a result, a junction of the otic canal with the occipital commissure and the main lateral line canal occurs in the tabular and not in the lateral extrascapular. These characters are frequently found correlated (e.g., *Dobrogeria*, *Whiteia* Moy-Thomas, 1935, *Axelrodichthys*, *Macropoma*, *Latimeria*; Forey 1998; Cavin & Grădinaru 2014), but differ in *Aemilia stellata* n. gen., n. sp. and other early coelacanths (e.g., *Miguashaia*, *Ngamugawi*; Cloutier 1996; Clement *et al.* 2024) and other sarcopterygians (e.g., onychodontids; Andrews *et al.* 2006; Mondéjar-Fernández 2020) in which the tabular is pierced by a single canal and the triple junction of lateral line canals occurs in the lateral extrascapular.

Cheek

Unfortunately, the cheek of *Aemilia stellata* n. gen., n. sp. is among the least well-preserved regions of the skull and little information can be obtained from it. All cheek bones are ornamented by rounded to slightly pointed tubercles (Figs 2A, C; 3E, G), similar to other Palaeozoic coelacanths like *Miguashaia* (Cloutier 1996), *Serenichthys* Gess & Coates, 2015 (Gess & Coates 2015), *Ngamugawi* (Clement *et al.* 2024), and *Rhabdoderma* (Forey 1981, 1998), but not quite as rounded as those of *Latimeria* and its close relatives (Millot & Anthony 1958; Forey 1998; Manuelli *et al.* 2024; Ferrante & Cavin 2025). Both the squamosal (Sq) and postorbital (Po; Figs 2E,G, 3E-G) are relatively large, different from the tube-like bones of various Mesozoic and Recent taxa (e.g., *Coccoderma*, *Coelacanthus*, *Ticinepomis*, *Axelrodichthys*, *Latimeria*; Forey 1998; Cavin *et al.* 2013; Ferrante *et al.* 2023; Ferrante & Cavin 2025). However, given the preservation of the specimen, it is unclear whether the cheek bones were tightly sutured to each other (representing the plesiomorphic condition known for instance in the Devonian *Miguashaia*, *Gavinia* Long, 1999, *Serenichthys*, *Diplocercides*, and the Carboniferous *Rhabdoderma*; Forey 1981; Cloutier 1996; Long 1999; Gess & Coates 2015) or not (as most post-Carboniferous taxa such as the Triassic *Sassenia* Stensiö, 1921; Forey 1998).

Palate

The few palatal elements found in *Aemilia stellata* n. gen., n. sp. comprise an ectopterygoid (Ectp; Fig. 6L, N, P, R), a bone barely known in fossil coelacanths. In *Aemilia stellata* n. gen., n. sp., it carries a combination of small pointed teeth and larger fangs posteriorly, a condition different from the solely denticulated ectopterygoid of the Triassic *Dobrogeria* (Cavin & Grădinaru 2014) and *Graulia* (Manuelli *et al.* 2024) and more similar to the combined occurrence of small teeth and fangs (albeit slightly reduced compared with the dermopalatine fangs) of the Cretaceous *Macropoma* (Forey 1998) and *Latimeria* (Millot & Anthony 1958).

An open buccohypophysial canal on the posterior portion of the parasphenoid is a plesiomorphic condition among coelacanths, present both in Palaeozoic (e.g., *Diplocercides*, *Euporosteus* Jaeckel, 1927, *Ngamugawi*, *Spermatodus*) and Mesozoic taxa (e.g., *Laugia*, *Piveteauaia* Lehman, 1952, *Parnaibaia* Yabumoto, 2008; Forey 1998; Clément 1999; Yabumoto 2008; Clement *et al.* 2024; Ferrante & Cavin 2025). *Aemilia stellata* n. gen., n. sp. retains an open buccohyphysial canal (bh.c; Fig. 6H, J), situated roughly at the ossification center of the parasphenoid, reminiscent of its position in *Diplocercides* (Bjerring 1993: fig.3). However, the patchy distribution of this character across coelacanth phylogeny is likely the result of a morphological disparity and the poor record of well-preserved braincases. For instance, in the case of *Parnaibaia maranhoensis* Yabumoto, 2008 (Yabumoto 2008), it may represent a reversion from a closed condition in the Latimerioidei and its Mesozoic close relatives (Manuelli *et al.* 2024), whereas in the Carboniferous *Rhabdoderma elegans* Newberry, 1856 the closed opening may represent an autapomorphic trait (Forey 1998).

Braincase

The reduction of the ossification and fragmentation of a primitively solidly ossified ethmosphenoid and otico-occipital portions of the neurocranium into separated smaller ossifications is one of the clearest evolutionary trends among coelacanths (Forey 1998; Ferrante & Cavin 2025); similar trends are also occurring in actinopterygians (Patterson 1975; Gardiner 1984). Until now, very few preserved braincases were known in Palaeozoic coelacanths, hampering the precise reconstruction of the evolutionary timing and the modalities of the separation of the components of the ethmosphenoid and otico-occipital units of the braincase. Fully ossified braincases are solely known in Devonian coelacanths like *Diplocercides*, *Euporosteus*, and *Ngamugawi* (Stensiö 1922; Clement *et al.* 2024) but also in the Triassic *Sassenia groenlandica* Forey, 1998 (Forey 1998), likely representing an autapomorphic reversal trait found into the early Mesozoic. *Aemilia stellata* n. gen., n. sp. displays the derived condition of an otico-occipital portion of the braincase formed of separate elements, with a clear separation between the parasphenoid, basisphenoid, and prootics (Fig. 9), common in all post-Palaeozoic taxa. This is the earliest occurrence of this feature, prior to the Mesozoic, since the only known braincases from the Carboniferous are those of *Rhabdoderma elegans* Newberry, 1856 where the otico-occipital portion of the braincase is still ossified as a unit (Forey 1981, 1998).

The prootic is the largest ossification of the otico-occipital portion of the neurocranium in coelacanths. In *Aemilia stellata* n. gen., n. sp., it is clearly detached from the rest of the braincase (Figs 8; 9) and its postero-lateral margins are unfinished, indicating that the lateral commissure was largely cartilaginous. Due to this, there is no clear evidence for the articulation facets of the hyomandibular, pharyngo- and epibranchials as seen in *Latimeria chalumnae* (Millot & Anthony 1958). The jugular vein runs along a prominent jugular canal and groove across the prootic of *Aemilia stellata* n. gen., n. sp. (c.ju; Fig. 8B, F, H), similar to *Laugia* (Forey 1998: fig. 6.7), a common and plesiomorphic condition of coelacanths, but secondarily absent in certain Mesozoic and Recent taxa (*Macropoma*, *Mawsonia*, *Sassenia*, and *Latimeria*; Maisey 1986; Forey 1998).

Aemilia stellata n. gen., n. sp. presents a basioccipital separated from the prootic with a complex digitating suture between both bones (Fig. 9), as in many Mesozoic and Recent Latimerioidei (e.g., *Graulia*, *Axelrodichthys*, *Undina* Münster, 1834, *Macropoma*, *Holophagus* Egerton, 1861, and *Latimeria*; Forey 1998; Manuelli *et al.* 2024; Ferrante & Cavin 2025). This condition was previously unknown in the Palaeozoic, thus currently corresponding to the earliest occurrence of this configuration among coelacanths. This new combination of features displayed in *Aemilia stellata* n. gen., n. sp. confirms that fully disjointed braincases in which both the ethmosphenoid (i.e., vomers, lateral ethmoids, basisphenoid, parasphenoid) and the otico-occipital (i.e., prootic, basioccipital, supraoccipital, exoccipital) portions are separated in different bones originated in coelacanths no later than the Upper Carboniferous.

It has also been stated that the development of descending processes in the skull roof may be associated with this overall reduction of the ossification of the neurocranium (Forey 1998). For instance, in *Latimeria* the neurocranium is securely attached to the roofing dermal bones through the descending processes of the parietals (corresponding to the posterior parietals), postparietals, and tabulars (Millot & Anthony 1958; Forey 1998; Manuelli *et al.* 2023, 2024). Descending processes occur in the ethmosphenoid division of the braincase, carried by the parietals, but only in post-Devonian coelacanths (e.g., *Rhabdoderma*, *Spermatodus*, *Coelacanthus*, *Sassenia*; Westoll 1939; Schaumberg 1978; Forey 1998; Ferrante & Cavin 2025). In the otico-occipital unit, descending processes appear first in the tabulars already in the Palaeozoic (e.g., the Carboniferous *Rhabdoderma* and the Permian *Coelacanthus* and *Spermatodus*; Forey 1998), but only later in the postparietals during the Mesozoic (e.g., the Triassic *Sassenia*, *Laugia*, *Dobrogeria*, and *Piveteauia*; Forey 1998; Clément 1999; Cavin & Grădinaru 2014; Ferrante & Cavin 2025). *Aemilia stellata* n. gen., n. sp. does not display any clear descending processes on the tabular, whereas the postparietals display a narrow a ridge, visible on the left postparietal (d.p.Pp; Fig. 5D), similar to certain Mesozoic coelacanths like *Laugia* (Forey 1998: fig. 3.9) and *Wimania* Stensiö, 1921 (Stensiö 1921: fig. 19), which could have fitted in a groove along the prefacial eminence of the prootic. However, in *Aemilia stellata* n. gen., n. sp. the autapomorphic occurrence in the prootic of a long postero-dorsal process probably articulating with the tabular (ov.Ta?; Fig. 5D, F, J) may constitute an analogous structure to the ventral process of the tabular known in other coelacanths, but it is currently challenging to support this statement.

Attachment surfaces between the palate and the braincase are also quite variable and diagnostic among coelacanths. A basipterygoid process on the ethmosphenoid unit is only known in *Diplocercides* (Forey 1998). Similarly, a suprapterygoid process occurs only in the Devonian *Diplocercides* (Stensiö 1922) and *Euporosteus* (Stensiö 1937), but also in the Triassic *Sassenia* (Forey 1998). The suprapterygoid process of the ethmoid unit of the braincase has usually been synonymized with the antotic process of the separated basisphenoid in coelacanths (e.g., Stensiö 1932; Jarvik 1954), but the condition in these three latter taxa reveals that these are different processes, with the suprapterygoid process located anterior to the antotic process, which truly constitutes an actinistian synapomorphy (Forey 1998). The suprapterygoid process also disappears in post-Devonian coelacanths, and is no longer present in the Carboniferous as illustrated by *Aemilia stellata* n. gen., n. sp. and *Rhabdoderma*, with the antotic process becoming larger and projecting farther laterally as the main articulation surface between the metapterygoid (palate) and the basisphenoid (braincase; Schaeffer & Gregory 1961).

The basisphenoid of *Aemilia stellata* n. gen., n. sp. (Figs 7A-D; 9) lacks its anterior and dorsal margins, but the ventral half is relatively complete and recalls in many aspects that of *Spermatodus* as described by Westoll (1939). The *processus connectens* is short and thus it could not have met the parasphenoid (Fig. 9). A separation between the *processus connectens* and the parasphenoid can be considered a plesiomorphic feature of coelacanths as displayed in Devonian taxa like *Diplocercides*, *Euporosteus*, and *Ngamugawi* (Forey 1998; Clement *et al.* 2024), as well as in the Latimeriidae *Macropoma* and *Latimeria* (Millot & Anthony 1958; Forey 1998). A contact between the *processus connectens* and the parasphenoid is mainly known in Mesozoic taxa (e.g., *Laugia*, *Diplurus* Newberry, 1878, *Dobrogeria*, *Wimania*, *Mawsonia*, *Megalocoelacanthus* Schwimmer, Stewart & Williams, 1994, *Undina*, *Axelrodichthys*; Maisey 1986; Forey 1998; Dutel *et al.* 2012; Cavin & Grădinaru 2014; Toriño *et al.* 2021b; Ferrante & Cavin 2025) but it also occurs in the Carboniferous *Rhabdoderma* (Forey 1998). The distribution of this character reveals that it is a relatively homoplastic feature, making it difficult to reconstruct its phylogenetic history, especially given the current absence of data from the braincase of many Palaeozoic and early Mesozoic coelacanths.

Pectoral girdle

The pectoral girdle is considered as remarkably conservative in coelacanths, with only minor differences in proportions of the cleithrum, clavicle, and shape of the anocleithrum among taxa (Forey 1998; Schaeffer 1941; Manuelli *et al.* 2024). However, the size and relationships of the extracleithrum with the other bones of the girdle shows a certain morphological disparity. The extracleithrum is a unique feature of actinistians among osteichthyans, located lateral to the cleithrum, and ventral to the level of the insertion of the pectoral fin on the scapulocoracoid. The extracleithrum is unornamented in *Latimeria* (Millot & Anthony 1958) but in fossil coelacanths it can be variably ornamented by rounded tubercles (e.g., *Miguashaia*, *Aemilia stellata* n. gen., n. sp., *Foreyia*, *Whiteia*; Cloutier 1996; Forey 1998; Cavin *et al.* 2017) or thin ridges (e.g., *Allenypterus* Melton, 1969, *Coelacanthus*, *Laugia*, *Macropoma*; Forey 1998). In *Aemilia stellata* n. gen., n. sp., the cleithrum and extracleithrum display a homogenous ornamentation of small tubercles (Fig. 13A, C), similar to the condition of *Miguashaia* (Cloutier 1996) or *Whiteia* (Forey 1998). In *Rhabdoderma*, only the dorsal portion of the cleithrum is ornamented while the extracleithrum is smooth (Forey 1981). However, in some taxa the ornamentation of the cleithrum and extracleithrum is slightly different from that of other dermal bones of the skull (e.g., *Allenypterus*, *Laugia*, *Macropoma*), represented by small ridges in the girdle as opposed to tubercles or larger ridges in the cheek and skull roof (Forey 1998).

The dorsal extension of extracleithrum is also quite variable. It projects more dorsally than the clavicle in *Aemilia stellata* n. gen., n. sp. (Fig. 13), as in many other taxa, both from the Palaeozoic (e.g., *Allenypterus*, *Caridosuctor* Lund & Lund, 1984, *Coelacanthus*; Moy-Thomas & Westoll 1935; Forey 1998), Mesozoic (e.g., *Laugia*, *Dobrogeria*, *Macropoma*; Forey 1998; Cavin & Grădinaru 2014), and Recent (*Latimeria*; Millot & Anthony 1958; Forey 1998). In certain cases, the dorsal edge of the extracleithrum is levelled with that of the clavicle (e.g., *Rhabdoderma*, *Mawsonia*, *Axelrodichthys*, *Holophagus*;

Forey 1998; Toriño *et al.* 2021b; Clement *et al.* 2024), whereas in *Rebellatrix*, the clavicle extends more dorsally than the extracleithrum (Wendruff & Wilson 2012). *Miguashaia* shows an interesting intrageneric disparity: in *M. bureaui* Schultze, 1973 the clavicle is levelled with the extracleithrum (Cloutier 1996) but in *M. grossi* Forey, Ahlberg, Lukševičs & Zupiņš, 2000 the clavicle extends more dorsally than the extracleithrum (Forey *et al.* 2000). In *Aemilia stellata* n. gen., n. sp., the suture of the extracleithrum with the cleithrum is more important than with the clavicle, similar to the condition of *Coelacanthus*, *Macropoma*, and *Laugia* (Stensiö 1932; Moy-Thomas & Westoll 1935; Schaumberg 1978; Forey 1998) but differing from the long contact between the extracleithrum and the clavicle in other taxa like *Holophagus*, *Rebellatrix* Wendruff & Wilson, 2012, or *Whiteia* (Forey 1998; Wendruff & Wilson 2012). It is currently difficult to determine the phylogenetic significance of these features.

The cleithrum and clavicle do not display a postbranchial lamina in *Aemilia stellata* n. gen., n. sp. (Fig. 13), as in many other coelacanths (e.g., *Rhabdoderma*, *Coelacanthus*, *Laugia*, *Axelrodichthys*, *Macropoma*, *Latimeria*; Stensiö 1932; Moy-Thomas & Westoll 1935; Schaumberg 1978; Forey 1998). The postbranchial lamina is a plesiomorphic feature for gnathostomes (Brazeau & Friedman 2014) as present for instance in *Psarolepis romeri* Yu, 1998 (Zhu *et al.* 1999) and the putative early coelacanth *Styloichthys changae* Zhu & Yu, 2002 (Zhu & Yu 2002; Friedman 2007). Postbranchial laminae are more common in Devonian coelacanths like *Miguashaia*, *Diplocercides*, and *Ngamugawi* (Forey 1998; Cloutier 1996; Clement *et al.* 2024) but are also known in younger taxa like the Triassic *Diplurus* (Schaeffer 1948, 1952; Forey 1998) and *Yunnancoelacanthus* Wen, Zhang, Hu, Benton, Zhou, Tiao, Huang & Chen, 2013 (Wen *et al.* 2013). The absence of a branchial lamina in post-Devonian coelacanths may indicate a slight shift in the position of the pectoral girdle relative to the opercular, in which the ventral portion of the cleithrum and clavicle no longer projects as anteriorly as in taxa with more consolidated dermal skulls (e.g., *Miguashaia*, *Diplocercides*), thus becoming more loosely attached to the opercular series and allowing more space to the water flow to be directed out of the gill chamber.

Finally, the scapulocoracoid of fossil coelacanths is poorly known, usually represented by small elements lying separated from the rest of the pectoral girdle (e.g., *Diplocercides*, *Rhaboderma*, *Laugia*, *Graulia*, *Macropoma*, *Axelrodichthys*; Stensiö 1922, 1932; Millot & Anthony 1958; Forey 1981, 1998; Manuelli *et al.* 2024). In *Aemilia stellata* n. gen., n. sp. it is particularly massive, despite being weakly ossified and internally hollow, and it is one of the largest preserved elements of the pectoral girdle, similar to the condition of *Latimeria chalumnae* (Mansuit *et al.* 2020). This preserved portion of the scapulocoracoid corresponds to the postero-dorsal articulatory portion, which associated with the internal concave and smooth surfaces of the cleithrum, extracleithrum, and clavicle, suggests that the unmineralized blade of the scapulocoracoid was largely developed, as in *Latimeria*, and probably in many other fossil coelacanths. This large cartilaginous ventral blade of the scapulocoracoid explains why the small articulatory process is usually the only preserved element in fossil specimens (Mansuit *et al.* 2020). The relatively large scapulocoracoid of coelacanths differs from many other osteichthyans, where the scapulocoracoid is usually small compared with other components of the pectoral girdle (Janvier 1996), whereas among sarcopterygians large scapulocoracoids also convergently evolved in the lungfish *Neoceratodus forsteri* Krefft, 1870 (Johanson *et al.* 2004) and among tetrapodomorphs (Vickaryous & Hall 2006).

Assembly and evolution of the coelacanth hyobranchial skeleton

The hyobranchial skeleton, a portion of the visceral skeleton (or splanchnocranium) of gnathostomes plays not only an essential role in breathing for aquatic jawed vertebrates, but also assists in the opening of the jaws and the expansion of the bucco-pharyngeal cavity during suction feeding (e.g., Lauder & Reilly 1994; Dutel *et al.* 2015a). Among piscine gnathostomes, the gills (or hemibranchs) are supported by endoskeletal segmented elements (or arches), lying medially to branchial blood vessels and nerves. The primitive configuration of the gnathostome hyobranchial skeleton consists of the hyoid arch and five branchial (or gill) arches (Nelson 1969; Pradel *et al.* 2014; Dearden *et al.* 2019, 2024). A reduction of the number of branchial arches is relatively common among crown gnathostomes (e.g., four branchial arches in lungfishes and tetrapodomorphs; Janvier 1996) while supernumerary gill arches are extremely unusual (one singular exception are hexanchiform sharks with six gill arches, and among them *Heptranchias* Rafinesque, 1810 with seven gill arches; Janvier 2004). Nevertheless, precise counting of the branchial arches is often difficult in fossil specimens due to their variable ossification degree, which usually decreases in the rearmost arches. Cases of completely preserved and ossified hyoid and branchial arches are rare in the Palaeozoic, not only among coelacanths, but also in gnathostomes as a whole (e.g., Brazeau *et al.* 2017; Coates *et al.* 2018; Dearden *et al.* 2019, 2024; Pradel *et al.* 2021).

The plesiomorphic configuration of the hyobranchial skeleton of osteichthyans consists of a hyoid arch, divided from ventral to dorsal into the hypohyal, ceratohyal, and hyomandibula, followed by the branchial arches, in turn divided into hypobranchials, ceratobranchials, epibranchials, and pharyngobranchials (infra- and suprapharyngobranchials in certain cases), with the whole system ventrally linked to the median basibranchial series, including an anterior basihyal, a variable number of basibranchials, and a posterior urohyal in certain cases (Nelson 1969; Pradel *et al.* 2014). One or two small bones may be interconnected between the ceratohyal and the hyomandibula in osteichthyans: the symplectic and the interhyal (Millot & Anthony 1958; Véran 1988; Argyriou *et al.* 2022). Five branchial arches are plesiomorphic for sarcopterygians (Janvier 1996) with coelacanths (Forey 1998) and porolepiforms (e.g., *Laccognathus panderi* Gross, 1941; Kanyukin 2006) displaying this condition. On the other hand, early dipnoans (e.g., *Griphognathus* Gross,

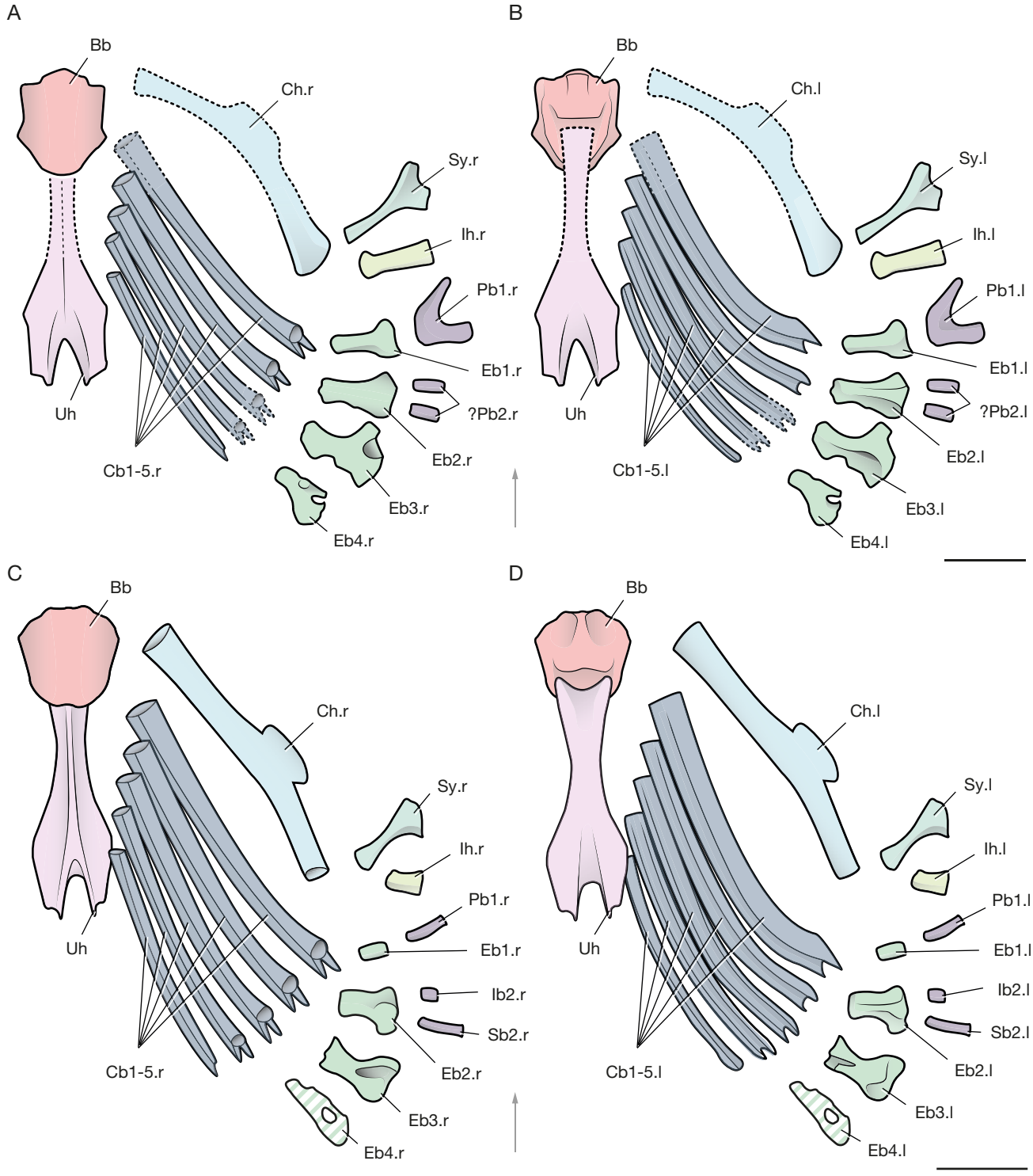

FIG. 14. — Hyobranchial skeleton of *Aemilia stellata* n. gen., n. sp. (AMNH FF 20686) and *Latimeria chalumnae* Smith, 1939 (based on direct observations on MNHN C7 and MHNG 1080.070): **A**-**D**, schematical reconstrution as if spread horizontally of the ossified elements of the hyobranchial skeleton of *Aemilia stellata* n. gen., n. sp. (**A**, **B**) and *Latimeria chalumnae* (**C**, **D**) in dorsal (**A**, **C**) and ventral (**B**, **D**) views. The symplectic, interhyal, and the epibranchial and pharyngobranchial series are seen in medial (**A**, **C**) and lateral (**B**, **D**) views. The fourth epibranchial of *Latimeria chalumnae* is cartilaginous and is represented hatched. The dental plates on the basibranchial and ceratobranchials and the cartilage extensions in *Latimeria chalumnae* have been omitted. Abbreviations: **Bb**, basibranchial; **Cb1.l**, first left ceratobranchial; **Cb1.r**, first right ceratobranchial; **Cb2.l**, second left ceratobranchial; **Cb2.r**, second right ceratobranchial; **Cb3.l**, third left ceratobranchial; **Cb3.r**, third right ceratobranchial; **Cb4.l**, fourth left ceratobranchial; **Cb4.r**, fourth right ceratobranchial; **Cb5.l**, fifth left ceratobranchial; **Cb5.r**, fifth right ceratobranchial; **Ch.l**, left ceratohyal; **Ch.r**, right ceratohyal; **Eb1.l**, first left epibranchial; **Eb1.r**, first right epibranchial; **Eb2.l**, second left epibranchial; **Eb2.r**, second right epibranchial; **Eb3.l**, third left epibranchial; **Eb3.r**, third right epibranchial; **Eb4.l**, fourth left epibranchial; **Eb4.r**, fourth right epibranchial; **Ib2.l**, second left infrapharyngobranchial; **Ib2.r**, second right infrapharyngobranchial; **Ih.l**, left interhyal; **Ih.r**, right interhyal; **?Pb.2.l**, second left infra- or supraphrayngobranchial; **?Pb.2.r**, second right infra- or supraphrayngobranchial; **Sb2.l**, second left suprapharyngobranchial; **Sb2.r**, second right suprapharyngobranchial; **Sy.l**, left symplectic; **Sy.r**, right symplectic. **Arrow** points anteriorly. Scale bars: A, B, 10 mm; C, D, 50 mm. Credits: drawings made by Jorge Mondéjar Fernández.

1956, *Chirodipterus* Gross, 1933) and their close relatives (e.g., *Youngolepis praecursor* Chang & Yu, 1981) only show four branchial arches (Miles 1977; Cui *et al.* 2022) and no more than four branchial arches can be confidently identified in tetrapodomorph fishes (e.g., *Eusthenopteron foordi* Whiteaves, 1881, *Medoevia lata* Lebedev, 1995, *Mandageria fairfaxi* Johanson & Ahlberg, 1997; Jarvik 1954; Lebedev 1995; Johanson & Ahlberg 1997) and early tetrapods (Witzmann 2013). The exact number of branchial arches in onychodontids is still unknown (Andrews *et al.* 2006; Mondéjar-Fernández 2020).

The organization of the coelacanth hyobranchial skeleton is considered unusual among bony fishes. Coelacanths, exemplified by *Latimeria*, are remarkable in lacking a basihyal (present in actinopterygians and other sarcopterygians) and hypobranchials, resulting in a direct contact of the single basibranchial with the ceratobranchials. A small cartilaginous hypohyal is present in *Latimeria chalumnae*, but it is unknown in all other coelacanths (Millot & Anthony 1958; Wiley 1979; Forey 1998). Indeed, gill arches in fossil coelacanths are rarely preserved, and when found they are greatly incomplete, fragmentary or displaced from their original position. Among these, the upper portion of the branchial skeleton is poorly known and, in many cases, confusingly illustrated. This is due to the fact that most of our knowledge on the branchial arches come from flattened specimens. Observations on *Latimeria* also revealed a reduction of ossification (decrease of periosteal thickness) occurring from lateral to medial in the cerato-, epi-, and pharyngobranchial series (Millot & Anthony 1958; Forey 1998; Manuelli *et al.* 2023, 2024). This pattern may explain why so many elements from the hyobranchial skeleton are often missing or unpreserved in fossil coelacanths. Moreover, the anatomy of many early coelacanths does not necessarily match that of *Latimeria*, thus complicating the identification of elements. Because of these issues, the gill arches of fossil coelacanths are among the least surveyed skeletal systems of their anatomy and thus few evolutionary trends can be recognized (Forey 1998). Nevertheless, exceptionally preserved fossil specimens like *Graulia* (Manuelli *et al.* 2024) and *Aemilia stellata* n. gen., n. sp. may reveal new and unexpected combinations of characters that could shed light on the organization and evolution of the hyobranchial skeleton in coelacanths.

Hyoid arch

Hyomandibula

The hyomandibula of *Latimeria chalumnae* carries functional gills supplied with blood from an anterior loop of the first branchial artery laterally lining the hyomandibula (Millot & Anthony 1958; Hughes 1976). There is a small vestigial afferent hyoidean artery, but it does not reach the hyomandibula (Millot *et al.* 1978). The hyomandibula is the only element from the hyoid arch to carry hemibranchs, as these are absent from the more ventral elements (i.e., symplectic, interhyal, and ceratohyal). The hyomandibula is rarely preserved in fossil coelacanths, with some notable exceptions in which it is partially ossified: *Miguashaia*, *Gavinia*, *Diplocercides*, *Laugia*, and probably *Coelacanthus* (Stensiö 1932, 1937; Schaumberg 1978; Long 1999; Forey 1998; Clement *et al.* 2024). The hyomandibula is entirely cartilaginous in *Latimeria chalumnae* (Millot & Anthony 1958).

In *Aemilia stellata* n. gen., n. sp., no distinctive hyomandibula has been identified, despite the fact that the complete hyobranchial skeleton is preserved in close proximity and almost in articulation. As such, we can confidently affirm that the absence of a hyomandibula in many fossil coelacanths preserving relatively complete skull remains (e.g., *Ngamugawi*, *Graulia*, *Ticinepomis*) is most likely due to its cartilaginous nature (Cavin *et al.* 2013; Manuelli *et al.* 2024; Clement *et al.* 2024). Moreover, given the distribution of partially ossified hyomandibulae, occurring almost exclusively in Devonian coelacanths (with the exception of *Laugia*, known by its exceptionally developed ossification for an early Mesozoic coelacanth; Stensiö 1932; Forey 1998), we can also state that cartilaginous hyomandibulae became common in post-Devonian taxa probably representing the first element associated with the braincase to become largely cartilaginous in coelacanth evolutionary history. *Ngamugawi* from the Upper Devonian (Frasnian) is currently the earliest representative of an inferred cartilaginous hyomandibula (Clement *et al.* 2024). The causes of the shift from ossified to cartilaginous hyomandibulae are still unknown but it may be related to a functional decoupling of the hyomandibula and the ceratohyal early in coelacanth evolutionary history.

Symplectic

The symplectic is a distinctive bone of coelacanths, listed as one of the synapomorphies of the Actinistia, forming part of the tandem jaw articulation between the quadrate and the articular anteriorly and between the sympletic and the retroarticular posteriorly (Forey 1998). In *Latimeria chalumnae*, the symplectic articulates via large cartilaginous caps with the ceratohyal and the interhyal dorsally, and with the retroarticular of the lower jaw ventrally (Millot & Anthony 1958) playing an important role in the complex mechanisms of the jaw opening (Dutel *et al.* 2015a). The symplectic is usually well ossified and thus it is known in many fossil coelacanths, both from the Palaeozoic and Mesozoic (Table 1), however, it may differ in size between taxa. This may be due to the incomplete ossification of its ends, which are cartilaginous in *Latimeria*. The symplectic of *Aemilia stellata* n. gen., n. sp. (Sy; Figs 3E-H; 4E-H; 10E, F, I, J; 12A-E; 14A, B) is reminiscent both in shape and length to that of *Laugia* (Forey 1998), suggesting that it may also have been substantially ossified, especially the double articulatory dorsal portion. Relatively smaller symplectics found in younger taxa (e.g., *Coccoderma*, *Libys* Münster, 1842, *Ticinepomis*, *Whiteia*, *Graulia*; Münster 1842; Forey 1998; Cavin *et al.* 2013; Yabumoto *et al.* 2019; Manuelli *et al.* 2024) may indicate a slight decrease in ossification of the extremities of this bone after the Carboniferous, as displayed in *Latimeria* (Fig. 14C, D).

Interhyal

The interhyal (sometimes called stylohyal) is a small ossification of the hyoid arch of osteichthyans. In *Latimeria chalumnae*, it articulates dorsally with the hyomandibula, and ventrally with the ceratohyal and the symplectic (Millot & Anthony 1958; Manuelli *et al.* 2023, 2024). Certain actinopterygians (i.e., *Polypterus* Lacepède, 1803 and neopterygians) also possess an interhyal, but its homology with the coelacanth interhyal or symplectic is difficult to decipher (Patterson 1982; Argyriou *et al.* 2022). The recent identification of an interhyal element in the stem chondrichthyan *Acanthodes confusus* Heidtke, 2011 (Dearden *et al.* 2024) suggests that, irrespective of its homology with the interhyal or symplectic of osteichthyans, a separate element between the ceratohyal and the hyomandibula may be a crown-group gnathostome symplesiomorphy. The interhyal is rarely found in fossil coelacanths, as it was small and probably only partly ossified. Among Palaeozoic coelacanths, it was only previously known in the Devonian *Diplocercides* (Stensiö 1937) and subsequently in the Triassic *Graulia* (Manuelli *et al.* 2024), *Ticinepomis* (Cavin *et al.* 2013), and *Wimania* (termed 'epihyal' by Stensiö 1921). In *Sassenia*, Stensiö (1921) also described an 'epihyal', but in this case it most likely corresponds to the symplectic. In *Aemilia stellata* n. gen., n. sp. (Ih; Figs 3E-H; 4E-H; 10C, D, G, H; 12A-E), the interhyal is preserved exceptionally as a small tubular element, representing the second confident occurrence of this bone in a Palaeozoic coelacanth. Size comparisons between taxa like *Aemilia stellata* n. gen., n. sp., *Graulia* (Manuelli *et al.* 2024), and *Latimeria* (Fig. 14) suggest that the relative reduction in size of the interhyal from the Palaeozoic to Recent may be due to a partial reduction of the ossification of this bone across coelacanth evolution.

Ceratohyal

The ceratohyal is a long and narrow bone that carries a remarkable blade-like process ventrally, giving it a characteristic shape in fossil coelacanths. As such, and as opposed to the ceratobranchials, the ceratohyal does not display a ventral groove for the passage of blood vessels (Millot *et al.* 1978; Fig. 14). In *Latimeria chalumnae*, both the anterior (ventral) and posterior (dorsal) ends of the ceratohyal are capped by cartilage, as is the blade-like process, resulting in a more rounded profile to the ventral edge (Millot & Anthony 1958). The cartilage pad is especially developed on the posterior (dorsal) end, laterally swollen and developed at a right angle with the rest of the bone for the articulation with the interhyal and the symplectic. The absence of this cartilaginous knob in fossil coelacanths always gives to the rear end of the ceratohyal a straight to slightly concave profile (e.g., *Dobrogeria*, *Graulia*, *Axelrodichthys*; Cavin & Grădinaru 2014; Fragoso *et al.* 2018; Manuelli *et al.* 2024). In *Aemilia stellata* n. gen., n. sp. (Ch; Figs 2F-H;3E-H; 4E-H; 10A, B; 12A-E; 14A, B), most of the bone has been preserved as an imprint in the nodule and few information can be obtained from it, but the left ceratohyal preserves the posterior end, which is also slightly concave in shape. The overall shape of the ceratohyal is usually constant across all coelacanths, as it is always well ossified when present, but in *Moenkopia* Schaeffer & Gregory, 1961 and *Axelrodichthys* they have been described as relatively shorter than in other taxa (Schaeffer & Gregory 1961; Fragoso *et al.* 2018).

In *Latimeria chalumnae*, a small and cartilaginous hypohyal occurs anterior to the ceratohyal, articulating with the basibranchial (Millot & Anthony 1958; Wiley 1979). Among sarcopterygians (e.g., onychodontids, porolepiforms, lungfishes, and tetrapodomorphs) a separate and ossified hypohyal is usually present and constitutes the anterior-most element of the hyoid arch (Jarvik 1954, 1972; Miles 1977; Cloutier & Schultze 1996; Andrews *et al.* 2006; Kanyukin 2006). Ossified hypohyals have not been found in any fossil coelacanth, suggesting that they have always been cartilaginous in coelacanths.

Branchial arches

Pharyngobranchials

The pharyngobranchial series of osteichthyans is divided into two separate elements: suprapharyngobranchials and infrapharyngobranchials. Suprapharyngobranchials have usually been considered a synapomorphy of osteichthyans (Friedman & Brazeau 2010), however their presence in the chondrichthyans *Ozarcus mapesae* Pradel, Maisey, Tafforeau, Mapes & Mallat, 2014 and perhaps in *Falcatus falcatus* Lund, 1985 suggests that the combined presence of supra- and infrapharyngobranchials is a plesiomorphic character in crown gnathostomes (Pradel *et al.* 2014). In osteichthyans, suprapharyngobranchials are posteriorly oriented, whereas the infrapharyngobranchials are anteriorly oriented, and likely homologous to the single pharyngobranchials of other crown gnathostomes, regardless of their orientation (Pradel *et al.* 2014; Dearden *et al.* 2024). In *Latimeria chalumnae*, only three pharyngobranchial elements are ossified, associated with the first two branchial arches (Millot & Anthony 1958; Manuelli *et al.* 2023, 2024; Fig. 14C, D). The first pharyngobranchial is a single rod-like element comparable to a suprapharyngobranchial owing to its posterodorsal orientation. Dorsally, it articulates with the braincase via a cartilaginous parampullary process. A separate infrapharyngobranchial is not present, suggesting that either it was completely missing or it may have fused with the suprapharyngobranchial (Nelson 1969). The second arch displays both a rod-like suprapharyngobranchial and a smaller, swollen infrapharyngobranchial. Further pharyngobranchials may be represented by small cartilages attached to the tips of the epibranchials on the third and fourth arches, but this is still unclear (Millot & Anthony 1958; Forey 1998).

In *Aemilia stellata* n. gen., n. sp., reconstructing the pharyngobranchial series is puzzling, as the small and barely ossified elements have been found slightly shifted from their original position (Fig. 4). *Aemilia stellata* n. gen., n. sp. preserves three putative pharyngobranchial elements: a large boomerang-shaped first pharyngobranchial (Pb1; Figs 3; 4; 11F, G; 12; 14A, B) and two small ossifications, probably corresponding to the supra- and infrapharyngobranchials of the second branchial arch (?Pb2; Figs 3; 4; 11H, I; 12; 14A, B). The latter identification is based on comparisons with *Latimeria*

chalumnae (JMF pers. obs., Manuelli *et al.* 2023, 2024) in which the infra- and suprapharyngobranchials of the second arch are the only ossified elements from the medial pharyngobranchial series (Fig. 14C, D). It is unclear whether pharyngobranchials associated with the third branchial arch may have been present in *Aemilia stellata* n. gen., n. sp. The absence of preserved pharyngobranchials in many fossil coelacanths (Table 1) may suggest that the more medial elements of the pharyngobranchial series were not ossified, as in *Latimeria*.

The element from the hyobranchial skeleton of *Aemilia stellata* n. gen., n. sp. that most differs in shape from that of other coelacanths is undoubtedly the first pharyngobranchial (Pb1; Fig. 11F, G; 14A, B). The characteristic boomerang shape contrasts with the rod-like first pharyngobranchial of *Laugia* (Forey 1998) and *Latimeria* (Millot & Anthony 1958; Fig. 14C, D), and no such shape is known in any other coelacanth. However, it is reminiscent of the pharyngobranchial of the Devonian tetrapodomorph *Eusthenopteron foordi* (Jarvik 1954). Most likely, the condition of *Eusthenopteron* represents a fusion between separate supra- and infrapharyngobranchial of early osteichthyans (Nelson 1969), resulting in a square-shaped element (Jarvik 1954: fig. 17), similar to that of *Aemilia stellata* n. gen., n. sp. However, in *Eusthenopteron* the left pharyngobranchial bears a foramen at its base, whereas the right one solely displays a notch. This groove or foramen allows the passage of the branchial artery and the glossopharyngeus nerve (Jarvik 1954: figs 43, 47) from the braincase into the branchial arches. Such foramina or grooves are absent in *Aemilia stellata* n. gen., n. sp., probably indicating that the course of the artery and nerve may have been more lateral to the first pharyngobranchial than in *Eusthenopteron*. In *Aemilia stellata* n. gen., n. sp., a putative articulatory surface on the prootic with the dorsal end of the suprapharyngeal portion of the pharyngobranchial (s.Pb1; Fig. 11G) has not been retrieved (the parampullary process in *Latimeria*), as it would have been made of cartilage as the major part of the lateral commissure of the prootic. In *Eusthenopteron*, Jarvik (1954) described that the articulation facet for the infrapharyngeal portion of the pharyngobranchial was located close to the groove for the lateral aorta, ventral to the lateral fontanelle and the ventral hyomandibular facet, but again, this portion of the prootic is too irregularly preserved in *Aemilia stellata* n. gen., n. sp. to be confidently reconstructed.

It is currently difficult to explain the similarities of the dorsal portion of the branchial apparatus between *Aemilia stellata* n. gen., n. sp. and *Eusthenopteron foordi*. Could they represent a retention of a plesiomorphic morphology for sarcopterygians or a convergence between coelacanths and 'osteolepiforms'? Moreover, could the simplification of the first pharyngobranchial with cylindrical shape as in *Laugia* (Forey 1998) and *Latimeria* (Fig. 14C, D) constitute another evolutionary trend in coelacanth evolution? If we consider the odd shape displayed by *Aemilia stellata* n. gen., n. sp. as the plesiomorphic state for the common ancestor of coelacanths and rhipidistians (including *Eusthenopteron*), the condition displayed in *Laugia* and *Latimeria* may be considered derived, illustrating a certain degree of morphological disparity and evolvability in the coelacanth hyobranchial skeleton. It is challenging to support this statement given the scarcity of well-preserved branchial series in fossil coelacanths and many other Palaeozoic sarcopterygians.

Epibranchials

The epibranchial series of coelacanths is remarkable among gnathostomes. As in other osteichthyans, coelacanths only possess four epibranchials (Forey 1998; Carvalho *et al.* 2013), as displayed in *Latimeria chalumnae*. However, in early osteichthyans, the size of the elements decreases from lateral to medial (or anterior to posterior; e.g., *Eusthenopteron foordi*, *Raynerius splendens* Giles, Darras, Clément, Blieck & Friedman, 2015, *Mimipiscis toombsi* Gardiner & Bartram, 1977, *Brachydegma caelatum* Dunkle, 1939; Jarvik 1954; Nelson 1969; Gardiner 1984; Giles *et al.* 2015; Argyriou *et al.* 2022), while in coelacanths the largest elements are more medial (or posterior) than lateral (or anterior). *Aemilia stellata* n. gen., n. sp. displays this pattern in which the largest epibranchial of the series is the third one (Eb3; Fig. 11N-Q; 13; 14A, B), as is the case in *Rhabdoderma* (Forey 1981, 1998) and *Graulia* (Manuelli *et al.* 2024). In these taxa, the epibranchial 3 carries a large canal for the passage of the efferent artery, as in *Latimeria* (Millot & Anthony 1958; Fig. 14C, D). In *Graulia* (Manuelli *et al.* 2024: fig. 12), the canal appears dorsally open, whereas in *Rhabdoderma* (Forey 1981: fig. 3) and *Aemilia stellata* n. gen., n. sp. it is fully closed. The epibranchial 1 (Eb1) of *Aemilia stellata* n. gen., n. sp. (Fig. 11J, K; 14A, B) is significantly larger than the rod-like and mainly cartilaginous epibranchial 1 in *Latimeria* (Fig. 14C, D), but it resembles more closely the stouter and well-ossified epibranchial 1 of *Laugia* (Forey 1998: fig. 6.6D) by its expanded anterior (dorsal) extremity. A similar shape and degree of ossification also occurs in the putative epibranchials of the Triassic *Dobrogeria* (Cavin & Grădinaru 2014). In *Eusthenopteron*, Jarvik (1954) described a dorsal groove on the epibranchials 1 and 2 for the passage of the efferent artery and the ramus posttrematicus of the nerve glossopharyngeus (rp.IX.v, Jarvik 1954: fig. 43, 47) running from the dorso-lateral side of the epibranchials to end on the medial side of the articulating ceratobranchial, where it is continued by the ceratobranchial ventral groove. A similar feature has also been identified in the "acanthodian" *Acanthodes confusus* (Dearden *et al.* 2024), revealing that this may be a generalized gnathostome character. In *Latimeria*, the epibranchial 1 is greatly reduced compared with that of *Aemilia stellata* n. gen., n. sp. (Fig. 14) and *Laugia* (Forey 1998), and the course of the groove is difficult to follow in the epibranchial 2 as it may have simply run along the dorso-lateral side of the bone. No distinct groove is present in the epibranchial 2 of *Graulia* (Manuelli *et al.* 2024). However, in *Aemilia stellata* n. gen., n. sp., the putative course of this groove is more marked, associated with a ridge medially framing it.

Aemilia stellata n. gen., n. sp. preserves the right and left epibranchial 4 (Eb4; Fig. 11R, S; 13; 14A, B), which is extremely morphologically reminiscent to that of *Latimeria chalumnae* (Millot & Anthony 1958: fig.14B, wrongly labelled as "*troisième épibranchial*" [third epibranchial]; Fig. 14). The epibranchial 4

in *Aemilia stellata* n. gen., n. sp. and *Latimeria* is pierced by a foramen for the branchial artery, but in *Latimeria* this element is entirely cartilaginous while in *Aemilia stellata* n. gen., n. sp. it is fully ossified. Variations in size and ossification degree of the epibranchial series identified in *Aemilia stellata* n. gen., n. sp. may reveal two different evolutionary trends: 1) the reduction in size and ossification degree of the epibranchial 1 as seen in *Latimeria* compared with taxa like *Laugia* (Forey 1998) and *Dobrogeria* (Cavin & Grădinaru 2014) could constitute a trend of post-Triassic coelacanths; and 2) the lack of preservation of the medial-most epibranchial of the series in younger, but otherwise well-preserved fossil coelacanths like the Triassic *Graulia* (Manuelli *et al.* 2024) may indicate that the loss of ossification of the epibranchial 4 occurred in post-Carboniferous coelacanths and was maintained until Recent. However, these hypothetical trends still need to be tested by additional discoveries of well-preserved and complete branchial material from Mesozoic taxa.

Ceratobranchials

The ceratobranchials are the most commonly found elements from the branchial skeleton in fossil coelacanths, certainly owing to their larger size and more ossified condition among the other bones forming the arches. The ceratobranchials are large and curved elements, always five in number (when fully preserved), carrying a ventral groove for the superficial afferent and the more internal efferent branchial arteries (Millot *et al.* 1978; Wiley 1979), with the exception of the ceratobranchial 5, which is always the smallest. The latter lacks a groove, and, as in other sarcopterygians, does not articulate with the basibranchial ventrally, but with the ceratobranchial 4 (Wiley 1979; Janvier 1996; Datovo & Johnson 2025). As such, only the first four branchial arches carry gills, as evidenced in *Latimeria* (Hughes 1976; Hughes & Morgan 1973). In fossil coelacanths, the ceratobranchials may have directly articulate with the basibranchial, without the occurrence of hypobranchials as in other sarcopterygians (Jarvik 1954, 1972; Miles 1977; Cloutier & Schultze 1996; Andrews *et al.* 2006; Kanyukin 2006). In *Latimeria chalumnae*, the anterior (ventral) and posterior (dorsal) tips of each ceratobranchial are capped with a cartilage knob, which can be significantly large, prolonging the bones in both directions (Millot & Anthony 1958); as such the ceratobranchials of fossil coelacanths are always relatively shorter than those of *Latimeria*. In *Latimeria*, the posterior (dorsal) cartilaginous articular heads of the ceratobranchials are complex in shape and display two swellings: one for the adjacent epibranchial and the other for the branchial elevator muscle related to the arch, impossible to retrieve in fossil specimens.

As seen in *Aemilia stellata* n. gen., n. sp. (Figs 4; 11A-F; 12; 14A, B), the ceratobranchials maintain the same width along their entire length in almost all coelacanths (e.g., *Coelacanthus*, *Dobrogeria*, *Axelrodichthys*, and *Latimeria*; Forey 1998; Cavin & Grădinaru 2014; Fragoso *et al.* 2018); however, slight morphological variations are also known. For instance, the ceratobranchials of *Ngamugawi* (Clement *et al.* 2024), *Luopingcoelacanthus* Wen, Zhang, Hu, Benton, Zhou, Tiao, Huang & Chen, 2013 (Wen *et al.* 2013), *Ticinepomis* (Cavin *et al.* 2013), and *Mawsonia* (Forey 1998; Toriño *et al.* 2021b, 2024) are expanded anteriorly at the articulation with the basibranchial, whereas in *Whiteia* (Stensiö 1921) and *Polyosteorhynchus* Lund & Lund, 1984 (Lund & Lund 1984, 1985), the expansion occurs posteriorly. The degree of curvature is also variable, with most taxa displaying straight to weakly curved ceratobranchials (e.g., *Caridosuctor*, *Rhabdoderma*, *Whiteia*, *Mawsonia*, and *Latimeria*; Forey 1998; Toriño *et al.* 2021b, 2024; Clement *et al.* 2024), whereas in others they are more strongly curved (e.g, *Ngamugawi*, *Dobrogeria*, *Parnaibaia* Yabumoto, 2008, *Luopingcoelacanthus*, *Macropoma*; Forey 1998; Wen *et al.* 2013; Cavin & Grădinaru 2014; Clement *et al.* 2024). These variations are unevenly distributed across coelacanth phylogeny and do not seem to constitute a particular evolutionary trend.

Basibranchial series

Basibranchial

The basibranchial series of coelacanths is relatively simple compared with other sarcopterygians (Janvier 1996). A distinct basihyal is absent, as in porolepiforms (e.g., *Laccognathus* Gross, 1941, *Glyptolepis* Agassiz, 1844; Jarvik 1972; Kanyukin 2006), but different to lungfishes, (e.g., *Griphognathus*, *Chirodipterus*, *Neoceratodus*; Miles 1977; Nelson, 1969) and tetrapodomorphs (e.g., *Eusthenopteron*, *Mandageria*) in which the sublingual rod may be considered a form of basihyal (Jarvik 1954; Johanson & Ahlberg 1997). Coelacanths are thus characterized by possessing a single basibranchial (or copula), similar to onychodontids (e.g., *Onychodus jandemarrai* Andrews, Long, Ahlberg, Barwick & Campbell, 2006; Andrews *et al.* 2006) and porolepiforms (Jarvik 1972; Kanyukin 2006) but again different from lungfishes and tetrapodomorphs which display two basibranchial elements (Miles 1977; Jarvik 1980; Janvier 1996). In certain specimens of *Latimeria chalumnae*, the cartilaginous portion can show traces of a partial division, leading to speculations that the single basibranchial of coelacanths is the result of a fusion between two (or more) separate ossifications present in early osteichthyans (Nelson 1969; Forey 1998). Millot & Anthony (1958) proposed that the copula in *Latimeria* results from the fusion of an anterior basihyal for the articulation with the hyoid arch and a posterior basibranchial for the articulation with the branchial arches. Comparisons with extant sarcopterygians, like the axolotl, suggest that the second basibranchial of certain tetrapods may be homologous with the urohyal of coelacanths and thus of other sarcopterygians (Sefton *et al.* 2015), not with the second basibranchial as seen in *Eusthenopteron* (Jarvik 1954).

In *Latimeria*, the basibranchial is large and diamond-shaped as formed mainly by cartilaginous expansions surrounding a smaller central ossification (Millot & Anthony 1958), which is the only portion found in fossil coelacanths, as seen in *Aemilia stellata* n. gen., n. sp. (Fig. 14). The coelacanth basibranchial is thus of endoskeletal origin and articulates anteriorly with the ceratohyal, laterally with the first four ceratobranchials, and ventrally with the urohyal (Wiley 1979). However, due to the cartilaginous nature of the connections between the

ceratobranchial and basibranchial as seen in *Latimeria* it is difficult to reconstruct the precise point of insertion of each ceratobranchial along the lateral margins of the ossified portion of the basibranchial in fossil coelacanths.

Urohyal

The urohyal is one of the most characteristic bones of coelacanths and is overall constant in shape throughout their evolution, although slight variations can be observed. Morphologically it resembles an inverted Y, with a narrow anterior section and a larger and bifid posterior portion overlapping the junction between the clavicles. This is different from the urohyal of other sarcopterygians like the porolepiform *Glyptolepis* (Jarvik 1972), the dipnoan *Griphognathus* (Miles 1977), and the 'osteolepiform' *Eusthenopteron* (Jarvik 1954), which is deeper and narrower and more plate-like, but it also differs from that of actinopterygians where it is plate-like and vertically expanded (e.g., *Birgeria* Stensiö, 1919) or rod-like (e.g., teleosts; Arratia & Schultze 1990). The urohyal of onychodontids is unknown (Andrews *et al.* 2006). Another important difference is that the coelacanth urohyal is of endoskeletal origin, as in other sarcopterygians (i.e., dipnomorphs and tetrapodomorphs; Jarvik 1954, 1972; Miles 1977) and thus generally considered not homologous to the urohyal of actinopterygians (Sefton *et al.* 2015) where it is a tendon bone (e.g., *Polypterus*) or a dermal bone (e.g., teleosts; Arratia & Schultze 1990). However, Millot & Anthony (1958) proposed that the urohyal of *Latimeria chalumnae*, and thus of coelacanths, may represent a compound bone: the thin, axial section articulating with the basibranchial is endochondral, whereas a peripheral sheat of bone surrounding it would be of dermal origin. To our knowledge, this hypothesis has not yet been tested.

The earliest evidence of the characteristic coelacanth urohyal can be found in *Diplocercides*, already in the Late Devonian (Stensiö 1922), revealing a rapid separation from the other morphologies of early osteichthyans. The main differences in urohyal shape among coelacanths usually include the width of the gap separating the posterior lobes and their acuteness, the width of the anterior portion, or the level of constriction between the anterior and posterior portions (Romano *et al.* 2016). Another notable variation concerns the anterior portion that articulates with the basibranchial, which is bifid in *Coelacanthus*, *Ticinepomis*, *Polyosteorhynchus*, *Whiteia*, and *Megalocoelacanthus* (Schaumberg 1978; Lund & Lund 1984, 1985; Forey 1998; Dutel *et al.* 2012; Cavin *et al.* 2013) as opposed to unifid in other taxa (e.g., *Ngamugawi*, *Diplocercides*, *Caridosuctor*, *Dobrogeria*, *Axelrodichthys*, *Latimeria*; Clement *et al.* 2024). In *Aemilia stellata* n. gen., n. sp., the anterior end is unfortunately missing and most of the middle section is preserved as an imprint in the nodule; only the posterior portion can be reconstructed (Fig. 14A, B). The gap between the two bifid projections is shorter but wider than in *Diplocercides* (Jarvik 1954) resulting in a larger and more massive urohyal overall, more similar to that of *Rhabdoderma*, *Coelacanthus*, *Wimania*, and *Trachymetopon* (Schaumberg 1978; Forey 1998; Dutel *et al.* 2015b) than the thin and elongate one of *Diplocercides*, *Ticinepomis*, and *Megalocoelacanthus* (Forey 1998; Dutel *et al.* 2012; Cavin *et al.* 2013). However, given the phylogenetic distribution of the different morphologies, no clear evolutionary pattern can explain the morphological disparity of the urohyal across coelacanths.

Branchial dentition

Numerous dental plates are associated with the ventral portion of the hyobranchial skeleton in coelacanths, covering the dorsal surface of the basibranchial and ceratobranchials. These dental plates are covered by small pointed denticles but are never modified into crushing plates as in certain actinopterygians (Nelson 1969), as such they were probably used for holding prey in the mouth cavity or as filtering systems, analogous in function to the gill rackers of some actinopterygians. The plates have undergone modifications, transforming the number and size of the plates, probably through processes of fusion of smaller plates into larger ones, especially on the basibranchial. A series of small tooth plates cover the ceratobranchials (e.g., three main rows in *Latimeria* and *Rhabdoderma*, two rows in *Graulia*, and one row in *Undina*; Reis 1888; Millot & Anthony 1958; Forey 1981, 1998; Forey *et al.* 1985; Manuelli *et al.* 2024) but these are sometimes difficult to count in other fossil coelacanths due to their small size and tendency to be found disarticulated.

A consolidation of the basibranchial dentition is one of the single evolutionary trends identified by Forey (1998: fig. 7.6) with respect to the hyobranchial skeleton. In the basibranchial series of early coelacanths, dental plates are usually arranged symmetrically in parallel rows composed of numerous quadrangular platelets of similar size (e.g., *Laugia*, *Whiteia*; Forey 1998), reminiscent of basal actinopterygians like *Polypterus* (Nelson 1969), whereas younger coelacanths display larger and more elongate plates (e.g., *Graulia*, *Diplurus*, *Axelrodichthys*, *Megalocoelacanthus*, and *Macropoma*; Forey 1998; Dutel *et al.* 2012; Manuelli *et al.* 2024; Ferrante & Cavin 2025). The case of the Cretaceous *Macropoma* and *Megalocoelacanthus* is of particular interest since the anterior pair of plates appears to have fused into a larger plate (Forey 1998; Dutel *et al.* 2012). Large plates arranged in two median pairs or less only occur in the Mesozoic among the Latimerioidei, probably representing a diagnostic feature of the clade (Manuelli *et al.* 2024). One remarkable aspect of the extant *Latimeria chalumnae* is that it presents a median plate developed between the anterior and posterior pairs of basibranchial plates (Millot & Anthony 1958; Nelson 1969; Forey 1998), a condition not known in any other coelacanth. Finally, as exemplified by *Aemilia stellata* n. gen., n. sp., tooth plates are usually found disarticulated in fossil coelacanths, especially in the Palaeozoic, and thus no clear evolutionary scenarios can be reconstructed besides the observation that larger plates appear to be more common in Middle to Late Mesozoic taxa than in the Palaeozoic.

Phylogenetic implications

The new phylogenetical analysis reveals two previously unrecognized radiation episodes during the Late Palaeozoic-Early Mesozoic coelacanth evolutionary history. These radiations

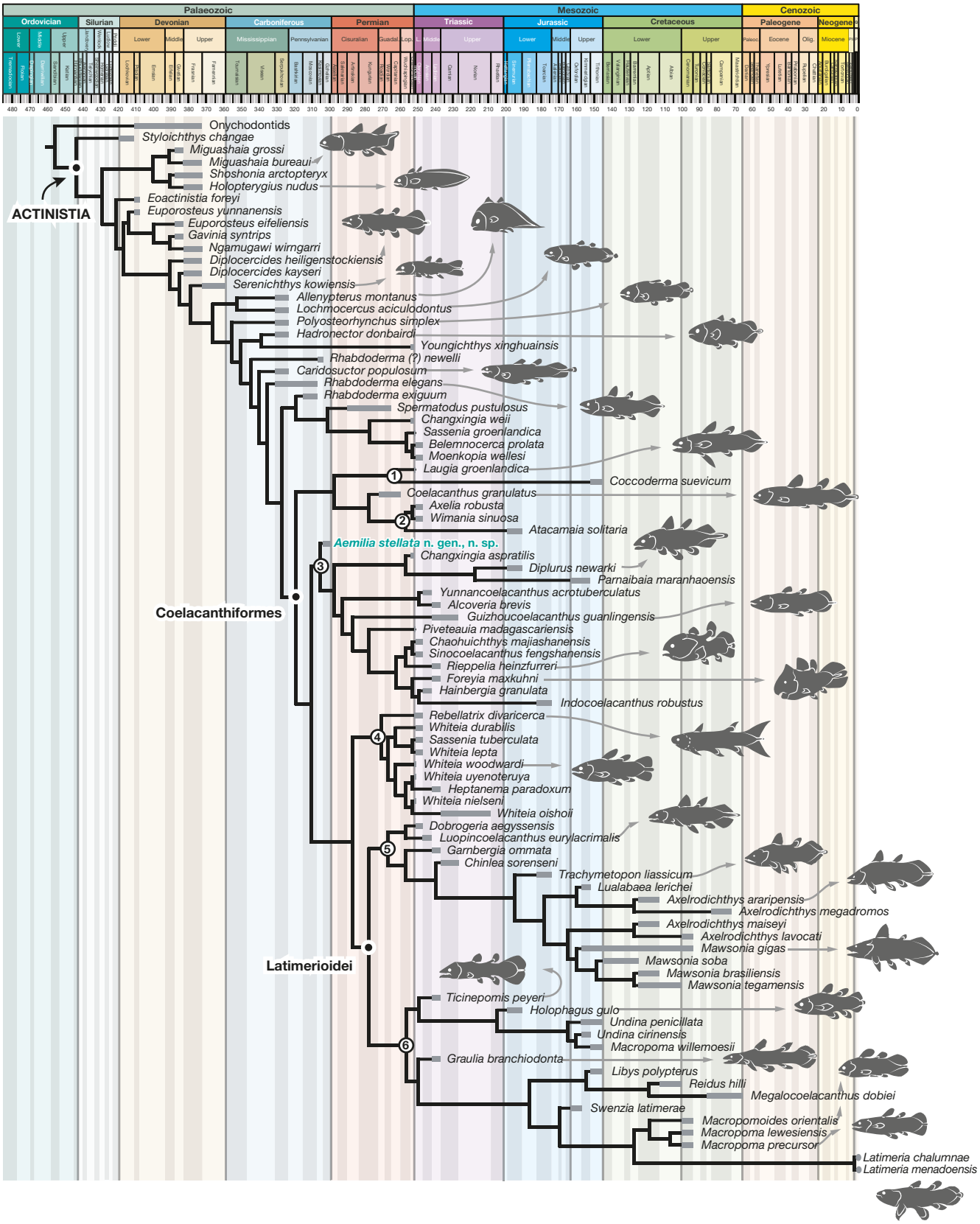

FIG. 15. — Phylogenetic relationships of coelacanths plotted against the International Stratigraphic Chart. Phylogenetic hypothesis after the Bayesian tip-dating analysis following the Fossilized Birth Death model (FBD). Clade divergence dates are based on tip-dated Bayesian inference. *Nodes*: **1**, Laugiidae; **2**, Axeliidae; **3**, unnamed clade; **4**, unnamed clade; **5**, Mawsoniidae; **6**, Latimeriidae. Coelacanth profiles not to scale (references provided in Appendix 3). Coelacanth profile silhouettes not to scale. Credits: Figure made by Jorge Mondéjar Fernández.

correspond to a Permian-Triassic-Jurassic clade to which *Aemilia stellata* n. gen., n. sp. is the sister group (clade 3; Fig. 15) and a clade including all species of *Whiteia* and other closely related taxa (clade 4; Fig. 15). The diversification of these clades encompasses the early radiation of the Latimerioidei, especially during the Triassic and Jurassic. Moreover, *Aemilia stellata* n. gen., n. sp. also constitutes the oldest representative of a larger clade comprising the main diversification episodes of coelacanths starting at the beginning of the Mesozoic. By using a phylogenetic definition, we name this clade Coelacanthiformes (Fig. 15). The recent study by Ferrante & Cavin (2025) was conducted in parallel to ours and in it they list the characters supporting the Coelacanthiformes clade, as well as other actinistian taxa. We will briefly discuss and compare their approach to ours.

The term Coelacanthini (or Coelacanthiformes) was first introduced by Huxley (1861) in his classification of fossil fishes to include the only coelacanths known at the time: *Undina penicillata* Münster, 1834, *Macropoma mantelli* Agassiz, 1835, and *Coelacanthus granulatus* Agassiz, 1839. The initial sense of Huxley's term was later synonymized with Actinistia Cope, 1871 but both names coexisted during much of the 20th century (e.g., Berg 1940; Echols 1963; Lund & Lund 1985; Long 1999). In an attempt of reinstating the term and assigning to it a proper phylogenetic definition, Forey (1998) defined the order Coelacanthiformes as "actinistians in which the otico-occipital portion of the neurocranium is fragmented to separate prootic, opisthotic, basioccipital and supraoccipital bones, with a complex suture between the prootic and the basioccipital, loss of vestibular fontanelle and buccohypophysial canal" (Forey 1998: 300), with the Permian *Coelacanthus granulatus* as its oldest member (Schultze 2004), but without a similarly rank-named sister group (Forey 1998; Ferrante & Cavin 2025). However, Forey's definition turned out to be problematic as it combined up to four different characters that have been revealed to have evolved independently among coelacanths (e.g., Ferrante & Cavin 2023, 2025; Manuelli *et al.* 2024; Clement *et al.* 2024). At the time of publication, these characters occurred simultaneously in the main taxa used by Forey to build his phylogenetic study. New discoveries have highlighted a greater morphological disparity than previously expected, resulting in a patchy distribution of these features, especially the occurrence of a closed buccohypophysial canal. Moreover, the poor record of well-preserved braincases among coelacanths makes it particularly challenging to test the putative combined occurrence of these characters in many fossil specimens.

The main characters defining the order Coelacanthiformes are found in the neurocranium, and concern the separate ossification of the otico-occipital portion and the presence or absence of buccohypophysial canal on the parasphenoid. The separation between the elements forming the otico-occipital portion of the braincase is indeed a derived character exclusively known in Mesozoic and Recent taxa (e.g., *Laugia groenlandica*, *Wimania sinuosa*, *Dobrogeria aegyssensis*, *Graulia branchiodonta*, *Rieppelia heinzfurreri*, *Diplurus newarki*, *Whiteia woodwardi*, *Axelrodichthys araripensis* Maisey, 1986, *Mawsonia gigas*, *Macropoma* (*M. lewesiensis* Agassiz, 1835 and *M. precursor* Woodward, 1909), *Holophagus gulo*, *Undina penicillata*, *Trachymetopon liassicum* Hennig, 1951, *Megalocoelacanthus dobiei* Schwimmer, Stewart & Williams, 1994, and *Latimeria chalumnae*). *Aemilia stellata* n. gen., n. sp. is the first Palaeozoic coelacanth to display this feature. Similarly, a closed buccohypophysial foramen occurs mainly in Mesozoic coelacanths like the Triassic *Axelia robusta*, *Wimania sinuosa*, *Graulia branchiodonta*, *Rieppelia heinzfurreri*, *Whiteia woodwardi*, *Luopingcoelacanthus eurylacrimalis* Wen, Zhang, Hu, Benton, Zhou, Tiao, Huang & Chen, 2013, the Jurassic *Diplurus newarki*, the Cretaceous *Axelrodichthys* (*A. araripensis*, *A. lavocati* Tabaste, 1963, *A. megadromos* Cavin, Valenti & Garcia, 2016), *Macropoma* (*M. lewesiensis* and *M. precursor*), *Undina penicillata*, *Megalocoelacanthus dobiei*, and the extant *Latimeria chalumnae*, but it has also been described in the Carboniferous *Polyosteorhynchus simplex* Lund & Lund, 1984 and *Rhabdoderma* (*R. elegans*, *R.? newelli* Hibbard, 1933). On the other hand, an open buccohypophysial foramen on the parasphenoid represents the plesiomorphic condition and is thus more common among Palaeozoic taxa (e.g., *Styloichthys changae*, *Miguashaia bureaui*, *Euporosteus eifeliensis*, *Ngamugawi wirngarri*, *Diplocercides kayseri*, *Allenypterus montanus*, *Caridosuctor populosum*, *Rhabdoderma exiguum*, *Coelacanthus granulatus*), but it also occurs in some Mesozoic taxa (e.g., *Laugia groenlandica*, *Piveteauia madagascarensis*, *Parnaibaia maranhoensis*). The case of intrageneric variation in *Rhaboderma* is remarkable: in *Rhabdoderma exiguum* Eastman, 1902 the foramen is open whereas in *Rhabdoderma elegans* it is closed.

According to Forey's (1998) initial diagnosis of the group, *Aemilia stellata* n. gen., n. sp. should not be considered a Coelacanthiformes since the buccohypophyseal foramen is plesiomorphically open (Figs 6G, H; 9B, C). However, *Aemilia stellata* n. gen., n. sp. also displays the derived conditions of a separate basioccipital and a prootic with a complex suture with the basioccipital (Figs 7Q-T; 8; 9). *Aemilia stellata* n. gen., n. sp. thus suggests that these features may not be evolutionary linked and thus their combined occurrence constitutes an unreliable argument for the definition of the order Coelacanthiformes as an apomorphy-based clade, sensu Forey (1998).

Recently, Ferrante & Cavin (2025) emended the diagnosis of the Coelacanthiformes as "actinistians characterised by the following unique combination of characters: neurocranium fragmented to separate prootic, opisthotic and basioccipital; premaxilla usually without a dorsal lamina; anterior opening of the rostral organ occurring usually within separated rostral ossicles; posterior margin of the skull roof usually embayed; subopercle usually absent; posterior opening(s) of the rostral organ usually mark as a notch(es); infraorbital sensory canal usually running through centre of the postorbital; pit lines usually not marking cheek bones; ventral margin of the basal plate of the anterior dorsal fin usually smooth." (Ferrante & Cavin 2025: 130). In their diagnosis, there is no reference to the buccohypophysial canal, as opposed to Forey (1998), and this character is not diagnostic of any node in their tree (Ferrante & Cavin 2025: fig. 73). In our Bayesian analysis, the

clade Coelacanthiformes is supported by four characters: 77 (anterior lacrymojugal sensory pore(s) expanded or forming a groove), 103 (absence of a suboperculum), 137 (deepest portion of the angular at approximately midway along the length of the angular, but also present in *Caridosuctor populosum*), and 184 (otico-occipital portion of the braincase separated into prootic and opisthotic).

Based on the homoplastic distribution of some of these characters and the lack of proper knowledge on many fossil coelacanths neurocrania, we propose instead to redefine the order Coelacanthiformes Huxley, 1861 as a node-based taxon consisting of the least inclusive clade comprising the last common ancestor of *Coelacanthus granulatus* Agassiz, 1839 and *Latimeria chalumnae* Smith, 1939, and all of its descendants. This definition is congruent with the character-based one proposed by Ferrante & Cavin (2025).

Finally, the Bayesian tip-dating analysis also suggests that the splitting of the main clades of Coelacanthiformes (i.e., Laugiidae+Axeliidae clade, clade 3 including *Aemilia stellata* n. gen., n. sp., and clade 4+Latimerioidei) may have occurred deep in the Carboniferous, while the vast majority of taxa belonging to these clades date from the beginning of the Mesozoic, especially the Triassic. However, the number of coelacanth taxa known from the Permian is extremely limited (e.g., *Coelacanthus granulatus*, *Spermatodus pustulosus*, *Changxingia* (*C. weii* Jin, 1997 and *C. aspratilis* Wang & Liu, 1981), and *Youngichthys xinghuainsis* Wang & Liu, 1981; Agassiz 1839; Moy-Thomas & Westoll 1935; Westoll 1939; Wang & Liu 1981; Friedman *et al.* 2007). The unexpected phylogenetic patterns revealed by our new phylogenetic analysis suggest that the diversity of Carboniferous and more particularly Permian coelacanths remains largely undersampled.

CONCLUSION

Coelacanth evolution has traditionally been described as conservative (e.g., Cloutier 1991a, b; Forey 1998; Clement *et al.* 2024; Ferrante & Cavin 2025) but not necessarily due to a simple lack of variation (which is now well established by new and sometimes odd morphologies; e.g., Friedman & Coates 2006; Wendruff & Wilson 2012; Cavin *et al.* 2017; Ferrante & Cavin 2023) but rather because these few limited, punctual variations span more than 400 million years of evolution, making coelacanths one of the most fascinating groups of vertebrates. Clement *et al.* (2024) pointed out that the early Palaeozoic (especially the Devonian) saw a rapid burst of morphological evolution and that major morphological innovations ceased to occur from the late Mesozoic, followed by a still unexistant fossil record of Cenozoic coelacanths.

It has been proposed that one of the key factors explaining the survival of extant coelacanths after the Cretaceous is their adaptation to moderate oceanic depths (Cupello *et al.* 2019a) and an incredibly slow metabolism that allows *Latimeria chalumnae* to live past one hundred years, despite an impressively late reach of sexual maturity at around fifty years (Mahé *et al.* 2021). An explanation to this slow metabolism lies in its extremely reduced proportion of oxygen absorbed by the gills (Hughes 1972, 1976, 1980, 1998). However, fossil coelacanths are also known to posses a lung to support bimodal respiration along with the gills, which allowed them to thrive in both fresh and shallow to moderate deep marine waters (Cupello *et al.* 2017a, b, 2019a, b). The lung was functional and surrounded by bony plates in many Palaeozoic and Mesozoic taxa (e.g., *Rhabdoderma*, *Coelacanthus*, *Laugia*, *Graulia*, *Macropoma*, *Mawsonia*, *Axelrodichthys*; Forey 1998; Brito *et al.* 2010; Cupello *et al.* 2017b; Manuelli *et al.* 2024), whereas in the extant *Latimeria chalumnae* the lung is present but vestigial and non-functional (Millot & Anthony 1965; Cupello *et al.* 2017b), and the gas exchange is made exclusively through the gills. Unfortunately, physiology does not fossilize so it is currently not possible to evaluate the evolution of oxygen intake in coelacanths. However, the skeleton supporting the gills, namely the hyobranchial skeleton, appears not to be affected by these metabolic changes as evidenced by the rather stable morphology and organization of the hyoid and branchial arches across coelacanth evolution, especially the elements carrying hemibranchs (i.e., the hyomandibula and ceratobranchials). Nevertheless, the dorsal portion of the branchial arches, comprising the epibranchial and pharyngobranchial series appears to have been more plastic, but unfortunately its components are among the least well-preserved elements of the hyobranchial skeleton in fossil coelacanths.

The new Carboniferous coelacanth *Aemilia stellata* n. gen., n. sp. fills an important gap in our knowledge of the morphological diversity of coelacanths during the Late Palaeozoic. *Aemilia stellata* n. gen., n. sp. preserves almost the entire hyoid and branchial arches in partial articulation. Other exceptionally preserved coelacanths also display a rather complete hyobranchial skeleton (e.g., *Ticinepomis*, *Ngamugawi*, *Graulia*; Cavin *et al.* 2013; Clement *et al.* 2024; Manuelli *et al.* 2024; Table 1), however *Aemilia stellata* n. gen., n. sp. is remarkable in that it uncovers elements never before described in a fossil coelacanth. Among these, the epibranchial and pharyngobranchial series have been revealed in great detail, allowing comparisons with only a few extinct forms (e.g., *Laugia*, *Dobrogeria*, *Graulia*) besides the extant *Latimeria*. The new anatomical information supports the idea that the hyobranchial skeleton of post-Carboniferous coelacanths may be considered derived relative to the plesiomorphic condition displayed in *Aemilia stellata* n. gen., n. sp., and that the hyoid and branchial arches of younger and Recent taxa like *Latimeria* are the evolutionary result of a morphological simplification and a reduction in ossification, especially in the epibranchial and pharyngobranchial series. Further comparative data on other Palaeozoic coelacanths is greatly desired in order to support this statement.

A new phylogenetic analysis with the addition of new taxa to the previously published matrix by Clement *et al.* (2024) has reconstructed *Aemilia stellata* n. gen., n. sp. as the oldest Coelacanthiformes (*sensu* our new phylogenetic definition of the order) and the earliest representative of a major

post-Palaeozoic radiation of coelacanths. This new middle Palaeozoic species bridges the gap between the Devonian and post-Carboniferous clades of coelacanths, shedding light on a relatively uncharted period of their evolutionary history and revealing that the fossil record of Carboniferous and especially Permian coelacanths is still greatly unexplored.

New taxa like *Aemilia stellata* n. gen., n. sp. unveil novel and unexpected combinations of features that reconfigure our understanding of the systematics and anatomical evolution of coelacanths, especially focusing on the neurocranial and hyobranchial skeleton. We predict that future studies on coelacanth anatomy will heavily focus on the yet untapped diversity of these skull systems as tomographic studies applied to exceptionally preserved fossils continue developing. We hope that the new data such as the ones presented here will establish a firm comparative basis for future descriptions of extinct coelacanths and will continue shedding light on some of the lesser-known episodes of the long evolutionary history of these iconic fishes.

Acknowledgements
We warmly thank Philippe Janvier (Muséum national d'Histoire naturelle, Paris), Per Ahlberg (Uppsala University), John Long and Alice Clement (Flinders University, Adelaide), Luigi Manuelli, Christophe Ferrante, and Lionel Cavin (Muséum d'Histoire naturelle, Genève) for insights and inspiring discussions on coelacanth anatomy and evolution. Dieter Uhl (Senckenberg Research Institute and Natural History Museum) is thanked for providing essential hardware and ressources. Florent Goussard (Muséum national d'Histoire naturelle, Paris) provided software and technical assistance, and Marc Herbin (Muséum national d'Histoire naturelle, Paris) granted access to the coelacanth collections at the MNHN under his care. Richard Dearden (University of Birmingham) shared precious advice and guidance on the use of Blender. JMF was supported by the Louis Gentil-Jacques Bourcart prize of the French Academy of Sciences. We acknowledge the work of Lionel Cavin and an anonymous reviewer and thank them for their constructive remarks.

REFERENCES

AGASSIZ L. 1839. — *Recherches sur les poissons fossiles*. Vol. 2. Imprimerie de Petitpierre, Neuchatel, 336 p. https://doi.org/10.5962/bhl.title.4275

AMEMIYA C., ALFÖLDI J., LEE A., […] & LINDBLAD-TOH K. 2013. — The African coelacanth genome provides insights into tetrapod evolution. *Nature* 496: 311-316. https://doi.org/10.1038/nature12027

ANDREWS M., LONG J., AHLBERG P., BARWICK R. & CAMPBELL K. 2006. — The structure of the sarcopterygian *Onychodus jandemarrai* n. sp. from Gogo, Western Australia: with a functional interpretation of the skeleton. *Earth and Environmental Science Transactions of the Royal Society of Edinburgh* 96 (3): 197-307. https://doi.org/10.1017/S0263593300001309

ARGYRIOU T., GILES S. & FRIEDMAN M. 2022. — A Permian fish reveals widespread distribution of neopterygian-like jaw suspension. *Elife* 11: e58433. https://doi.org/10.7554/eLife.58433

ARRATIA G. & SCHULTZE H. P. 1990. — The urohyal: development and homology within osteichthyans. *Journal of Morphology* 203 (3): 247-282. https://doi.org/10.1002/jmor.1052030302

ARRATIA G. & SCHULTZE H. P. 2015. — A new fossil actinistian from the Early Jurassic of Chile and its bearing on the phylogeny of Actinistia. *Journal of Vertebrate Paleontology* 35 (5): e983524. https://doi.org/10.1080/02724634.2015.983524

BERG L. S. 1940. — Classification of fishes, both recent and fossil. *Travaux de l'Institut de l'Academie des Sciences de l'URSS* 5 (2): 87-517.

BJERRING H. C. 1993. — Yet another interpretation of the coelacanthiform basicranial muscle and its innervation. *Acta Zoologica* 74 (4): 289-299. https://doi.org/10.1111/j.1463-6395.1993.tb01244.x

BOUCKAERT R., VAUGHAN T. G., BARIDO-SOTTANI J., DUCHÊNE S., FOURMENT M., GAVRYUSHKINA A., HELED J., JONES G., KÜHNERT D., DE MAIO N., MATSCHINER M., MENDES F. K., MÜLLER N. F., OGILVIE H. A., DU PLESSIS L., POPINGA A., RAMBAUT A., RASMUSSEN D., SIVERONI I., SUCHARD M. A., WU C.-H., XIE D., ZHANG C., STADLER T. & DRUMMOND A. J. 2019. — BEAST 2.5: an advanced software platform for Bayesian evolutionary analysis. *PLOS Computational Biology* 15 (4): e1006650. https://doi.org/10.1371/journal.pcbi.1006650

BRAZEAU M. D. & FRIEDMAN M. 2014. — The characters of Palaeozoic jawed vertebrates. *Zoological journal of the Linnean Society* 170 (4): 779-821. https://doi.org/10.1111/zoj.12111

BRAZEAU M. D., FRIEDMAN M., JERVE A. & ATWOOD R. C. 2017. — A three-dimensional placoderm (stem-group gnathostome) pharyngeal skeleton and its implications for primitive gnathostome pharyngeal architecture. *Journal of Morphology* 278 (9): 1220-1228. https://doi.org/10.1002/jmor.20706

BRITO P. M., MEUNIER F. J., CLÉMENT G. & GEFFARD-KURIYAMA D. 2010. — The histological structure of the calcified lung of the fossil coelacanth *Axelrodichthys araripensis* (Actinistia: Mawsoniidae). *Palaeontology* 53 (6): 1281-1290. https://doi.org/10.1111/j.1475-4983.2010.01015.x

CARVALHO M., BOCKMANN F. A. & DE CARVALHO M. R. 2013. — Homology of the fifth epibranchial and accessory elements of the ceratobranchials among Gnathostomes: insights from the development of ostariophysans. *PLOS ONE* 8 (4): e62389. https://doi.org/10.1371/journal.pone.0062389

CARVALHO M. S. DE & MAISEY J. G. 2008. — New occurrence of *Mawsonia* (Sarcopterygii: Actinistia) from the Early Cretaceous of the Sanfranciscana Basin, Minas Gerais, southeastern Brazil. *Geological Society, London, Special Publications* 295 (1): 109-144. https://doi.org/10.1144/SP295.8

CARVALHO M. S. DE, GALLO V. & SANTOS H. R. S. 2013. — New species of coelacanth fish from the Lower Cretaceous (Albian) of the Grajaú Basin, NE Brazil. *Cretaceous Research* 46: 80-89. https://doi.org/10.1016/j.cretres.2013.09.006

CAVIN L. & GRĂDINARU E. 2014. — *Dobrogeria aegyssensis*, a new early Spathian (Early Triassic) coelacanth from North Dobrogea (Romania). *Acta Geologica Polonica* 64 (2): 161-187. https://doi.org/10.2478/agp-2014-0010

CAVIN L., FURRER H. & OBRIST C. 2013. — New coelacanth material from the Middle Triassic of eastern Switzerland and comments on the taxic diversity of actinistans. *Swiss Journal of Geosciences* 106: 161-177. https://doi.org/10.1007/s00015-013-0143-7

CAVIN L., MENNECART B., OBRIST C., COSTEUR L. & FURRER H. 2017. — Heterochronic evolution explains novel body shape in a Triassic coelacanth from Switzerland. *Scientific Reports* 7 (1): 13695. https://doi.org/10.1038/s41598-017-13796-0

CLEMENT A. M., CLOUTIER R., LEE M. S., KING B., VANHAESEBROUCKE O., BRADSHAW C. J., DUTEL H., TRINAJSTIC K. & LONG J. A. 2024. — A Late Devonian coelacanth reconfigures actinistian phylogeny, disparity, and evolutionary dynamics. *Nature Communications* 15 (1): 7529. https://doi.org/10.1038/s41467-024-51238-4

CLÉMENT G. 1999. — The actinistian (Sarcopterygii) *Piveteauia madagascariensis* Lehman from the Lower Triassic of northwestern Madagascar: a redescription on the basis of new material. *Journal of Vertebrate Paleontology* 19 (2): 234-242. https://doi.org/10.1080/02724634.1999.10011137

CLÉMENT G. 2005. — A new coelacanth (Actinistia, Sarcopterygii) from the Jurassic of France, and the question of the closest relative fossil to *Latimeria*. *Journal of Vertebrate Paleontology* 25 (3): 481-491. https://doi.org/10.1671/0272-4634(2005)025[0481:ANCASF]2.0.CO;2

CLOUTIER R. 1991a. — Patterns, trends, and rates of evolution within the Actinistia. *Environmental Biology of Fishes* 32: 23-58. https://doi.org/10.1007/BF00007444

CLOUTIER R. 1991b. — Interrelationships of Palaeozoic actinistians: patterns and trends, *in* CHANG M.-M., LIU Y.-L. & ZHANG G.-N. (eds), *Early vertebrates and related problems of evolutionary biology*. Science Press, Beijing: 379-428.

CLOUTIER R. 1996. — The primitive actinistian *Miguashaia bureaui* Schultze (Sarcopterygii), *in* SCHULTZE H.-P. & CLOUTIER R. (eds), *Devonian fishes and plants of Miguasha, Quebec, Canada*. Verlag Dr Friedrich Pfeil, Munchen: 227-247.

CLOUTIER R. & SCHULTZE H.-P. 1996. — Porolepiform fishes (Sarcopterygii), *in* SCHULTZE H.-P. & CLOUTIER R. (eds), *Devonian fishes and plants of Miguasha, Quebec, Canada*. Verlag Dr Friedrich Pfeil, Munchen: 248-270.

COATES M. I., FINARELLI J. A., SANSOM I. J., ANDREEV P. S., CRISWELL K. E., TIETJEN K., RIVERS M. L. & LA RIVIERE P. J. 2018. — An early chondrichthyan and the evolutionary assembly of a shark body plan. *Proceedings of the Royal Society B: Biological Sciences* 285 (1870): 20172418. https://doi.org/10.6084/m9.figshare.c.3952948.

COPE E. D. 1871. — Contributions to the ichthyology of the Lesser Antilles. *Transactions of the American Philosophical Society* 14 (3): 445-483. https://doi.org/10.2307/1005256

CUI X., FRIEDMAN M., QIAO T., YU Y. & ZHU M. 2022. — The rapid evolution of lungfish durophagy. *Nature communications* 13 (1): 2390. https://doi.org/10.1038/s41467-022-30091-3

CUPELLO C., MEUNIER F. J., HERBIN M., JANVIER P., CLÉMENT G. & BRITO P. M. 2017a. — The homology and function of the lung plates in extant and fossil coelacanths. *Scientific Reports* 7 (1): 9244. https://doi.org/10.1038/s41598-017-09327-6

CUPELLO C., MEUNIER F. J., HERBIN M., CLÉMENT G. & BRITO P. M. 2017b. — Lung anatomy and histology of the extant coelacanth shed light on the loss of air-breathing during deep-water adaptation in actinistians. *Royal Society Open Science* 4 (3): 161030. https://doi.org/10.1098/rsos.161030

CUPELLO C., CLÉMENT G. & BRITO P. M. 2019a. — Evolution of air breathing and lung distribution among fossil fishes, *in* JOHANSON Z., UNDERWOOD C. & RICHTER M. (eds), *Evolution and Development of Fishes*, Cambridge University Press, Cambridge: 252-262.

CUPELLO C., CLÉMENT G., MEUNIER F. J., HERBIN M., YABUMOTO Y. & BRITO P. M. 2019b. — The long-time adaptation of coelacanths to moderate deep water: reviewing the evidences. *Bulletin of the Kitakyushu Museum of Natural History and Human History, Series A (Natural History)* 17: 29-35. https://doi.org/10.34522/kmnh.17.0_29

DATOVO A. & JOHNSON D. 2025. — Coelacanths illuminate Deep-time evolution of cranial musculature in jawed vertebrates. *Science Advances* 11 (18): eadt1576. https://doi.org/10.1126/sciadv.adt1576

DEARDEN R. P., STOCKEY C. & BRAZEAU M. D. 2019. — The pharynx of the stem-chondrichthyan *Ptomacanthus* and the early evolution of the gnathostome gill skeleton. *Nature Communications* 10 (1): 2050. https://doi.org/10.1038/s41467-019-10032-3

DEARDEN R. P., HERREL A. & PRADEL A. 2024. — The pharynx of the iconic stem-group chondrichthyan Acanthodes Agassiz, 1833 revisited with micro-computed tomography. *Zoological Journal of the Linnean Society* 203 (2): zlae058. https://doi.org/10.1093/zoolinnean/zlae058

DEESRI U., CAVIN L., AMIOT R., BARDET N., BUFFETAUT E., CUNY G., GINER S., MARTIN J. E. & SUAN G. 2018. — A mawsoniid coelacanth (Sarcopterygii: Actinistia) from the Rhaetian (Upper Triassic) of the Peygros quarry, Le Thoronet (Var, southeastern France). *Geological Magazine* 155 (1): 187-192. https://doi.org/10.1017/S0016756817000619

DEMANET F. 1939. — Filtering appendices on the branchial arches of *Coelacanthus lepturus*. *Geological Magazine* 76 (5): 215-219. https://doi.org/10.1017/S0016756800071004

DUTEL H., MAISEY J. G., SCHWIMMER D. R., JANVIER P., HERBIN M. & CLÉMENT G. 2012. — The giant Cretaceous coelacanth (Actinistia, Sarcopterygii) *Megalocoelacanthus dobiei* Schwimmer, Stewart & Williams, 1994, and its bearing on Latimerioidei Interrelationships. *PLoS ONE* 7: e49911. https://doi.org/10.1371/journal.pone.0049911

DUTEL H., HERREL A., CLÉMENT G. & HERBIN M. 2013. — A reevaluation of the anatomy of the jaw-closing system in the extant coelacanth *Latimeria chalumnae*. *Naturwissenschaften* 100: 1007-1022. https://doi.org/10.1007/s00114-013-1104-8

DUTEL H., HERBIN M., CLÉMENT G. & HERREL A. 2015a. — Bite force in the extant coelacanth Latimeria: the role of the intracranial joint and the basicranial muscle. *Current Biology* 25 (9): 1228-1233. https://doi.org/10.1016/j.cub.2015.02.076

DUTEL H., HERBIN M. & CLÉMENT G. 2015b. — First occurrence of a mawsoniid coelacanth in the Early Jurassic of Europe. *Journal of Vertebrate Paleontology* 35 (3): e929581. https://doi.org/10.1080/02724634.2014.929581

DUTEL H., GALLAND M., TAFFOREAU P., LONG J. A., FAGAN M. J., JANVIER P., HERREL A., SANTIN M. D., CLÉMENT G. & HERBIN M. 2019. — Neurocranial development of the coelacanth and the evolution of the sarcopterygian head. *Nature* 569 (7757): 556-559. https://doi.org/10.1038/s41586-019-1117-3

ECHOLS J. 1963. — A new genus of Pennsylvanian fish (Crossopterygii, Coelacanthiformes) from Kansas. *University of Kansas Publications* 12 (10): 475-501.

FERRANTE C. & CAVIN L. 2023. — Early Mesozoic burst of morphological disparity in the slow-evolving coelacanth fish lineage. *Scientific Reports* 13 (1): 11356. https://doi.org/10.1038/s41598-023-37849-9

FERRANTE C. & CAVIN L. 2025. — A deep dive into the coelacanth phylogeny. *PLoS One* 20 (6): e0320214. https://doi.org/10.1371/journal.pone.0320214

FERRANTE C., MENKVELD-GFELLER U. & CAVIN L. 2022. — The first Jurassic coelacanth from Switzerland. *Swiss Journal of Palaeontology* 141 (15). https://doi.org/10.1186/s13358-022-00257-z

FERRANTE C., FURRER H., MARTINI R. & CAVIN L. 2023. — Revision of the Middle Triassic coelacanth *Ticinepomis* Rieppel 1980 (Actinistia, Latimeriidae) with paleobiological and paleoecological considerations. *Swiss Journal of Palaeontology* 142 (1): 18. https://doi.org/10.1186/s13358-023-00276-4

FERRING R. 2007. — *The Geology of Texas*. CENGAGE Learning Custom Publishing, University of North Texas, Denton, Texas, 24 p.

FOREY P. L. 1981. — The coelacanth *Rhabdoderma* in the Carboniferous of the British Isles. *Palaeontology* 24: 203-229.

FOREY P. L. 1991. — *Latimeria chalumnae* and its pedigree. *Environmental Biology of Fishes* 32: 75-97. https://doi.org/10.1007/BF00007446

FOREY P. L. 1998. — *History of the Coelacanth fishes*. Chapman and Hall, London, 419 p.

FOREY P. L., AHLBERG P. E., LUKŠEVIČS E. & ZUPINŠ I. 2000. — A new coelacanth from the Middle Devonian of Latvia. *Journal of Vertebrate Paleontology* 20 (2): 243-252. https://doi.org/10.1671/0272-4634(2000)020[0243:ANCFTM]2.0.CO;2

FOREY P. L., MONOD O. & PATTERSON C. 1985. — Fishes from the Akkuyu Formation (Tithonian), Western Taurus, Turkey. *Geobios* 18 (2): 195-201. https://doi.org/10.1016/S0016-6995(85)80013-9

FRAGOSO L. G. C., BRITO P. & YABUMOTO Y. 2018. — *Axelrodichthys araripensis* Maisey, 1986 revisited. *Historical Biology* 31 (10): 1350-1372. https://doi.org/10.1080/08912963.2018.1454443

FRIEDMAN M. 2007. — *Styloichthys* as the oldest coelacanth: implications for early osteichthyan interrelationships. *Journal of Systematic Palaeontology* 5 (3): 289-343. https://doi.org/10.1017/S1477201907002052

FRIEDMAN M. & BRAZEAU M. D. 2010. — A reappraisal of the origin and basal radiation of the Osteichthyes. *Journal of Vertebrate Paleontology* 30 (1): 36-56. https://doi.org/10.1080/02724630903409071

FRIEDMAN M. & COATES M. I. 2006. — A newly recognized coelacanth highlights the early morphological diversification of the clade. *Proceedings of the Royal Society B,* 273: 240-245. https://doi.org/10.1098/rspb.2005.3316

FRIEDMAN M., COATES M. I. & ANDERSON P. 2007. — First discovery of a primitive coelacanth fin fills a major gap in the evolution of lobed fins and limbs. *Evolution and Development* 9 (4): 329-337. https://doi.org/10.1111/j.1525-142X.2007.00169.x

GARDINER B. G. 1984. — The relationships of the palaeoniscoid fishes, a review based on new specimens of *Mimia* and *Moythomasia* from the Upper Devonian of Western Australia. *Bulletin of the British Museum (Natural History), Geology* 37: 173-428.

GESS R. W. & COATES M. I. 2015. — Fossil juvenile coelacanths from the Devonian of South Africa shed light on the order of character acquisition in actinistians. *Zoological Journal of the Linnean Society* 175 (2): 360-383. https://doi.org/10.1111/zoj.12276

GILES S., DARRAS L., CLÉMENT G., BLIECK A. & FRIEDMAN M. 2015. — An exceptionally preserved Late Devonian actinopterygian provides a new model for primitive cranial anatomy in ray-finned fishes. *Proceedings of the Royal Society B: Biological Sciences* 282 (1816): 20151485. https://doi.org/10.1098/rspb.2015.1485

GOLOBOFF P. A. & MORALES M. E. 2023. — TNT version 1.6, with a graphical interface for MacOS and Linux, including new routines in parallel. *Cladistics* 39 (2): 144-153. https://doi.org/10.1111/cla.12524

GOLONKA J. 2000. — *Cambrian-Neogene plate tectonic maps*. Wydavnictwa Universytetu Jagiellonskiego, Krakow b Wydawn, 125 p.

HEATH T. A., HUELSENBECK J. P. & STADLER T. 2014. — The fossilized birth–death process for coherent calibration of divergence-time estimates. *Proceedings of the National Academy of Sciences* 111 (29): E2957-E2966. https://doi.org/10.1073/pnas.1319091111

HUGHES G. M. 1972. — Gills of a living coelacanth, *Latimeria chalumnae*. *Experientia* 28: 1301-1302. https://doi.org/10.1007/BF01965307

HUGHES G. M. 1976. — On the respiration of *Latimeria chalumnae*. *Zoological Journal of the Linnean Society* 59 (2): 195-208. https://doi.org/10.1111/j.1096-3642.1976.tb01014.x

HUGHES G. M. 1980. — Ultrastructure and morphometry of the gills of *Latimeria chalumnae*, and a comparison with the gills of associated fishes. *Proceedings of the Royal Society of London Series B* 208: 309-328. https://doi.org/10.1098/rspb.1980.0053

HUGHES G. M. 1998. — The gills of the coelacanth, *Latimeria chalumnae* Latimeriidae. What can they teach us? *Italian Journal of Zoology* 65 (issue sup 1): 425-429. https://doi.org/10.1080/11250009809386859

HUGHES G. M. & MORGAN M. 1973. — The structure of fish gills in relation to their respiratory function. *Biological Reviews* 48 (3): 419-475. https://doi.org/10.1111/j.1469-185X.1973.tb01009.x

HUXLEY T. H. 1861. — Preliminary essay upon the systematic arrangement of the fishes of the Devonian epoch. *Memoirs of the Geological Survey of the United Kingdom* 10: 1-40.

HUXLEY T. H. 1880. — On the application of the laws of evolution to the arrangement of the Vertebrata and more particularly of the Mammalia. *Proceedings of the Zoological Society of London* 1880: 649-662.

JAIN S. L. 1974. — *Indocoelacanthus robustus* n. gen., n. sp. (Coelacanthidae, Lower Jurassic), the first fossil coelacanth from India. *Journal of Paleontology* 48 (1): 49-62. https://www.jstor.org/stable/1303105

JANVIER P. 1996. — *Early vertebrates*. Clarendon Press (Oxford Monographs on Geology and Geophysics; 33), Oxford, 393 p.

JANVIER P. 2004. — Early specializations in the branchial apparatus of jawless vertebrates: a consideration of gill number and size, *in* ARRATIA G., WILSON M. V. H. & CLOUTIER R. (eds), *Recent Advances in the Origin and Early Radiation of Vertebrates*. Verlag Dr. Friedrich Pfeil, Munich: 29-52.

JARVIK E. 1954. — On the visceral skeleton in *Eusthenopteron* with a discussion of the parasphenoid and palatoquadrate in fishes. *Kungliga Svenska Vetenskapsakademiens Handlingar. Fjärde Serien* 5 (1): 1-104.

JARVIK E. 1972. — Middle and Upper Devonian Porolepiformes form East Greenland with special reference to *Glyptolepis groenlandica* n. sp. *Meddelelser om Grønland* 187: 1-307. https://tidsskrift.dk/meddrgroenland/article/view/151880

JARVIK E. 1980. — *Basic structure and evolution of vertebrates*, *Volume 1*. Academic Press, London: 575 p.

JESSEN H. 1973. — Weitere Fischreste aus dem Oberen Plattenkalk der Bergisch-Gladbach-Paffrather Mulde (Oberdevon, Rheinisches Schiefergebirge). *Palaeontographica Abteilung A* 1-6: 159-187.

JOHANSON Z. & AHLBERG P. E. 1997. — A new tristichopterid (Osteolepiformes; Sarcopterygii) from the Mandagery Sandstone (Famennian) near Canowindra, N.S.W., Australia. *Transactions of the Royal Society of Edinburgh: Earth Sciences* 88 (1): 39-53. https://doi.org/10.1017/S0263593300002303

JOHANSON Z., JOSS J. M. & WOOD D. 2004. — The scapulocoracoid of the Queensland lungfish *Neoceratodus forsteri* (Dipnoi: Sarcopterygii): morphology, development and evolutionary implications for bony fishes (Osteichthyes). *Zoology* 107 (2): 93-109. https://doi.org/10.1016/j.zool.2004.01.001

JOHANSON Z., LONG J. A., TALENT J. A., JANVIER P. & WARREN J. W. 2006. — Oldest coelacanth from the Early Devonian of Australia. *Biology Letters* 2 (3): 443-446. https://doi.org/10.1098/rsbl.2006.0470

KADARUSMAN, SUGEHA H. Y., POUYAUD L., HOCDÉ R., HISMAYASARI I. B., GUNAISAH E., WIDIARTO S. B., ARAFAT G., WIDYASARI F., MOUILLOT D. & PARADIS E. 2020. — A thirteen-million-year divergence between two lineages of Indonesian coelacanths. *Scientific Reports* 10 (1): 192. https://doi.org/10.1038/s41598-019-57042-1

KANYUKIN A. A. 2006. — Hyobranchial skeleton and hypobranchial muscles of rhipidistians. *Paleontological Journal* 40: 297-311. https://doi.org/10.1134/S0031030106030117

LAMBERS P. H. 1991. — The identity of the type specimen of *Coelacanthus harlemensis* Winkler (Pisces, Actinistia) from the lithographic limestone of Solmhofen (Tithonian), Bavaria. *Paläontologische Zeitschrift* 65: 173-189. https://doi.org/10.1007/BF02985782

LAUDER G. V. & REILLY S. M. 1994. — Amphibian feeding behavior: comparative biomechanics and evolution, *in* BELS V. L., CHARDON M. & VANDEWALLE P. (eds), *Biomechanics of feeding in vertebrates. Advances in Comparative and Environmental Physiology*. Vol. 18. Springer, Berlin, Heidelberg: 163-195. https://doi.org/10.1007/978-3-642-57906-6_7

LEBEDEV O. A. 1995. — Morphology of a new osteolepidid fish from Russia. *Bulletin du Muséum National d'Histoire Naturelle. 4e Série. Section C. Sciences de la Terre. Paléontologie, Géologie, Minéralogie* 17: 287-341.

LONG J. A. 1999. — A new genus of fossil coelacanth (Osteichthyes: Coelacanthiformes) from the Middle Devonian of southeastern Australia. *Records of the Western Australian Museum* Supplement No. 57: 37-53.

LUND R. & LUND W. 1984. — New genera and species of coelacanths from the Bear Gulch Limestone (Lower Carboniferous) of Montana (U.S.A.). *Geobios* 17 (2): 237-244. https://doi.org/10.1016/S0016-6995(84)80145-X

LUND R. & LUND W. 1985. — Coelacanths of the Bear Gulch Limestone (Namurian) of Montana and the evolution of the coelacanthiformes. *Bulletin of Carnegie Museum of Natural History* 25: 1-74. https://doi.org/10.5962/p.228604

MAHÉ K., ERNANDE B. & HERBIN M. 2021. — New scale analyses reveal centenarian African coelacanths. *Current Biology* 31 (16): 3621-3628. https://doi.org/10.1016/j.cub.2021.05.054

MAISEY J. G. 1986. — Coelacanths from the Lower Cretaceous of Brazil. *American Museum Novitates* 2866: 1-30. http://hdl.handle.net/2246/5188

MANSUIT R., CLÉMENT G., HERREL A., DUTEL H., TAFFOREAU P., SANTIN M. D. & HERBIN M. 2020. — Development and growth of the pectoral girdle and fin skeleton in the extant coelacanth Latimeria chalumnae. *Journal of Anatomy* 236 (3): 493-509.

MANUELLI L., COVAIN R. & CAVIN L. 2023. — A 3D reconstruction of the skull of the West Indian Ocean coelacanth *Latimeria chalumnae*. *MorphoMuseuM* 9 (3): e211. https://doi.org/10.18563/journal.m3.211

MANUELLI L., MONDÉJAR FERNÁNDEZ J., DOLLMAN K., JAKATA K. & CAVIN L. 2024. — The most detailed anatomical reconstruction of a Mesozoic coelacanth. *PLoS ONE* 19 (11): e0312026. https://doi.org/10.1371/journal.pone.0312026

MILES R. S. 1977. — Dipnoan (lungfish) skulls and the relationships of the group: a study based on new species from the Devonian of Australia. *Zoological Journal of the Linnean Society* 61 (1-3): 1-328. https://doi.org/10.1111/j.1096-3642.1977.tb01031.x

MILLOT J. & ANTHONY J. 1958. — *Anatomie de* Latimeria chalumnue. *Vol. I. Squelette, muscles et formation de soutien*. CNRS, Paris, 122 p.

MILLOT J. & ANTHONY J. 1965. — *Anatomie de Latimeria chalumnae. Vol. 2. Système nerveux et organes des sens*. CNRS, Paris, 131 p.

MILLOT J. A., ANTHONY J. & ROBINEAU D. 1978. — *Anatomie de Latimeria chalumnae. Vol. 3. Appareil digestif, appareil respiratoire, appareil urogénital, glandes endocrines, appareil circulatoire, téguments, écailles, conclusions générales*. CNRS, Paris, 198 p.

MONDÉJAR-FERNÁNDEZ J. 2020. — A new onychodont (Osteichthyes; Sarcopterygii) from the Middle Devonian of Morocco and its bearing on early osteichthyan evolution. *Journal of Systematic Palaeontology* 18 (7): 573-606. https://doi.org/10.1080/14772019.2019.1655495

MOY-THOMAS J. A. 1937. — The Carboniferous coelacanth fishes of Great Britain and Ireland. *Proceedings of the Zoological Society of London* B107 (3): 383-415. https://doi.org/10.1111/j.1469-7998.1937.tb00016.x

MOY-THOMAS J. A. & WESTOLL T. S. 1935. — On the Permian coelacanth, *Coelacanthus granulatus*, Ag. *Geological Magazine* 72 (10): 446-457. https://doi.org/10.1017/S0016756800094516

MÜNSTER G. VON. 1842. — Beitrag zur Kenntniss einiger neuen seltenen Versteinerungen aus den lithographischen Schiefern in Baiern. *Neues Jahrbuch für Mineralogie, Geognosie, Geologie und Petrefakten-Kunde* 1842: 35-46.

NELSON G. J. 1969. — Gill arches and the phylogeny of fishes, with notes on the classification of vertebrates. *Bulletin of the American Museum of Natural History* 141 (4): 475-552. http://hdl.handle.net/2246/1162

NEWBERRY J. S. 1856. — Description of several new genera and species of fossil fishes, from the Carboniferous strata of Ohio. *Proceedings of the Academy of Natural Sciences of Philadelphia* 8: 96-100.

PATTERSON C. 1975. — The braincase of pholidophorid and leptolepid fishes, with a review of the actinopterygian braincase. *Philosophical Transactions of the Royal Society of London. B, Biological Sciences* 269 (899): 275-579. https://doi.org/10.1098/rstb.1975.0001

PATTERSON C. 1982. — Morphology and interrelationships of primitive actinopterygian fishes. *American Zoologist* 22 (2): 241-259. https://doi.org/10.1093/icb/22.2.241

POUYAUD L., WIRJOATMODJO S., RACHMATIKA I., TJAKRAWIDJAJA A., HADIATY R. & HADIE W. 1999. — Une nouvelle espèce de coelacanthe. Preuves génétiques et morphologiques. *Comptes Rendus de l'Académie des Sciences-Series III-Sciences de la Vie* 322 (4): 261-267. https://doi.org/10.1016/S0764-4469(99)80061-4

PRADEL A., MAISEY J. G., TAFFOREAU P., MAPES R. H. & MALLATT J. 2014. — A Palaeozoic shark with osteichthyan-like branchial arches. *Nature* 509: 608-611. https://doi.org/10.1038/nature13195

PRADEL A., DEARDEN R. P., CUCKOVIC A., MANSUIT R. & JANVIER P. 2021. — The visceral skeleton and its relation to the head circulatory system of both a fossil, the Carboniferous *Iniopera*, and a modern, *Callorhinchus milii* holocephalan (Chondrichthyes), *in* PRADEL A., DENTON J. S. S. & JANVIER P. (eds), *Ancient Fishes and Their Living Relatives: A Tribute to John G Maisey.* Verlag Dr. Friedrich Pfeil, München: 183-192.

RAMBAUT A. 2018. — *FigTree–Tree Figure Drawing Tool Version v. 1.4. 4*. Institute of Evolutionary Biology, University of Edinburgh, Edinburgh.

RAMBAUT A., DRUMMOND A. J., XIE D., BAELE G. & SUCHARD M. A. 2018. — Posterior summarization in Bayesian phylogenetics using Tracer 1.7. *Systematic Biology* 67 (5): 901-904. https://doi.org/10.1093/sysbio/syy032

REIS O. M. 1888. — Die Coelacanthinen, mit besonderer Berticksichtigung der im Weissen Jura Bayerns vorkommender Gattungen. *Palaeontographica* 35: 1- 94.

RENESTO S. & STOCKAR R. 2018. — First record of a coelacanth fish from the Middle Triassic Meride Limestone of Monte San Giorgio (canton Ticino, Switzerland). *Rivista Italiana di Paleontologia e Stratigrafia* 124 (3): 639-653.

ROMANO C., WARE D., BRÜHWILER T., BUCHER H. & BRINKMANN W. 2016. — Marine Early Triassic Osteichthyes from Spiti, Indian Himalayas. *Swiss Journal of Palaeontology* 135: 275-294. https://doi.org/10.1007/s13358-015-0098-6

ROMER A. S. 1955. — Herpetichthyes, Amphibioidei, Choanichthyes or Sarcopterygii? *Nature* 176: 126-127. https://doi.org/10.1038/176126b0

SAINT-SEINE P. D. 1949. — Les poissons des calcaires lithographiques de Cerin (Ain). *Publications du Musée des Confluences* 2 (1): 3-79.

SCHAEFFER B. 1941. — A revision of *Coelacanthus newarki* and notes on the evolution of the girdles and basal plates of the median fins in the Coelacanthini. *American Museum Novitates* 1110: 1-17.

SCHAEFFER B. 1948. — A study of *Diplurus longicaudatus* with notes on the body form and locomotion of the Coelacanthini. *American Museum Novitates* 1378. https://www.biodiversitylibrary.org/page/63975949

SCHAEFFER B. 1952. — The Triassic coelacanth fish *Diplurus*, with observations on the evolution of the Coelacanthini. *Bulletin of the AMNH* 99 (2): 25-78.

SCHAEFFER B. & GREGORY J. T. 1961. — Coelacanth Fishes from the Continental Triassic of the Western United States. *American Museum Novitates* 2036: 1-17. http://hdl.handle.net/2246/3465

SCHAUMBERG G. 1978. — Neubeschreibung von *Coelacanthus granulatus* Agassiz (Actinistia, Pisces) aus dem Kupferschiefer von Richelsdorf (Perm, W.-Deutschland). *Palaeontologische Zeitschrift* 52: 169-197. https://doi.org/10.1007/BF02987700

SCHINDELIN J., ARGANDA-CARRERAS I., FRISE E. *ET AL.* 2012. — Fiji: an open-source platform for biological-image analysis. *Nature Methods* 9 (7): 676-682. https://doi.org/10.1038/nmeth.2019

SCHULTZE H.-P. 1973. — Crossopterygier mit heterozerker Schwanzflose aus dem Oberdevon Kanadas, Nebst einer Beschreibung von Onychodontida-Resten aus dem Mittledevon Spaniens und dem Karbon der USA. *Palaeontographica* 143A: 188-208.

SCHULTZE H.-P. 1993. — Osteichthyes: Sarcopterygii, *in* BENTON M. J. (ed.), *The Fossil Record 2*. Chapman and Hall, London: 657-663.

SCHULTZE H.-P. 2004. — Mesozoic sarcopterygians, *in* ARRATIA G. & TINTORI A. (eds), *Mesozoic fishes 3 - Systematics, Paleoenvironments and Biodiverity*. Verlag Dr Friedrich Pfeil, München: 463-492.

SCHWEIZER R. 1966. — Ein Coelacanthide aus dem Oberen Muschelkalk Göttingens. *Neues Jahrbuch für Geologie und Paläontologie, Abhandlungen*, 125: 215-226.
SEFTON E. M., PIEKARSKI N. & HANKEN J. 2015. — Dual embryonic origin and patterning of the pharyngeal skeleton in the axolotl (*Ambystoma mexicanum*). *Evolution & Development* 17 (3): 175-184. https://doi.org/10.1111/ede.12124
SMITH J. L. B. 1939. — A living fish of Mesozoic type. *Nature* 143 (3620): 455-456. https://doi.org/10.1038/143455a0
STADLER T., KÜHNERT D., BONHOEFFER S. & DRUMMOND A. J. 2013. — Birth–death skyline plot reveals temporal changes of epidemic spread in HIV and hepatitis C virus (HCV). *Proceedings of the National Academy of Sciences* 110 (1): 228-233. https://doi.org/10.1073/pnas.1207965110
STENSIÖ E. A. 1921. — *Triassic fishes from Spitzbergen, Part 1*. Adolf Holzhausen, Vienna, 307 p.
STENSIÖ E. A. 1922. — Über zwei Coelacanthiden aus dem Oberdevon von Wildungen. *Palaeontologischen Zeitschrift* 4: 167-210. https://doi.org/10.1007/BF03041548
STENSIÖ E. A. 1932. — Triassic fishes from East Greenland, collected by the Danish expeditions in 1929-1931. *Meddelelser om Grønland* 83: 1-305.
STENSIÖ E. A. 1937. — On the Devonian coelacanthids of Germany with special reference to the dermal skeleton. *Kungliga Svenska Vetenskapsakademiens Handligar, Stockholm Series 3* 16: 1-56.
TENG C. S., CAVIN L., MAXSON R. E., SÁNCHEZ-VILLAGRA M. R. & CRUMP J. G. 2019. — Resolving homology in the face of shifting germ layer origins: lessons from a major skull vault boundary. *Elife* 8: e52814. https://doi.org/10.7554/eLife.52814
TORIÑO P., SOTO M. & PEREA D. 2021a. — A comprehensive phylogenetic analysis of coelacanth fishes (Sarcopterygii, Actinistia) with comments on the composition of the Mawsoniidae and Latimeriidae: evaluating old and new methodological challenges and constraints. *Historical Biology* 33 (12): 3423-3443. https://doi.org/10.1080/08912963.2020.1867982
TORIÑO P., SOTO M., PEREA D. & DE CARVALHO M. S. S. 2021b. — New findings of the coelacanth *Mawsonia* Woodward (Actinistia, Latimerioidei) from the Late Jurassic-Early Cretaceous of Uruguay: novel anatomical and taxonomic considerations and an emended diagnosis for the genus. *Journal of South American Earth Sciences* 107: 103054. https://doi.org/10.1016/j.jsames.2020.103054
TORIÑO P., DUTEL H., SOTO M., NORBIS W., EZQUERRA V. & PEREA D. 2024. — Reconstructing an ancient fish: three-dimensional skeletal restoration of the head of *Mawsonia* (Sarcopterygii, Actinistia) using CT scan, and an adjusted model for body size estimation in fossil coelacanths. *Journal of Anatomy* 245 (3): 467-489. https://doi.org/10.1111/joa.14054
VÉRAN M. 1988. — Les éléments accessoires de l'arc hyoïdien des poissons téléostomes (Acanthodiens et Osteichthyens) fossiles et actuels. *Mémoires du Muséum national d'Histoire naturelle* 54: 1-98.
VICKARYOUS M. K. & HALL B. K. 2006. — Homology of the reptilian coracoid and a reappraisal of the evolution and development of the amniote pectoral apparatus. *Journal of Anatomy* 208 (3): 263-285. https://doi.org/10.1111/j.1469-7580.2006.00542.x
WANG N. & LIU H. 1981. — Coelacanth fishes from the marine Permian of Zhejiang, South China. *Vertebrata Palasiatica* 19: 305-312, 4 figs. [In Chinese with English summary.]
WEN W., ZHANG Q.-Y., HU S.-X., BENTON M. J., ZHOU C.-Y., TAO X., HUANG J.-Y. & CHEN Z.-Q. 2013. — Coelacanths from the Middle Triassic Luoping Biota, Yunnan, South China, with the earliest evidence of ovoviviparity. *Acta Palaeontologica Polonica* 58 (1): 175-193. https://doi.org/10.4202/app.2011.0066
WENDRUFF A. J. & WILSON M. V. H. 2012. — A fork-tailed coelacanth, *Rebellatrix divaricerca*, gen. et sp. nov. (Actinistia, Rebellatricidae, fam. nov.), from the Lower Triassic of Western Canada. *Journal of Vertebrate Paleontology* 32 (3): 499-511. https://doi.org/10.1080/02724634.2012.657317
WESTOLL T. S. 1939. — *On Spermatodus pustulosus* Cope, a coelacanth from the "Permian" of Texas. *American Museum Novitates*: 1017.
WILEY E. O. 1979. — Ventral gill arch muscles and the interrelationships of gnathostomes, with a new classification of the Vertebrata. *Zoological Journal of the Linnean Society* 67 (2): 149-179. https://doi.org/10.1111/j.1096-3642.1979.tb01110.x
WITZMANN F. 2013. — Phylogenetic patterns of character evolution in the hyobranchial apparatus of early tetrapods. *Earth and Environmental Science Transactions of the Royal Society of Edinburgh* 104 (2): 145-167. https://doi.org/10.1017/S1755691013000480
YABUMOTO Y. 2002. — A new coelacanth from the Early Cretaceous of Brazil (Sarcopterygii, Actinistia). *Paleontological Research* 6 (4): 343-350. https://doi.org/10.2517/prpsj.6.343
YABUMOTO Y. 2008. — A new Mesozoic coelacanth from Brazil (Sarcopterygii, Actinistia). *Paleontological Research* 12 (4): 329-343. https://doi.org/10.2517/prpsj.12.329
YABUMOTO Y. & BRITO P. M. 2016. — A new Triassic Coelacanth, *Whiteia oishii* (Sarcopterygii, Actinistia) from West Timor, Indonesia. *Paleontological Research* 20 (3): 233-246. https://doi.org/10.2517/2015PR033
YABUMOTO Y., BRITO P. M., IWATA M. & ABE Y. 2019. — A new Triassic coelacanth, *Whiteia uyenoteruyai* (Sarcopterygii, Actinistia) from Madagascar and paleobiogeography of the family Whiteiidae. *Bulletin of the Kitakyushu Museum of Natural History and Human History, Series A (Natural History)* 17: 15-27. https://doi.org/10.34522/kmnh.17.0_15
ZHU M. & YU X. 2002. — A primitive fish close to the common ancestor of tetrapods and lungfish. *Nature* 418: 767-770. https://doi.org/10.1038/nature00871
ZHU M., YU X. & JANVIER P. 1999. — A primitive fossil fish sheds light on the origin of bony fishes. *Nature* 397: 607-610. https://doi.org/10.1038/17594
ZHU M., YU X., LU J., QIAO T., ZHAO W. & JIA L. 2012. — Earliest known coelacanth skull extends the range of anatomically modern coelacanths to the Early Devonian. *Nature Communications* 3: 772. https://doi.org/10.1038/ncomms1764

Submitted on 16 June 2025;
accepted on 22 September 2025;
published on 16 June 2026.

APPENDICES

Appendix 1. — Image stacks (CT scan microtomography) of *Aemilia stellata* n.gen, n.sp (AMNHN FF 20686). Available at: https://doi.org/10.17602/M2/M859331

Appendix 2. — 3D meshes (.ply files) of *Aemilia stellata* n.gen, n.sp (AMNHN FF 20686). Available at: https://doi.org/10.17602/M2/L859329

Appendix 3. — Supplementary information: **1**, Coelacanth phylogeny including *Aemilia stellata* n.gen., n.sp. Character matrix, parsimony and Bayesian (BDSKY and FBD) analyses; **2**, table of fossil coelacanths with preserved hyoid, branchial and basibranchial elements; **3**, Coelacanth silhouettes and supplementary references. Available at: https://doi.org/10.7934/P6353